
















## Sea ice mechanics

F. Paul<sup>1</sup> , C. Schwarz<sup>2</sup> , R.R. Audh<sup>3</sup> , J. Bluhm<sup>2</sup>, S. Johnson<sup>4</sup> ,  
K. MacHutchon<sup>5</sup> , T. Mielke<sup>1</sup> , A. Mishra<sup>6</sup>, T. Rampai<sup>4</sup> , T. Ricken<sup>7</sup> ,  
A. Schwarz<sup>2</sup> , S. Skatulla<sup>5</sup> , A. Thom<sup>7</sup> , R. Verrinder<sup>6</sup> , J. Schröder<sup>2</sup> ,  
M. Vichi<sup>3</sup> , D.C. Lupascu<sup>1\*</sup> 

<sup>1</sup>Institute for Materials Science and Center for Nanointegration Duisburg-Essen (CENIDE), University of Duisburg-Essen, Germany.

<sup>2</sup>Institute of Mechanics, University of Duisburg-Essen, Germany.

<sup>3</sup>Department of Oceanography and Marine and Antarctic Research Centre for Innovation and Sustainability (MARiS), University of Cape Town, South Africa.

<sup>4</sup>Department of Chemical Engineering and Marine and Antarctic Research Centre for Innovation and Sustainability (MARiS), University of Cape Town, South Africa.

<sup>5</sup>Department of Civil Engineering, University of Cape Town, South Africa.

<sup>6</sup>Department of Electrical Engineering and Marine and Antarctic Research Centre for Innovation and Sustainability (MARiS), University of Cape Town, South Africa.

<sup>7</sup>Institute of Mechanics, Structural Analysis and Dynamics of Aerospace Structures, University of Stuttgart, Germany.

### Abstract

Earth System Models (ESM), simulating sea ice and its interaction with the atmosphere and open ocean, require reliable physical, chemical, and biological input from measurements. There is limited data available from the Marginal Ice Zone of the Antarctic, where sea ice growth mechanisms differ from the Arctic. The main objective of this study is to review existing work related to Antarctic sea ice and highlight gaps in the available literature. The mechanical properties of sea ice and the numerical modeling of sea ice across all scales are covered. We summarize the genesis, physical mechanics, static and dynamic properties, strength, toughness, and transport of young sea ice as well as medium to large scale observation. On the computational mechanics side large- and small-scale modeling, ocean-sea ice and atmosphere-sea ice models, as well as sea ice rheology models, sea ice fracture mechanics, and bio-geo-chemical interaction processes are captured. The synergy between the physical and computational mechanics brings to light missing information from both fields.

#### Plain language summary (PLS)

Sea ice determines the interaction of the ocean with the atmosphere in both the southern and northern hemispheres. Its formation and annual development is subject to mechanical interaction with ocean currents and winds. This review covers the mechanics of sea ice in the Antarctic and its relation to the Arctic covering experiment and modelling. Impact on the climate is discussed.

**Keywords:** sea ice mechanics, polar regions, review, Antarctic MIZ

\*Corresponding author: [doru.lupascu@uni-due.de](mailto:doru.lupascu@uni-due.de)

ORCID ID's: 0000-0002-2328-4048 (F. Paul), 0000-0001-7964-1908 (C. Schwarz), 0000-0002-4163-4515 (R.R. Audh), 0000-0003-0157-6338 (S. Johnson), 0000-0003-2327-8518 (K. MacHutchon), 0009-0002-4835-2817 (T. Mielke), 0000-0002-5808-947X (T. Rampai), 0000-0001-8515-5009 (T. Ricken), 0000-0003-2276-5947 (A. Schwarz), 0000-0003-1061-3356 (S. Skatulla), 0000-0003-1825-2604 (A. Thom), 0000-0003-4266-9274 (R. Verrinder), 0000-0001-7960-9553 (J. Schröder), 0000-0002-0686-9634 (M. Vichi), 0000-0002-6895-1334 (D.C. Lupascu)

© 2023 Authors. This is an open access publication, which can be used, distributed and reproduced in any medium according to the Creative Commons CC-BY 4.0 License requiring that the original work has been properly cited.

## 1. Introduction

Sea ice and its interaction with the atmosphere and ocean are essential parts of the earth's climate system. Earth System Models (ESM) aim to simulate the physical, chemical, and biological processes of components contributing to the climate system including sea ice, ocean circulation, atmosphere, ocean ecology, and biogeochemistry, as well as the interactions between these. Polar sea ice is a dynamic, mosaic interface between the ocean and the atmosphere. It is seasonal in composition and coverage. Atmosphere-ice-ocean interactions are key components of global climate cycles, influencing momentum transfer, gaseous exchange and primary production capacity (Kennicutt II et al., 2014, 2016, 2019; Parkinson, 2004). Within these interactions, sea ice is an insulating layer, filtering and reflecting incoming solar radiation, buffering the ocean surface temperature and limiting gaseous exchange between the ocean surface and the atmosphere (DeConto & Pollard, 2003). In addition, the physical properties of sea ice affect surface wave formation and propagation mostly through dampening ocean kinetic energy and surface wave attenuation (Ardhuin et al., 2020; Parkinson, 2004; Squire, 2020). The formation of sea ice, itself, is affected by the climate. High winds and prominent wave activity at the open ocean front promote complex ice formation behavior. To describe sea ice formation, its influence on the climate, surface wave damping, insulating properties, gaseous exchange, and numerous other processes, sea ice properties need to be investigated on different scales, as shown in Fig. 1.

The Marginal Ice Zone (MIZ) describes the interface region between open ocean and packed ice (Wadhams et al., 1987) typically comprised of unconsolidated mixture of heterogeneous ice floe types with a sea ice concentration between 15% and 80% (Strong & Rigor, 2013). The MIZ sea ice-floe concentration and coverage fundamentally influence the atmosphere-ocean-sea ice interaction in the polar regions with their formation and coverage following seasonal cycles. The maximum polar sea ice extent is observed in early spring, with a minimum extent found in late summer (Lee et al., 2017). The most pronounced changes have been observed in the Arctic region over the past 40 years, where there are dramatic reductions in sea ice thickness, compactness and extent during the summer months (Kwok, 2018; Lee et al., 2017; Squire, 2020; Turner et al., 2017). This results in greater areas of open ocean, allowing larger waves to form resulting in sea ice formation more similar to that observed in the MIZ of the Southern Ocean surrounding Antarctica (Squire, 2020). Limited understanding of the cycles of

sea ice formation, growth and impact on the MIZ of both polar regions limits the ability to model the sea ice system. Climate models are impacted by the environmental feature in particular reducing the accuracy of long term predictions (Kennicutt II et al., 2014, 2016; Kohout et al., 2015; Lee et al., 2012, 2017; Thomson J. et al., 2013). Metocean measurement variables which inform these processes and models include thermal structure of the atmosphere-snow-ice-ocean interface, sea surface and air temperature, barometric pressure, humidity, wind velocity, solar radiation, dissolved oxygen, salinity, vertical ocean profiles, currents, turbulent dissipation from breaking waves, sea ice drift, wave-in-ice properties (significant wave height, period, direction and spectra), sea ice extent, coverage and seasonal composition, snow and sea ice thickness, ice flexure, ice roughness, altimetry, Synthetic Aperture Radar and ship-borne wave radar and lidar measurements, camera images and acoustic measurements (Massom et al., 2001; Nicolaus et al., 2021; Rayner et al., 2003).

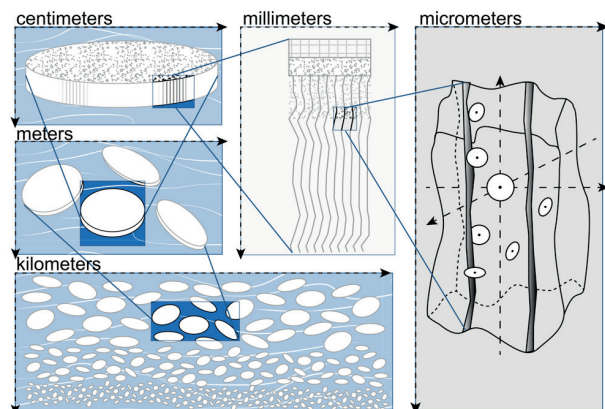


**Fig. 1.** The different scales of sea ice from the mikrometer scale up to the kilometer scale

Due to its topographic configuration, surrounded by a circumpolar channel, the Southern Ocean is subject to strong westerly winds and atmospheric circulation events that are, on average, of greater magnitude and severity than in the Arctic and result in a generally rougher sea state. Consequently, Antarctic sea ice growth is the result of turbulent sea conditions that strongly influence its initial phase, which occurs in the MIZ. Due to the strong atmospheric and oceanic forces in the Southern Ocean, the MIZ can extend for several hundred kilometers south of its edge. Accordingly, the MIZ represents an essential part of the Antarctic sea ice cover, playing a key role in sea ice growth and retreat and having a distinct but highly variable influence on atmosphere-ocean interactions.

Thus, valid, experimental determination of the material properties of sea ice and robust modeling of its individual components significantly contribute to reliable Earth System Models (ESM). Consequently, experimental studies as well as modeling of sea ice are long-standing areas of research. Important findings address the physical, mechanical, and biogeochemical characterization of sea ice, its dynamics, and complex constitutive description. These features already indicate the breadth of the research field, which poses particular challenges not only because of the interactions between the aforementioned disciplines, but also because of a wide range of scales that the research must cover.

In this paper, we aim to compile the main work on physical investigations and numerical modeling approaches for the MIZ sea ice in the Southern Ocean and to survey the current state of research. In particular, we would like to highlight recent achievements in the two research fields and illustrate which gaps between experimental investigation and modeling need to be closed in the coming years of research.

In *Section 2*, we summarize the main testing techniques and results of the physical description of sea ice in the Antarctic region.

In *Section 3*, we give an overview of sea ice observation and in situ measurement in both the Arctic and Antarctic regions from their historical origins to the present day.

In *Section 4*, we highlight the state of the art in numerical modeling of sea ice at all scales. In doing so, we consider the range of approaches and observational variations. Finally, we highlight in *Section 5* the gaps that need to be addressed in both disciplines and between disciplines in the field of sea ice research in the Antarctic MIZ. It is shown in *Section 5* that an interdisciplinary approach is promising to fill the gaps of the Antarctic Ocean “data desert” to continuously improve numerical models. Data on metoceanic conditions and sea ice observations, floe motions, sea ice texture and composition etc. need to be increasingly collected and integrated into computer model development. Such integrated research can improve the accuracy and detail in predicting the Southern Ocean metoceanic conditions and ultimately in global climate and Earth System Models (ESM).

## 2. Formation and mechanical properties

The mechanical properties of sea ice in the Arctic and Antarctic have been under scientific observation for many years. Three general states can be distinguished:

the initial frazil ice, compacted forms thereof, and consolidated ice. The latter can be part of a single ice floe or extended ice cores. Depending on the formation history, all three stages can exhibit widely varying individual properties at different locations and samples moment. The mechanical properties of consolidated sea ice depend on several factors such as its porosity, the strain rate at which the load is applied to the material, the aspect ratio of the material tested and the orientation of the sample when it is cored. Dependent on the material property investigated and test type, the above-mentioned properties have different influences on the test result and cannot be generalized for all mechanical properties. In contrast to the Arctic, there is still a lack of studies of the mechanical properties of Antarctic sea ice (Timco & Weeks, 2010).

### 2.1. Genesis

#### 2.1.1. Freezing

Ice formation in the Arctic is dominated by congelation ice, which forms by downwards freezing under relatively calm sea conditions (Petrich & Eicken, 2017). In contrast, Antarctic sea ice is typically exposed to rough sea conditions influencing its growth. Variations in the growth process are caused by different large scale heat fluxes in the Arctic and Antarctic regions (Maksym et al., 2012). The low ocean heat flux in the Arctic enhances thick multiyear ice to grow, whereas a higher heat flux in the Antarctic limits basal ice growth due to the presence of deep warm water and weak ocean stratification limits the ice thickness (Stammerjohn & Maksym, 2017). The first ice crystals to form in the annual freezing cycle in the Antarctic are frazil ice crystals. For frazil ice crystals to grow, two prerequisites must be fulfilled: the water must be supercooled and under turbulent conditions (Schneck et al., 2019). Supercooling describes the state, when the water temperature is below its freezing point. Turbulence is induced into the ocean by wind and waves. If a sufficient number of frazil ice crystals are present, they start to form flocs of ice by freezing several ice crystals together. If these frazil ice flocs increase in size, they appear on the water surface, increasingly interact, and finally develop into pancake ice. The shape of the pancake ice floes is uneven, and the edges are upturned due to interaction between pancake ice floes (Hicks, 2009; Lange et al., 1989).

The pancake ice floes are rafted by wind and waves, leading to closed ice cover (Lange et al., 1989; Shen H.H. et al., 2001). The whole freezing and melting process in the Marginal Ice Zone is displayed in Figure 2.

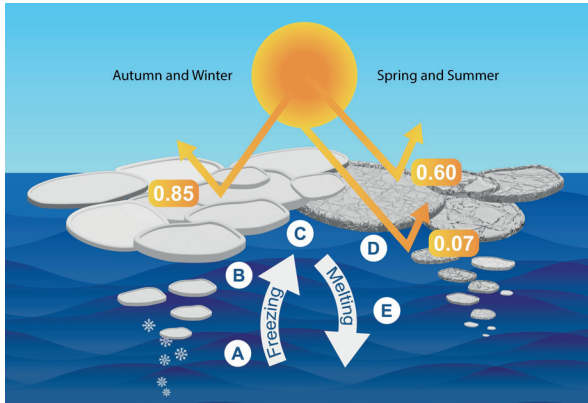


**Fig. 2.** Full-year sea ice cycle. Numbers denote the albedo of the current state: A – frazil ice; B – pancake ice; C – consolidated ice in the freezing period; D – consolidated ice in the melting period; E – sea ice floes (see e.g. Thomas 2017).

### 2.1.2. Mechanical impact

Forging describes the process when a metal object is subjected to heat and force impacts (Bargel et al., 2008). Sea ice is always close to its melting point, the swell leads to frequent bumping of the ice floes among each other. Besides bumping, the pancakes are freely floating in a frazil ice layer. Some deformation related ice growth processes, such as ridging and rafting, try to explain why frazil ice can be present at arbitrary places within the ice core (Lange & Eicken, 1991). However, the interaction with the frazil ice crystals and their influence on the growth has not yet been fully described in the literature. The frequent bumping between the pancake ice floes close to the melting point will influence the crystal structure in the outer pancake, as it is the case for traditional forging mechanisms. A study by Damsgaard et al. (2021) tried to identify the influence of pancake interaction on the sea ice strength numerically. The forces acting on pancake ice have never been measured in the field nor have the influence on the mechanical properties been evaluated.

Inferences about grain growth, crystallization and crystals structure cannot be drawn.

### 2.1.3. Ice accretion

Ice accretion describes the process where large masses of ice accumulate on a vessel's deck or offshore structure, see Figure 3 for an example. Ice accretion is a safety problem for offshore vessels as it affects the vessel's stability and seaworthiness, as well as on-deck operations (Ryerson, 2013). For this reason, sea ice accretion is mostly described in the context of vessel safety but not in the context of sea ice growth. Depending on the different sources, sea ice accretion is either divided into

three (Mintu et al., 2016) or four (Kulyakhtin et al., 2016) steps. About 90% of the ice accretion is caused by seawater spray and only 10% originate from atmospheric sources. The first step for accretion ice to occur is the generation of seawater spray while the air temperature is below the freezing point of seawater. Spray is generated either through interaction between the vessel and waves or through the wind. Thereby most of the spray originates from vessel wave interaction, nevertheless, this phenomenon is still not completely understood. The second step describes the spray flow in the air and the droplet impingement on the vessel's structure. The third step is the heat transfer of the water droplets, freezing and, run-off of surplus water. The rate of accretion ice growth mostly depends on the spray flux and heat transfer (Kulyakhtin & Tsarau, 2014). In summary, ice accretion is nearly not considered for sea ice growth, the physical process of spray generation by ship or sea ice impact is only poorly understood and cannot be described by existing models (Kulyakhtin & Tsarau, 2014; Mintu et al., 2016). As of now, it is unclear in how much accretion ice can form on ice floes. Much accretion ice droplets are found for harsh weather conditions concurrently the waves may wash over the floes and carry away the accretion crystals immediately.

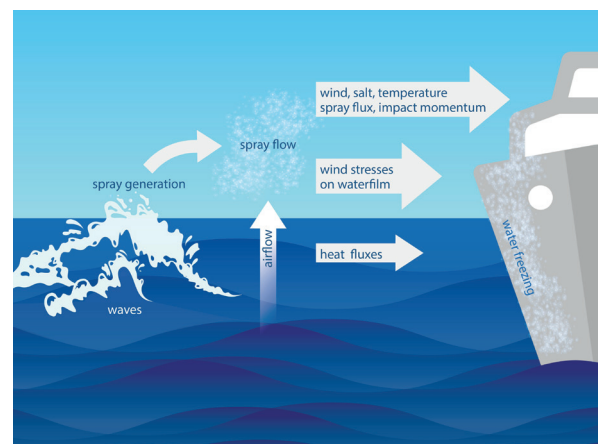


**Fig. 3.** Growth of accretion ice (after Samuelson et al. 2015)

### 2.1.4. Snow

Snow in the Antarctic MIZ is highly variable and plays an important role in air-sea-ice interaction (Massom et al., 2001). Snow nucleates on dust particles in the air at a high degree of supercooling and only below  $-38^{\circ}\text{C}$  homogeneous snow flake nucleation will arise (Belosi et al., 2014). The growth and shape of the snowflakes are governed by kinetics rather than equilibrium thermodynamics. The broad variety in different shapes of snowflakes is due to its sensitivity to variations in temperature and humidity.

As soon as the snow touches the ground, structural changes take place (Blackford, 2007). Snow has a high influence on sea ice: Snow has a high albedo, serves as an insulator between the ice and atmosphere and its changing properties, is driven by snow metamorphism, and influences the sea ice characteristics (*Section 2.1.5*).

Sea ice without snow has an albedo of 0.5 to 0.7, whereas with snow on top the albedo increases up to 0.9, meaning that 90% of the solar radiation gets reflected. On the other side, the open ocean absorbs most of the solar radiation due to an albedo of only 0.06. Large snow cover, therefore, slows down the annual sea ice decay in the Antarctic (Eayrs et al., 2019).

Snow is thermodynamically instable due to its large ice-air interface. The large ice-air interface leads to different metamorphism processes compacting the snow (Colbeck, 1982). One process driving this is sintering. Small particles get bonded without melting and, depending on the snow flake shape, geometry, orientation, and dimensions, each flake undergoes structural changes. These changes result in a structural evolution of the snow pack. The driving force behind sintering is the reduction of the crystals surface energy by reducing the surface area (Hosford, 2006). Due to the lower interface energy, the grain boundary surface area grows in between the ice crystals, reducing the ice-air interface area.

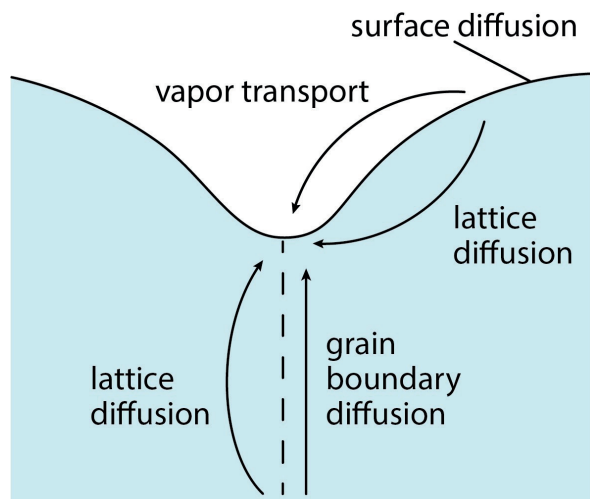


**Fig. 4.** Growth of a neck by transport from the spherical surface (left) and from the grain boundary formed between the particles (right) (after Hosford, 2006)

Sintering mechanisms can be separated into two groups: mechanisms where the material is transported along the surface, or mechanisms where material is transported through the bulk or along grain boundaries. The former typically dominates early compaction, then taken over by grain boundary diffusion. Both mechanisms are displayed in Figure 4. The main driver

under isothermal pressureless conditions for sintering of snow is vapor diffusion. Sintering not only plays a role for the densification of ice, but also for the densification in glaciers, ice sheets and the healing of flaws (Blackford, 2007).

It is known from transport engineering that sodium chloride weakens snow hardness by up to 60%. With increasing sodium content, the hardness can be reduced by up to 20% of the initial hardness. The weakening is probably caused by the attenuation of grain-grain bonds. The extent to which this affects the changes of snow properties and sea ice growth is not yet known (Wählén et al., 2014).

### 2.1.5. Snow metamorphism

Depth and surface hoar, frost flowers, and advection frost are different forms of surface ice occurring in the Antarctic MIZ and influence the sea ice behavior on different levels but have barely been considered in the context of mechanical testing of sea ice. The structural changes of snow known as snow metamorphism take place as soon as the snow has fallen on the ground. Fallen snow will change over time and by the impact of cold temperatures and wind into depth hoar. Depth hoar is a layer of loosely bonded, large snow crystals and accounts for up to 50% of the snow in Antarctica (Hall et al., 1986; Massom et al., 2001). For depth hoar to form, a large temperature gradient between the ice at the bottom and the air must be present. Depth hoar will then form in the warmer portion of the snow by constructive metamorphism (Colbeck, 1982). Large ice crystals will form at the bottom until all initial snow grains are replaced by depth hoar crystals. The newly formed depth hoar crystals are hollow and cup-shaped. This lowers the density per unit volume and also lowers the overall strength of the snow pack compared to the initial snow crystals (Hall et al., 1986).

Another kind of snow metamorphism is the growth of surface hoar also known as advection hoar frost. In contrast to depth hoar, surface hoar only grows in the night (Manninen et al., 2016). Surface hoar influences the surface roughness, the reflectivity of the snow, the surface mass balance and the energy budget, but, nevertheless, the formation of surface hoar is still not completely understood (Champollion et al., 2013). It is known that surface hoar forms during the night by deposition of relatively warm water vapor on to cold snow or ice surfaces. The crystals can be classified into seven groups: plates, cups, scrolls, needles, columns, dendrites, or composite forms (Ozeki et al., 2020). The hoar crystals have only a very weak inter-crystalline bonding and accumulations of surface hoar are mechanically weak. Surface hoar disappears

either with strong winds, when wind changes direction or the temperature increases (Champollion et al., 2013; Lang et al., 1984).

Frost flowers grow on very young and thin sea ice, where the surface temperature is much higher than the atmosphere temperature while it does not form on thicker neighboring ice. They either grow from a supersaturated atmosphere or pure ice sublimating into an unsaturated atmosphere, consisting of pure ice and being covered with highly concentrated brine. As sea ice becomes thicker and the temperature of the ice and atmosphere become similar, the frost flowers sublimate away (Style & Worster, 2009).

## 2.2. Static properties

### 2.2.1. Crystallography and texture

The morphology of the micro-structure of sea ice comprises the sizes, the shapes, and the orientations of (i) its crystals and grains, (ii) its brine inclusions and (iii) its air voids at the centimeter, millimeter and micrometer scales. This morphology strongly affects the thermal, mechanical and optical properties of sea ice (Shokr & Sinha, 2015). It is thus important to well describe the micro-structure so that the dependent properties can be fully understood, compared, and modeled (Lieblappen et al., 2017). A collage of different sea ice textures is presented in Figure 5.

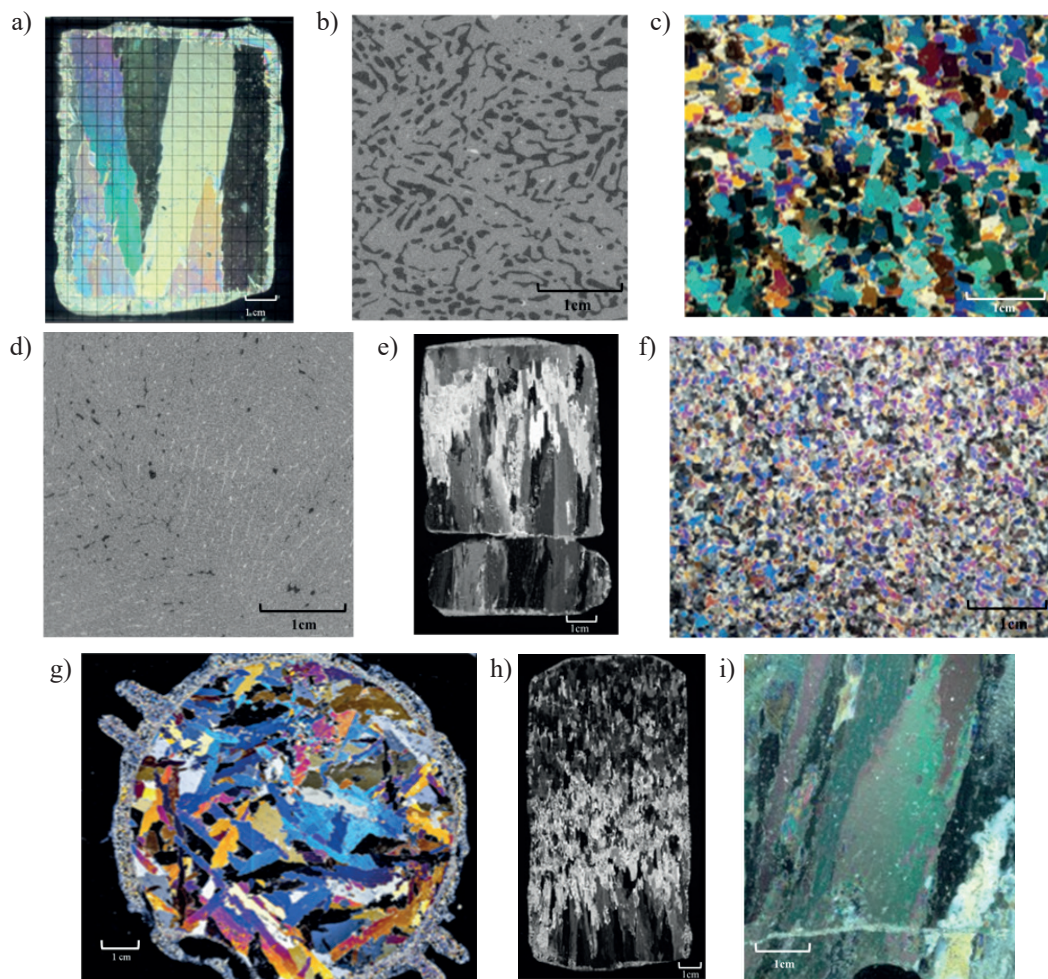


**Fig. 5.** Collage of sea ice textures and structures imaged using cross-polarization and  $\mu$ CT scan imaging: a) vertical thin section of laboratory-grown columnar sea ice texture visualized through cross-polarization (Bailey, 2011); b)  $\mu$ CT scan image of porous sea ice, with air inclusions shown as black, sea ice shown in gray and brine pockets in white (Maus et al., 2021); c) vertical thin section of granular sea ice from Terra Nova Bay polynya visualized through cross-polarization (Tison et al., 2020 – reproduced with permission from Cambridge University Press); d)  $\mu$ CT scan image of sea ice, with air inclusions shown as black, sea ice shown in gray and brine pockets in white (Maus et al., 2021); e) vertical thin section of columnar sea ice from Baffin Bay visualized through cross-polarization (Kawamura et al., 2001 – reproduced with permission from rights holder); f) vertical thin section of granular sea ice from Terra Nova Bay polynya visualized through cross-polarization (Tison et al., 2020 – reproduced with permission from Cambridge University Press); g) horizontal thin section of platelet sea ice from Atka Bay visualized through cross-polarization (Hoppmann et al., 2020); h) vertical thin section of transitional sea ice from Baffin Bay visualized through cross-polarization (Kawamura et al., 2001 – reproduced with permission from rights holder); i) vertical thin section of laboratory-grown columnar sea ice visualized through cross-polarization (Crabeck et al., 2016)

The crystal structure of sea ice consists of hexagonal rings of ( $\text{H}_2\text{O}$ ) water molecules, with hydrogen bonds between them. The hexagonal lattice structure of the ice crystal is made up of ordered parallel arrays of the molecular rings in the basal planes of the hexagonal structure. The crystal axis, at right angles to the basal plane, is the hexagonal  $c$ -axis (Eicken & Lange, 1989). In reality, the crystal lattice structures deviate from the typical structure defined above due to misalignment of molecules due to vacancies or line dislocations and stacking faults.

The term “grain” in sea ice is used to refer to either (i) a single ice crystal, or (ii) lumped groups of crystals with similar alignment. If the two terms are not specified, a single crystal can be referred to as a grain (Shokr & Sinha, 2015). Grains of crystals can be separated by a misalignment boundary (the classical grain boundary), interstitial trapped layers of brine, by brine pockets, or air voids. When the temperature of the ice increases, the ice crystals melt and the trapped brine is released to flow under gravity into vertical drainage channels.

The size, shape and orientation of crystal/grain structures change during the freezing of sea ice as a result of variations in (i) the different weather conditions governing the way frazil crystals freeze together to form compact floes during the formation of young ice (see 2.1.1), (ii) the rate and frequency of changing air temperatures during the growth of the floes, (iii) the degree of surface snow/hoar freeze coverage during freezing (see 2.1.5), and (iv) the impact of deformation (Lange & Eicken, 1991) like ridging and rafting (see 2.1.2).

The history of these changes, as well as their effect on the mechanical properties of sea ice, can be studied and quantified by birefringence techniques, based on the analysis of the crystal orientations in thin ice sections. After birefringence analysis, the differently orientated crystals in the thin section of ice all appear as separately colored entities depending on their orientation and refractive index, as shown in Figure 6.

If the crystal face is normal to the linear polarized incoming light, it passes straight through the crystal without being refracted and is therefore prevented from passing through the analyzer, with the result that the

crystal is extinct (black or very dark) on an image of the cross polarized crystal. This process allows one to measure the orientation of crystal faces by means of either:

- a classic separate Rigsby stage which is capable of being rotated around two normal horizontal axis ( $x$  and  $y$ ), and one central vertical ( $z$ ) axis;
- integrated computer-controlled systems for ice-fabric analysis with a Rigsby stage.

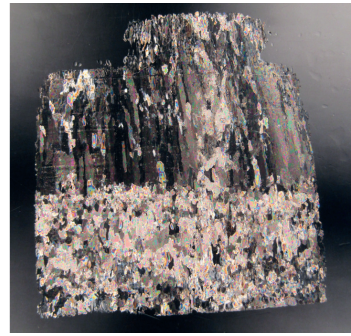


**Fig. 6.** Example of a sea ice sample analyzed with the birefringence technique. The bottom part shows a granular ice structure, the top part a columnar ice structure (Johnson et al., 2022)

It also allows us to obtain the sea ice texture.

Texture is a key parameter required for an in depth understanding of a number of physical and mechanical sea ice characteristics. It serves to record the various environmental conditions under which the ice froze, and it defines the stratigraphy of an ice core, which is important for the analysis, interpretation, and comparison of physical and mechanical test results.

Granular crystals are typically associated with random  $c$ -axis orientations while columnar crystals typically have a  $c$ -axis that is uniformly aligned. Intermediate, mixed granular and columnar crystals have mixed random and horizontally aligned  $c$ -axis. Eicken & Lange (1989) identified five classes of texture:

- polygonal and orbicular granular (see Fig. 7a);
- transitional or intermediate granular/columnar (see Fig. 7b);
- mixed granular/columnar, (iv) columnar (see Fig. 7c), and (v) platelet textures.

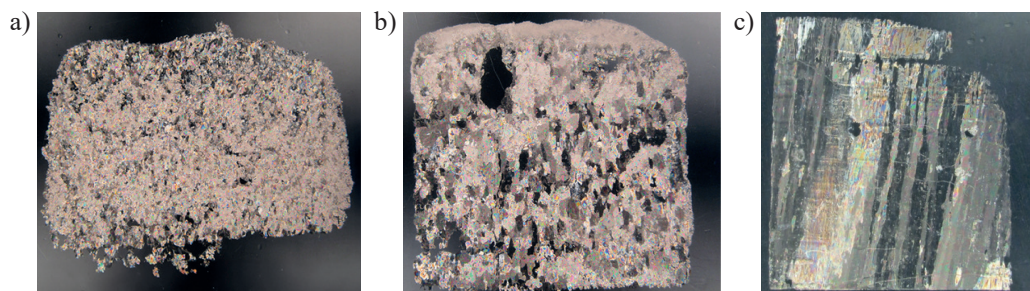


**Fig. 7.** Granular ice (a), transitional ice (b), and columnar ice (c) (Johnson et al., 2022)

The morphology of the ice crystals and grains, with their interstitial trapped layers and pockets of brine and air voids, can be studied using nondestructive X-ray micro-computed tomography ( $\mu$ CT) techniques, to derive three-dimensional images of a sample of ice with its internal structure (Frantz et al., 2019).

Nevertheless, pure optical analysis of sea ice cores cannot give accurate information about the origin of orbicular granular ice. It can either originate from the flooding of snow or frazil ice. Stable oxygen isotope data (as shown in Fig. 8) is necessary to distinguish between snow ice and frazil ice (Lytle & Ackley, 2001).

### 2.2.2. Salinity and temperature

As sea ice forms, brine is expelled from the growing ice matrix. A high concentration of brine is typically found at the surface and the ocean-exposed bottom of the sea ice (Petrich & Eicken, 2010). The brine is entrapped in pockets or channels because it cannot escape as fast as the heat at the ice ocean interface due to the thermal diffusivity being much higher than the diffusivity of salt (McGuinness, 2007). Based on the freezing temperatures and salinity, the salts either dissolve into and increase the salinity of the brine inclusions or start to dehydrate into solid minerals. The increase in salinity causes a depres-

sion of the freezing temperature of seawater (Vancoppenolle et al., 2018), the cryoscopic effect (Berti A. et al., 2016). A temperature below  $-8.2^{\circ}\text{C}$  triggers the precipitation of salt ions (Petrich & Eicken, 2010).

Ice warming leads to the expansion of the brine pockets, which enables an interconnection between the pockets and formation of a brine network. There are four identified salinity curves that are associated with different sea ice types and ages (Eicken, 2003). Shown in Figure 8, the most common is the C-curve, where a high salinity is found at the top and bottom of the sample. This profile is typical of young sea ice and is indicative of significant brine movement and drainage within the sea ice. The S-type curve is common within first-year sea ice and has a lower surface salinity than that of young sea ice with a C-curve salinity profile (Eicken, 1992).

A “?”-shaped (question mark-shaped) salinity profile has been identified in sea ice that has begun its melting, and has a profile that mirrors that of the S-shaped profile. The low surface salinity is indicative of the melting that has begun from increased atmospheric temperatures. Lastly, an I-shaped profile shows a steadily decreasing salinity gradient from the surface to the bottom of the sea ice. This profile is associated with multi-year sea ice.

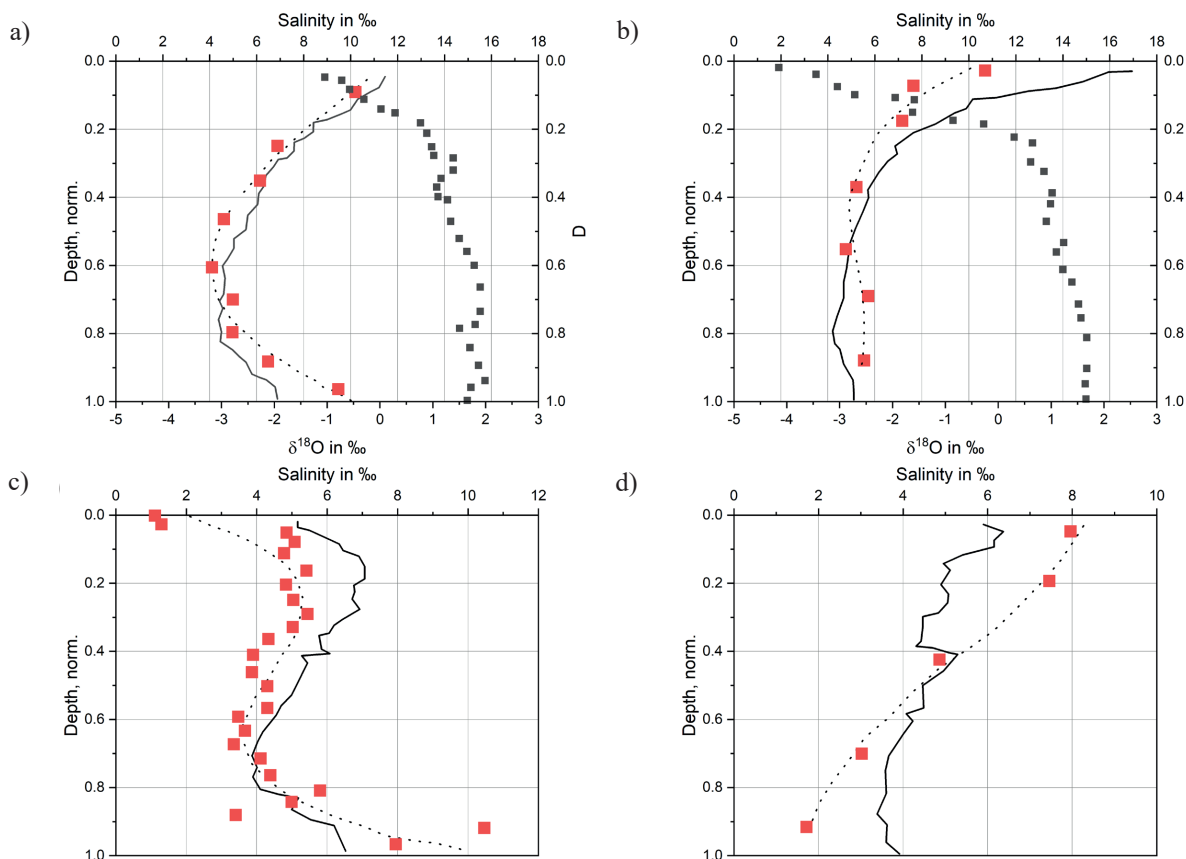


**Fig. 8.** Normalized salinity profiles of sea ice (Eicken, 1992) a) a common C-type profile that is typical of young sea ice; b) the S-type salinity profile; c) the converse, which is the “?”-type salinity curve; d) displays of the I-type salinity profile. Also shown in a) and b), are the oxygen isotope profile for the sea ice studied by Eicken (1992)



Induced by a higher density than that of seawater, the brine runs out in the course of time and is replaced with less salty seawater. The replacement by seawater provides new nutrients for the biological community.

Temperature gradients in growing sea ice are commonly found to be linear with low temperature at the surface exposed to the cold air. The gradient is linear towards the warmer ocean-exposed bottom of the sea ice, where the temperature is close to that of the freezing point of sea water (Eicken, 2003). It has to be noted that temperature and porosity are an inseparable pair for sea ice. A higher temperature gives rise to porosity due to the change in size and shape of the brine pockets and a lower temperature decreases porosity (Richter-Menge et al., 1993).

### 2.2.3. Porosity

Brine is not the only major component in sea ice, but air pockets and pores contribute a significant portion to the volume of sea ice. The air trapped inside the ice can come about during the freezing process under turbulent conditions as well as during the process of brine drainage. Visualization of the porosity of sea ice has been accomplished using the X-ray micro-computed tomography ( $\mu$ CT) techniques (Golden et al., 2006).

The permeability and porosity of sea ice are closely related, and relationships have been empirically estimated.

$$\Phi_{young\ ice} = 10^{-19} \frac{\Phi_3^{3.9}}{1000} \quad (1)$$

$$\Phi_{first\ year} = 10^{-14} \frac{\Phi_3^{1.6}}{1000} \quad (2)$$

where:  $\Phi_3$  – the image-derived porosity;  $\Phi$  – the calculated permeability (Freitag & Eicken, 2003).

### 2.2.4. Young's modulus

Sea ice naturally exists at high homologous temperatures, generally in the region of 0.9 or higher, meaning that, compared to other solids, the temperature of ice is always close to its melting point. This yields a large range of material characteristics comprising of elastic, inelastic, brittle and viscous properties as well as time-delayed behavior under constant load (Schulson et al., 2006; Timco & Weeks, 2010). This variability is linked to the temperature dependent material composition of sea ice. Its strain rate response is due to spatial gradients in the external forcing and internal damping and dissipative effects (Hutchings et al., 2012). The elastic behavior of sea ice is moderately anisotropic whereas the inelastic behavior is markedly anisotropic (Schulson, 1999). Sea ice convergence, divergence and fracture are driven by wave dynamics, ocean currents and atmospheric winds. These drivers play an important role in ice formation and retreat during a seasonal cycle (Horvat & Tziperman, 2015; Squire, 2018; Weiss

& Dansereau, 2017) and synoptic events like storms may further modify this picture in an unpredictable way (Vichi et al., 2019). The elastic properties and strength of sea ice depend on factors including temperature, salinity, porosity and ice structure (Karulina et al., 2019), which all change with the annual change in season. The elastic modulus respectively Young's modulus of sea ice ( $E$  [GPa]) can be measured by investigating the propagation of an elastic wave in an ice sheet or through measuring the ultrasonic velocity in ice samples (Timco & Weeks, 2010). The Young's modulus value of sea ice is said to decrease linearly with an increase in brine volume ( $V_b$  [g/kg]) the following relationship (Timco & Weeks, 2010):

$$E = 10 - 0.0351V_b \text{ [GPa]} \quad (3)$$

Ice is said to behave as an elastic material following Hooke's law at temperatures between  $-3^\circ\text{C}$  and  $-40^\circ\text{C}$  provided that the applied stress does not exceed 10 bar with a stress rate of 5 bar/s and with a duration less than 10 s (Gold, 1958). The Young's modulus of sea ice decreases with an increase in the strain rate (Snyder et al., 2015).

The elastic properties of sea ice vary with vertical position in the floe. At the top, sea ice can be usually considered isotropic due to its polycrystalline composition with randomly oriented  $c$ -axes of  $I_h$  ice crystals and the a priori isotropic distribution of pores and micro-cracks. The rate of growth of the basal plane is much greater than the growth rate in the direction of the  $c$ -axis, even though the thermal conductivity in the direction of the  $c$ -axis is on the order of 5% higher than that of the basal plane. As the basal plane, which is orthogonal to the  $c$ -axis, becomes aligned with the vertical direction of maximum heat flux, a columnar structure develops in the ice and the material becomes increasingly anisotropic with depth (Kennedy et al., 2013). Since the mechanical behavior of sea ice is rate-dependent, Young's modulus is typically determined by measuring the speed of ultrasonic waves, a pressure  $p$  and shear  $s$  waves, traveling through the ice (Timco & Weeks, 2010). The combined P- and S-wave signals are initiated by a pair of transducers put on opposite surfaces of a specimen. The Young's and shear moduli, as well as the Poisson's ratio of an ice specimen, can then be calculated on the basis of its length (the distance between the transducers) and density as well as the speed of transmission of the P- and S-waves in accordance with the following formula:

$$E_i = \rho c_s^2 \frac{3c_p^2 - 4c_s^2}{c_p^2 - c_s^2} \quad (4)$$

$$G_i = \rho c_s^2 \quad (5)$$

where  $E_i$  and  $G_i$  denote the Young's and shear moduli, respectively, associated with the material direction  $x_i$ ,

$\rho$  is the bulk density of ice,  $c_p$  the transmission speed of the P-wave and  $c_s$  the transmission speed of the Swave, both measured along direction  $x_i$ .

### 2.2.5. Influence of pores on Young's modulus

Sea ice consists of the solid ice matrix as well as gas and brine pockets as explained in *Section 2.1. Pores* with and without brine filling influence Young's modulus of sea ice. One attempt to calculate the influence of pores mathematically on Young's modulus is to homogenize the ice by smearing out the heterogeneity on the fine micro-scale and treating the material as homogeneous with new material parameters (Gross & Seelig, 2011). Using these calculations after Gross & Seelig (2011) and assuming that the porosity is 15% and consists of spherical pores which are filled with brine would reduce Young's modulus from 10 GPa for pure fresh-water ice to 8.5 GPa. The same amount of pores filled with air would decrease Young's modulus to 7.9 GPa. Whereas the shear modulus is independent of the pore filling. Another theoretical calculation using a random pore model showed that 15% porosity reduces Young's modulus to around 7 GPa, being in agreement with experimental results (Zong, 2022). Both calculations show that porosity, either filled with brine or not, does have a crucial impact on sea ice behavior. Therefore porosity of the ice must always be considered for mechanical testing. This leads to the conclusion that it is important to test sea ice *in-situ* or very quickly after the sampling to prevent any changes in the composition of sea ice e.g. brine drainage or size changes of the pores.

## 2.3. Dynamic Properties

### 2.3.1. Viscosity

Viscosity describes the ability of a material to deform under a given stress. It can be measured as dynamic viscosity [Pa·s] or kinematic viscosity [m<sup>2</sup>/s]. Viscosity of the ice is essential for the later consolidated state. Viscosity has been calculated for different stages of ice formation: pure frazil ice (A at Fig. 2), frazil and pancake mixture (B at Fig. 2) and floes of ice (E at Fig. 2) (Newyear, 1999; Rogers et al., 2016; Wadhams et al., 2006; Wang R. & Shen, 2010a; Zhao & Shen, 2015). Even though frazil ice is mostly present in the Antarctic, it has also been observed in the Northern Hemisphere (Smedsrud & Skogseth, 2006). Measurements of the viscosity have been conducted in laboratory wave tanks as well as in the field. Measurements in laboratory tanks used the amplitude attenuation to calculate the viscosity. These calculations require an assumption for the material behavior

e.g. the viscoelastic sea ice model (Wang R. & Shen, 2010b) or the viscous two layer model (Keller, 1998) etc. The assumptions of the sea ice model then affect the calculated viscosity. Some examples for the viscosity values: Newyear obtained a viscosity between 15 Pa·s  $\pm$  0.3 Pa·s to 30 Pa·s  $\pm$  0.6 Pa·s (Newyear, 1999), Wang R. & Shen (2010a) calculated a viscosity between 20 Pa·s  $\pm$  0.4 to 60 Pa·s  $\pm$  1.2 Pa·s and Zhao & Shen (2015) calculated the viscosity to be 14 Pa·s  $\pm$  0.3 Pa·s. Another attempt to calculate viscosity is through the use of SAR images 50 Pa·s  $\pm$  1 Pa·s (Wadhams et al., 2006) and a combination of buoy and SAR measurements (Rogers et al., 2016). The viscosity of frazil ice was obtained on a smaller scale by Paul et al. (2021) in the Marginal Ice Zone of the Antarctic with a vane rheometer. A vane rheometer is a suitable *in-situ* testing device for different kinds of liquids. The rheometer works by measuring the resisting torque of a fluid to an applied deformation, afterwards, the viscosity can be calculated. They obtained a shear thinning flow behavior with a maximum of 400 Pa·s, which decreases to about 30 Pa·s.

Most of the available viscosity data were obtained by indirect measurement techniques and therefore depend on assumptions about the sea ice behavior. Also only a minority of the tests were conducted in the MIZ of the Antarctic, which may, due to different growth conditions, influence the results. In summary, the viscosity of sea ice is an essential parameter for numerical calculations, but there is still a lack of knowledge on data from the MIZ with direct measurement techniques.

### 2.3.2. Solid flow

For numerical calculations, ice is often treated as a viscous fluid (Schulson & Duval, 2010). Flow of solid ice is caused by many different mechanism, but the most important one for ice single crystals is gliding along the basal plane. Gliding along the basal plane is called basal slip, on the classical hexagonal glide plane. Strong gliding along the basal plane (Fig. 9) and weak gliding along the other glide planes results in a strong plastic anisotropy of ice single crystals. The identified easy glide directions are  $\langle 1010 \rangle$  and  $\langle 1120 \rangle$  in hexagonal representation (Glen & Perutz, 1954). The brackets denote the class of equivalent crystal planes. However, sea ice consist of many grains, therefore its mechanical behavior depends on single crystal properties and the interaction between the grains (Cuffey & Paterson, 2010). If polycrystalline ice is loaded, not all grains can deform by basal slip due to the different grain orientations. Non-basal deformation requires a much higher stress compared to basal slip, leading to a non-uniform state of stress with high stress concentrations (Duval et al., 1983).

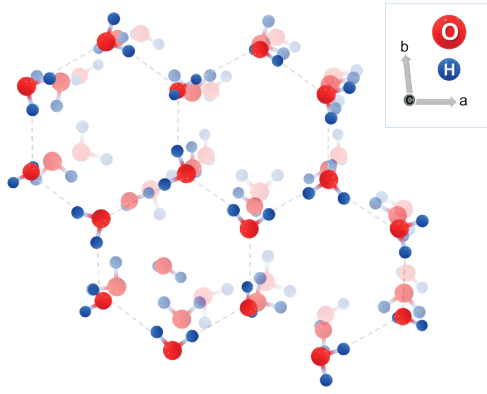


**Fig. 9.** Crystal structure of ice. The water molecules have been arranged so that each oxygen atom is surrounded by four hydrogen atoms in tetrahedral geometry. Two of these atoms are covalently bound to oxygen, while the other two are hydrogen, bonding with the oxygen

Flow or creep of granular sea ice can be separated into primary, secondary and tertiary creep (Azizi, 1989). Primary creep consists of recoverable strain and viscous strain. Secondary creep is the state between primary creep and a steady state (tertiary) creep. At a strain above 0.1 a quasi-steady state is reached, called tertiary creep (Schulson & Duval, 2010). If ice is unloaded reverse creep and strain are observed. The local stresses on reverse straining can amount up to 10 times of the initial global loading stress due to a heterogeneous micro-structure, leading to directional or kinematic hardening (Duval et al., 1983; Schulson & Duval, 2010). Nevertheless, in contrast to the numerical calculations of glaciers, the flow behavior of sea ice is often neglected, due to its smaller influence on the sea ice motion. Especially for large scale sea ice calculations, ice is often treated as an elastic brittle material and creep is ignored (Cuffey & Paterson, 2010; Weiss & Dansereau, 2017). In this case inelastic deformation is caused by fracture and frictional sliding (Weiss et al., 2007). On the local scale, and in particular during the impact forging of the individual floes, plastic strain may effectively alter the densification of ice.

## 2.4. Strength

Before we enter into details, and even though this should be common knowledge, we want to define strength and toughness. Strength is the stress value at which a piece of material deforms irreversibly. In metals this is the same as the yield stress and in brittle materials the initiation of failure by internal cracking. Strength depends on microstructure. Toughness, on the other hand, is the resistance of a material to crack advance for an already existing flaw. It is an intrinsic material property and does not depend on microstructure.

### 2.4.1. Compressive strength

The Uniaxial Compression Strength test is a destructive method of testing the compressive strength of a sample through the application of a uniaxial load at a constant rate. The resultant compressive strength is the maximum load that the sample can withstand before failure. Similarly, the triaxial compressive strength test is a destructive test whereby the sample is subjected to an applied load from all three directions until the sample fails. Triaxial tests apply axial loads with various pressure-axial ratios. The pressure-axial ratio is the ratio between the applied load bearing down on the sample ( $\sigma_1$ ) and the two loads applied to the sample sides ( $\sigma_2, \sigma_3$ ). A pressure-axial ratio of 0, indicates that no axial loads were applied, thus the test is essentially a Uniaxial Compression Strength test.

The strength of a material depends on several factors, such as its porosity, the strain rate at which the load is applied to the material, the aspect ratio of the material tested and the orientation of the sample when it is cored. Sea ice samples are recommended to be cylindrical with a diameter between 7 cm and 10 cm and an aspect ratio of approximately 2.5 (Schwarz J. et al., 1981), but prismatic structures are also suitable (Fig. 10).

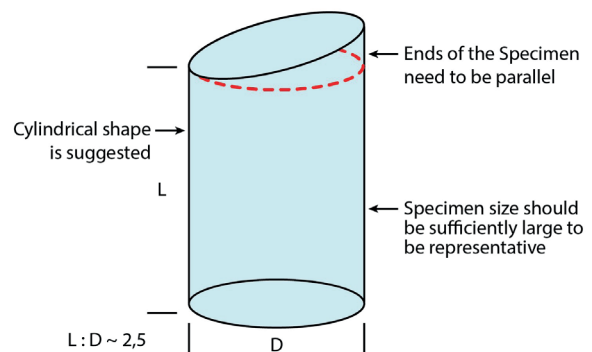


**Fig. 10.** Factors that must be given special attention for brittle compressive strength specimens (Schulson & Duval, 2009)

There are several studies on the compressive strength of sea ice from the Arctic. Each study investigated various variables, such as strain rate, loading direction and testing temperature which all had effects on the resulting compressive strength of the samples. The inferred typical range, from Table 1, of the Uniaxial Compression Strength of sea ice is approximately between 2 MPa and 8 MPa, depending on the testing conditions and the sample properties and the triaxial strength exhibits slightly wider range between 2 MPa and 25 MPa.

Temperature is a crucial part of the testing procedure. Almost all of the studies mentioned in Table 1 investigate the change in compressive strength with a variation of the ambient testing temperature.

**Table 1.** Uniaxial and triaxial compressive strength measured in the Arctic and Antarctic at different loading directions ( $0^\circ$  = vertical;  $90^\circ$  = horizontal), different temperatures and different strain rates

| Source                      | Sample location | Season      | Ice type                        | Testing apparatus                             | Loading direction | Sample dimensions [cm]            | Strain rates [1/s]                      | Test temperature [ $^\circ\text{C}$ ] | Uniaxial compressive strength [MPa] | Triaxial-compressive strength [MPa] |
|-----------------------------|-----------------|-------------|---------------------------------|---|-------------------|-----------------------------------|---|---------------------------------------|-------------------------------------|-------------------------------------|
| Cox & Richter-Menge (1984)  | Arctic          | summer      | multi-year ice                  | Mark II Triaxial Cell                         | 0                 | D = 10.8<br>L = 35.6              | $10^{-3}$ ;<br>$10^{-5}$                | -20; -5                               | -                                   | 2.48–23.5                           |
| Frederking & Timco (1983)   | Arctic          | winter      | not disclosed                   | Soiltest CT-405                               | 0                 | D = 7.56<br>L = 10;<br>15; 20; 23 | $2 \cdot 10^{-4}$                       | -11                                   | 1.07–5.22                           | -                                   |
| Han et al. (2015)           | Arctic          | summer      | multi-year ice                  | PPM226-LS2-1 and LM10                         | 0                 | D = 9<br>L = 20                   | $10^{-3}$                               | -3; -6;<br>-9                         | 0.3–6                               | -                                   |
| Liferov & Høyland (2004)    | Arctic          | late winter | first-year ice                  | not disclosed                                 | 0; 90             | D = 7.0<br>L = 17.5               | $10^{-3}$                               | -15 to<br>-20                         | 2.4–6.0                             | -                                   |
| Li et al. (2011)            | Arctic          | winter      | multi-year ice                  | CSS-44100                                     | 0                 | D = 17.5<br>L = 7                 | $10^{-6}$ to<br>$10^{-1}$               | -4; -7; -10;<br>-13; -16              | 1.69–3.58                           | -                                   |
| Murrell et al. (1991)       | Arctic          | summer      | multi-year ice                  | Triaxial Testing Machine                      | 0; 90             | D = 3.8<br>L = 10.0               | $10^{-7}$ to<br>$10^{-2}$               | -10; -15;<br>-20                      | 0.6–18.4                            | 1.23–36.3                           |
| Poplin & Wang (1994)        | Arctic          | spring      | multi-year ice                  | MTS fitted with extensometers                 | 0; 90             | D = 7.6<br>L = 17.6               | $10^{-3}$ ;<br>$10^{-4}$ ;<br>$10^{-5}$ | -10                                   | 0.64–8.32                           | -                                   |
| Richter-Menge (1992)        | Arctic          | summer      | first-year ice                  | closed loop electro-hydraulic testing machine | 0; 90             | D = 10.8<br>L = 25.4              | $10^{-2}$ ;<br>$10^{-3}$ ;<br>$10^{-5}$ | -10                                   | 0.59–7.3                            | 1.01–26.8                           |
| Richter-Menge et al. (1986) | Arctic          | summer      | first-year ice                  | closed loop electro-hydraulic testing machine | 0; 90             | D = 10.16<br>L = 25               | $10^{-2}$ ;<br>$10^{-3}$ ;<br>$10^{-5}$ | -10                                   | 1.59–7.30                           | 1.37–26.79                          |
| Sammonds et al. (1998)      | Arctic          | summer      | first-year ice; multi-year ice; | Triaxial Testing Machine                      | 0; 90             | D = 3.8<br>L = 10                 | $10^{-7}$ to<br>$10^{-2}$               | -40 to<br>-3.5                        | 0.6–23.9                            | 4.1–25                              |
| Sinha (1984)                | Arctic          | winter      | first-year ice; multi-year ice  | Soiltest CT-405                               | 0                 | B = 10<br>W = 5<br>L = 25         | $10^{-6}$ to<br>$3.8 \cdot 10^{-3}$     | -10                                   | 0.8–4.9                             | -                                   |
| Sinha (1986)                | Arctic          | winter      | first-year ice                  | Soiltest CT-405                               | 0                 | B = 10<br>W = 5<br>L = 25         | $6 \cdot 10^{-4}$<br>to $10^{-3}$       | -10                                   | 4.7–9.0                             | -                                   |
| Timco & Frederking (1986)   | Arctic          | summer      | multi-year ice                  | Soiltest CT-405                               | 0; 90             | B = 8<br>W = 5<br>L = 19          | $6 \cdot 10^{-4}$<br>to $10^{-3}$       | -10                                   | 4.7–9.0                             | -                                   |
| Urabe & Inoue (1988)        | Antarctic       | winter      | land-fast ice                   | screw drive type universal machine            | 0; 90             | B = 10<br>W = 10<br>L = 25        | $10^{-6}$ to<br>$10^{-2}$               | -5 to -30                             | 0.5–8.3                             | -                                   |
| Wang R. & Poplin (1988)     | Arctic          | winter      | not disclosed                   | MTS with extensometers                        | 0                 | D = 6.92<br>L = 14.6              | $10^{-6}$ to<br>$10^{-4}$               | -3 to -18                             | 0.16–1.97                           | -                                   |
| Wang Q. et al. (2018)       | Arctic          | summer      | not disclosed                   | hydraulic pump compression machine            | 0                 | D = 7<br>L = 17.5                 | $10^{-7}$ to<br>$10^{-2}$               | -3; -6; -9                            | 1.00–8.5                            | -                                   |
| Hill et al. (1994)          | Antarctic       | summer      | first-year ice; multi-year ice  | electro-hydraulic testing system              | 0                 | D = 10.5<br>L = 20–25             | $10^{-3}$                               | -3.0 t<br>-1.5                        | 1.2–4.5                             | -                                   |

On average, it is found that a decrease in the ambient testing temperature results in an increased yield strength. It can be speculated that with a decrease in temperature, brine inclusions become smaller and the proportion of pure ice within the sample increases which yields higher strengths. Additionally, the effect of changes in mechanical properties when bringing samples from *in-situ* to laboratory temperatures has still to be fully realized but it can be assumed that possible changes in mechanical properties may occur during this change in temperature.

The strain rate imposed on the sample during the testing procedure is an important variable to consider and has been found to have a significant effect on the observed compressive strength. Typical testing strain rates for sea ice range between  $10^{-6} \text{ s}^{-1}$  and  $10^{-2} \text{ s}^{-1}$ . At higher strain rates brittle failure may occur (Timco & Weeks, 2010). Compressive and yield strength was found to be at its maximum in the ductile-to-brittle transition zone when strain rates between  $10^{-3} \text{ s}^{-1}$  and  $10^{-4} \text{ s}^{-1}$  are applied (Han et al., 2015; Li et al., 2011; Poplin & Wang, 1994; Sinha, 1984; Timco & Frederking, 1986; Urabe & Inoue, 1988). The relationship between compressive strength and the strain rate is subject to change and depends on several sea ice properties, such as ice texture (Wang Q. et al., 2018).

As a result of the crystal structure of columnar ice, horizontal loading thus yields comparatively lower compressive strength results. This is because fractures parallel to the basal plane are easier to achieve than those along the plane normal to the basal plane. Typical compressive strength results for horizontal loading are approximately between 0.6 MPa and 5 MPa (Moslet et al., 2005; Poplin & Wang, 1994; Richter-Menge, 1992; Timco & Frederking, 1986) whilst vertical loading yields the upper range of compressive strength results.

Granular and columnar sea ice textures within a sample also influence the resulting mechanical properties. Timco & Frederking (1990) and Wang R. & Poplin (1988) researched the difference between columnar and granular textures and concluded that the samples with columnar ice textures had greater compressive strengths (Timco & Frederking, 1990; Wang R. & Poplin, 1988). Additionally, Timco & Frederking (1990) found empirical relationships to determine the compressive strength  $\sigma_c$  of horizontally loaded columnar ice (Equation (6)), vertically loaded columnar ice (Equation (7)) and granular ice (Equation (8)) where  $\dot{\epsilon}$  is the strain rate and  $v_t$  in parts per thousand is the porosity of the sample.

The models presented above by Timco & Frederking (1990) relate compressive strength in megapascals to the testing strain rate and the porosity of the sample. As suggested by the models, the porosity and by extension the brine and air volumes within the ice, may differ between ice type, age and texture, which will thus

yield different ranges of compressive strengths. Likewise, Moslet (2007) studied the directional dependency of strength in ice.

$$\sigma_c = 37 \cdot \dot{\epsilon}^{0.22} \left[ 1 - \sqrt{\frac{v_t}{270}} \right] \quad (6)$$

$$\sigma_c = 160 \cdot \dot{\epsilon}^{0.22} \left[ 1 - \sqrt{\frac{v_t}{200}} \right] \quad (7)$$

$$\sigma_c = 49 \cdot \dot{\epsilon}^{0.22} \left[ 1 - \sqrt{\frac{v_t}{280}} \right] \quad (8)$$

Extensive studies have taken place to characterize the mechanical properties, namely the compressive strength of sea ice in the Arctic region. However, with more insights into how the properties change with differing sea ice types, it is thus reasonable to assume that Antarctic sea ice differs in compressive strength from its northern counterpart owing to the different growth conditions and thus the different proportions of sea ice type found in each area. Additionally, sea ice properties are intrinsically linked to each other, thus requiring further investigation into the respective mechanical properties for different ice types and ice textures which will further characterize and yield a better understanding of compressive strength in sea ice in a warming world.

#### 2.4.2. Tensile strength

Tensile strength tests, in contrast to compressive strength or fracture toughness tests, have not been performed *in-situ* due to the difficult preparation of the test sample. Nevertheless, tensile strength is an essential engineering property as it limits the flexural strength ice can withstand and is especially important for the behavior of very young and thin sea ice (Voermans et al., 2020). Different kinds of direct and indirect testing methods are known from literature:

- direct tests:
  - end-capping method:
    - O-rings with synthane caps (Cole et al., 1985),
    - fresh-water bond for end caps (Richter-Menge et al., 1993);
  - variation of cross section:
    - increase of the end diameters (Hawkes & Mellor, 1972) by Peyton,
    - decrease of the middle diameter (Bonath et al., 2019; Cox & Richter-Menge, 1985; Dykins, 1967);
- indirect tests:
  - Brazil test (Chen & Ji, 2019; Mellor & Hawkes, 1971);
  - ring-tensile test (Butkovich, 1959; Mellor & Hawkes, 1971; Weeks, 1961).

The testing geometries are shown in Figure 11. The benefit of the direct tensile strength measurement is that pure tensile strength values are obtained which do not need further calculations. A disadvantages are the difficult and time consuming sample preparations. On the other hand, indirect measurements have an easier sample preparation procedure but need calculations afterwards to generate a tensile strength value. Another problem is the poor comparability of direct and indirect measurements. The Brazil test conducted by Chen (Chen & Ji, 2019) seems to overestimate the tensile strength, which is also shown in Figure 12. Earlier studies suggested an underestimation by the ring test and Brazil test in comparison to the uniaxial tensile test (Schulson, 2001). Nevertheless, trends can be captured with indirect tests. The test results are influenced by temperature, porosity, and crystal orientation, while the loading rate only has a minor influence.

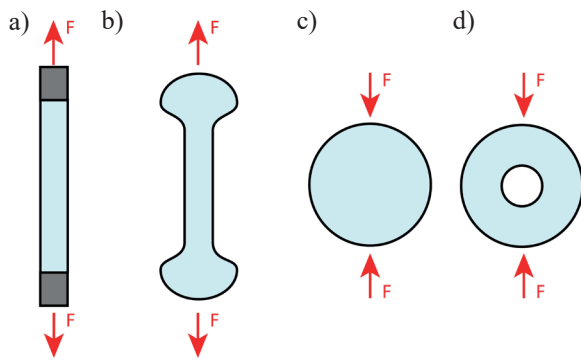


**Fig. 11.** Direct and indirect test methods to determine the tensile strength: a) direct measurement with end caps; b) direct measurement with cross section variation; c) indirect measurement with Brazil test; d) indirect measurement with the ring test

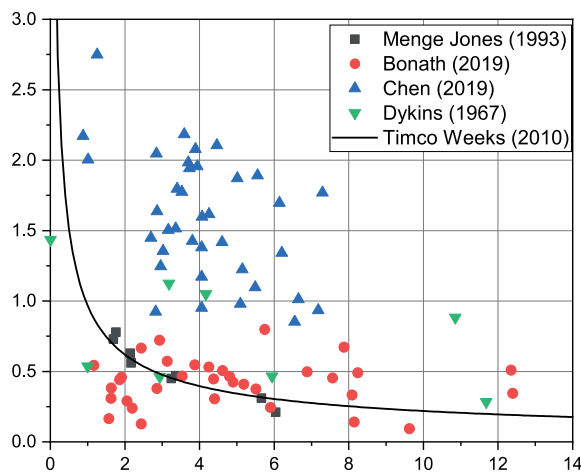


**Fig. 12.** Tensile strength for direct across column tensile tests of first year ice (Bonath et al., 2019; Richter-Menge et al., 1993), artificial first year ice (Dykins, 1967), and granular first year ice tested with an indirect test (Chen & Ji, 2019)

The crystal orientation has a large influence on the tensile strength, with samples loaded along the columns having up to three times higher tensile strength than if they were loaded across the columns (Kuehn et al., 1990). The difference in the two loading directions is not influenced by a varying stiffness in the two directions, but when loaded across the columns, the brine pockets in combination with the columns concentrate the stress, and thus, the material is weaker (Schulson & Duval, 2010).

To date, no tests on the tensile strength have been conducted on first year ice from the Antarctic. Results from the Arctic and laboratory ice is presented in Figure 12. The tensile strength is affected by crystal orientation, temperature, and porosity, which are different in the MIZ compared to multi-year ice in the Arctic, thus tests of the tensile strength should also be conducted in the MIZ.

### 2.4.3. Flexural Strength

Besides Young's modulus, the flexural strength (modulus of rupture) is an essential parameter to describe sea ice breakup (Voermans et al., 2020). In contrast to Young's modulus, the flexural strength is regarded as an index test (Timco & Weeks, 2010). This is due to the complex stress conditions within the material during the test, and therefore assumptions about the material behavior must be made to interpret the results (Timco & O'Brien, 1994). Besides the importance of flexural strength for ice loads on ships as well as other engineering constructions, it is essential to describe ice ridging and rafting (Aly et al., 2019). The flexural strength test is well suited for *in-situ* testing, thus it needs only little sample preparation. The importance of the test and its simplicity are the main reasons why this test has been conducted by many investigators (see a list in Timco & O'Brien (Timco & O'Brien, 1994)). Nevertheless, most of the measurements were conducted in the Arctic and only measurements by two investigators were performed in the Antarctic (Dykins, 1971; Williams et al., 1992). The most commonly used tests are the cantilever beam test, the three point bending test, and the four point bending test. The cantilever beam test is presented in Figure 14b and the three point bending test, which was used for measurements in the Antarctic (Dykins, 1971; Williams et al., 1992), is displayed in Figure 14c. Even though the three-point bending test is preferred in the Antarctic, most *in-situ* tests were conducted with the cantilever beam test. The cantilever beam test is well suited for *in-situ* testing as the ice sample stays in the seawater. This means that brine drainage is kept as low as possible, and so the sample can be tested over the whole thickness and the temperature gradient is maintained. On the other hand, the three and four-point

bending tests are mostly used on smaller samples under laboratory conditions. Four-point bending produces a stress state of pure bending, leading to the failure to occur at the weakest point, whereas for the three-point bending test the failure occurs at the loading point (Aly et al., 2019). The flexural strength is influenced by temperature, brine volume, and sample size, while the strain rate does not influence the flexural strength. It is discussed in literature how far the sample size influences the flexural strength. Differences in the flexural strength according to sample size were recognized by many investigators (Frederking & Sudom, 2013). The question discussed in literature is whether the differences are due to the varying size itself or due to different testing conditions for large and small samples. On the one hand, it is argued that large beams are mostly tested *in-situ* where the brine volume is high and temperature is low which subsequently leads to lower flexural strength (Timco & O'Brien, 1994). However, on the other hand, a recent study normalized the flexural strength of small and large samples to the salinity and came to the conclusion that for an increasing size the flexural strength decreases (Aly et al., 2019). This is in accordance with statistical fracture mechanics of porous brittle solids (Munz & Fett, 1999).

#### 2.4.4. Shear Strength

Materials experience shear stress during slip along a plane parallel to the imposed stress. In sea ice, shear stress is often experienced by floes when two or more

floes move past each other, imposing the shear stress on to one another. Shear stress is also involved in multi-axial compressive failure and known as shear fault. It is also a basic mechanical property for sea ice dynamics (Ji et al., 2013). Few studies have been carried out on Antarctic sea ice to determine the shear strength of the material, which have all been laboratory-based to date at sub-zero temperatures.

Butkovich (1956) conducted shear stress tests using a double shear testing device (Fig. 13a) which loads the center of the cylindrical specimen at  $90^\circ$  angles causing shear in the two adjacent sections of ice. Paige & Lee (1967) also conducted tests with cylindrical samples. The samples were loaded against a semicircular area at both ends of the core and a load was applied at both ends until failure (Fig. 13b). Frederking & Timco (1984, 1986) conducted tests on a sample block of sea ice using a 4 point bending apparatus. The load is applied at four points on the platens that hold the sample block (Fig. 13c). The load application points, two balls and two beams, are positioned on the sample such that shear forces are applied to the sample creating a bending moment until a failure envelope is generated. Saeki et al. (1985) conducted studies on Arctic sea ice using a shear box powered by a hydraulic jack. Vertical load application on the cylindrical samples induces shear forces and is controlled by the hydraulic pressure from the jack (Fig. 13d).

More recently, tests were conducted on Bohai Sea ice by Ji et al. (2013), using a laterally confined single-shear device (Fig. 13e).

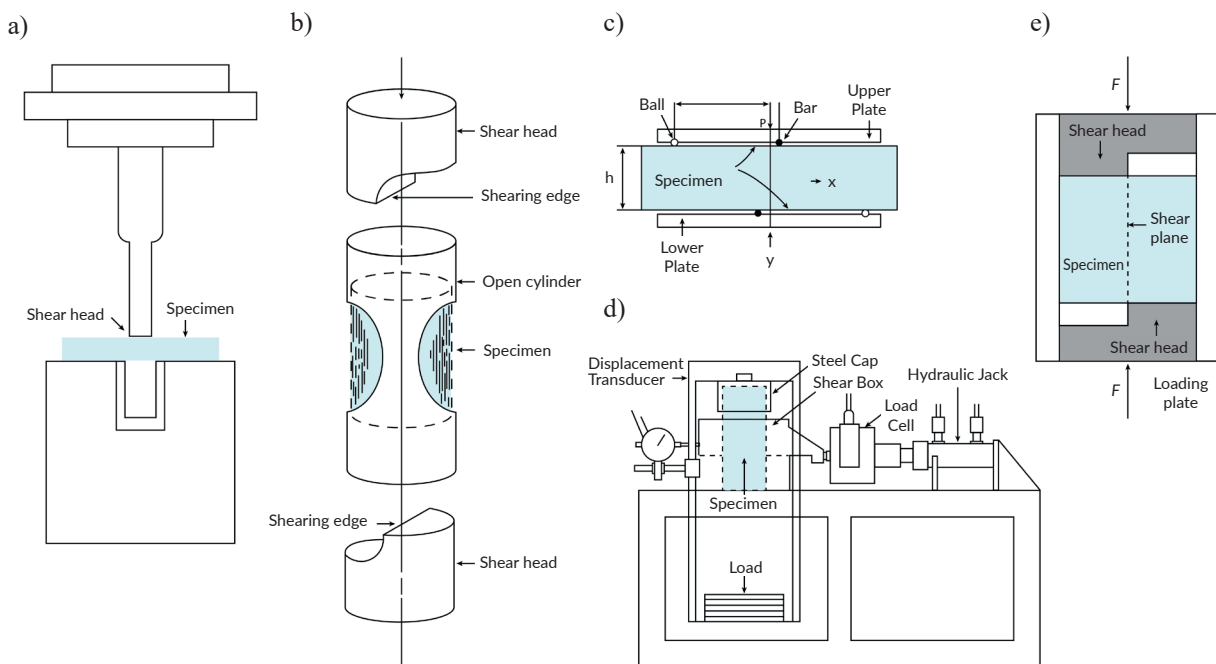


**Fig. 13.** Five different types of shear tests used for ice testing: a) according to Butkovich (1956); b) according to Paige & Lee (1967); c) according to Frederking & Timco (1984, 1986); d) according to Saeki et al. (1985); e) according to Ji et al. (2013)

Table 2 summarizes the test conditions and results of the aforementioned studies. Various factors affect the shear stress of samples, such as:

- temperature,
- brine volume,
- shear area,
- shear or strain rate,
- sample orientation.

Paige & Lee (1967) found an inverse exponential correlation between the shear strength and the square root of the brine volume of the sample. The results are based on columnar-grained sea ice collected from McMurdo Sound, Antarctica. According to Newtons law, shear strength is proportionally related to shear strain

with a proportional coefficient of viscosity. Therefore, the greater the brine volume within the sea ice sample, the less viscous the sample becomes, which thus can be related to the reduction in shear stress according to Newtons law. It must be noted however, that sea ice is a multi-phase material with solid and liquid phases that are in flux. Therefore, Newton’s law of viscosity may not be accurate for such a material but the overall reasoning may still hold. With similar reasoning, temperature reduction within a sample increases its shear strength according to the results by Paige and Lee. A reduction in temperature reduces the liquid component of the sea ice material, thus reducing the brine volume and increasing the shear strength compared to Paige & Lee (1967).

**Table 2.** Shear strength measured in the Arctic and Antarctic at different loading directions (0° = vertical; 90° = horizontal), different temperatures and different strain rates

|                           | Sample location | Season | Ice type       | Testing apparatus                         | Loading orientation [°] | Sample dimensions [cm]        | Strain rates [Mpa/s] | Test temperature [°C] | Shear strength [MPa] |
|---------------------------|-----------------|--------|----------------|---|-------------------------|-------------------------------|----------------------|-----------------------|----------------------|
| Sacki et al. (1985)       | Arctic          | summer | multi-year ice | shear box                                 | 0                       | D = 10<br>L = 15              | 0.1 to 10            | -20 to -2             | 0.2–3                |
| Paige & Lee (1967)        | Antarctic       | summer | multi-year ice | open cylinder                             | 0                       | D = 7.6<br>L = 7.6            | not given            | -11 to -1             | 0.5–1.1              |
| Sakharov et al. (2019)    | Arctic          | summer | multi-year ice | shear box                                 | 0                       | D = 20–25<br>L = 43–71        | not given            | -5 to -2.2            | 0.18–0.9             |
| Ji et al. (2013)          | Bohai Sea       | winter | multi-year ice | open cylinder                             | 0                       | L = 7.0<br>W = 7.0<br>H = 5.0 | 0.03 to 0.18         | -17 to -3             | 0.35–1.95            |
| Frederking & Timco (1984) | Beaufort Sea    | summer | multi-year ice | asymmetrical four-point bending apparatus | 0; 90                   | L = 40<br>W = 5<br>H = 10     | 0.004 to 0.1         | -13                   | 0.35–0.65            |
| Frederking & Timco (1986) | Labrador coast  | summer | multi-year ice | asymmetrical four-point bending apparatus | 0; 45 90                | L = 35<br>W = 5<br>H = 10     | not given            | -14; -2               | 0.55–0.9             |

Stress is applied force over shear area. Thus a reduction in sheared area results in an increase in the shear stress experienced in the sample. The results from Sacki et al. (1985) concur with this statement. They varied the sample diameter and length and additionally collected and tested samples along two planes; parallel and perpendicular to the growth direction of the sea ice crystals. The resulting shear strength is greater when the loading force is applied perpendicular to the growth direction of crystals.

The dependence of the shear strength on the strain rate was noted for the Bohai Sea ice in Ji et al. (2013). Comparable to the compressive strength, the shear strength increases with increasing strain rate until

a maximum value is reached and decreases afterwards. Besides that, a relation between the square root of the brine volume and the shear strength, as well as a temperature dependence of the shear strength were found.

### 2.5. Toughness

Experiments to determine the mode I fracture toughness of sea ice have been performed on both a large and small scale, under laboratory conditions, as well as in the field. Papers with good review chapters about the fracture toughness of ice have been published for freshwater ice (Dempsey, 1991), sea ice (Adamson et al., 1995;



Dempsey et al., 1999) and a combination of both (Schulson & Duval, 2009; Timco & Weeks, 2010).

Different methods to obtain the fracture toughness of sea ice have been used in previous studies, some *in-situ* testing techniques are displayed in Figure 14:

- three-point-bending under laboratory conditions (Adamson et al., 1995; Goodman & Tabor, 1978; Totman et al., 2007; Urabe & Inoue, 1988);
- *in-situ* vertical three-point-bending (Tuhkuri, 1988; Urabe & Yoshitake, 1981b; Urabe et al., 1980; Wei & Dai, 2021);
- four-point-bending under laboratory conditions (DeFranco et al., 1991; Timco & Frederking, 1983; Vaudrey, 1977);
- Vickers and conical indenter (Goodman & Tabor, 1978);
- short rod chevron notched specimen (Rist et al., 1999; Sammonds et al., 1998; Stehn, 1991, 1994);
- cantilever beam test (Adamson et al., 1995);
- wedge loaded tapered double-cantilever-beam (Dempsey et al., 1986);
- edge Cracked Rectangular Plate (Lu et al., 2015);
- circumferentially notched right circular cylinders (Mackey et al., 2007; Nixon & Schulson, 1988);
- reverse tapered-crack-line wedge load fracture geometry (Adamson et al., 1995; DeFranco & Dempsey, 1994).

The three and four-point bending tests are used in reference to ASTM E399 written for metallic materials, to conduct the fracture toughness test. It is also the most commonly used test in literature, even though different groups have used different sample sizes for the tests, thus making them hard to compare. The main question for the three and four-point bending tests is whether the samples fulfill the criteria for the linear elastic-fracture-mechanics concept. The major parameters to receive good measurements are sample size, notch-acuity, and loading rate.

It is important to note that sample size, notch-sharpness, and loading rate all affect one another and thus all three of them must be taken into account for a precise measurement. For freshwater ice a minimum size in all dimensions is inferred to be at least 10 (Nixon & Schulson, 1988), 12 (Dempsey, 1991) or 15 (Tuhkuri, 1988) times the grain size of the ice. The minimum in dimensions relative to the grain size diameter is necessary to provide polycrystalline constrains in the material and not just multicrystalline ones (Nixon & Schulson, 1988). For sea ice it is recommended to use a size of at least 200 times the average grain size to obtain homogeneity in the sample (Mulmule & Dempsey, 2000), requiring much larger samples for sea ice. These size

criteria have not been mathematical proven, but they are best practice values.

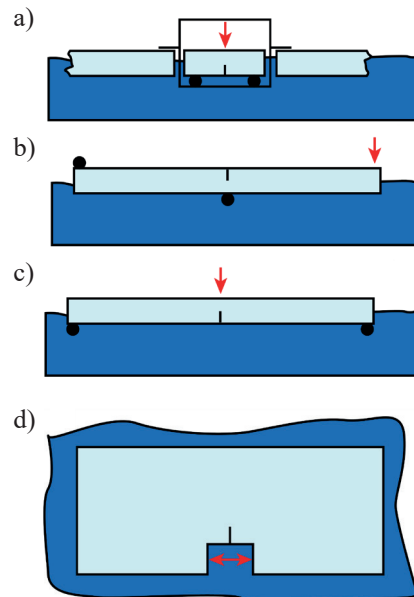


**Fig. 14.** Examples of different configurations for *in-situ* testing devices: a) three-point bending test (Urabe et al., 1980); b) cantilever beam test (Tuhkuri, 1988); c) three-point bending test (Vaudrey, 1977); d) crack opening geometry (Lu et al., 2015) (top view)

The notch must be small compared to the other dimensions of the sample, the notch tip must be sharp and larger than any other existing flaw in the sample (Timco & Frederking, 1983). Even though the notch sharpness is less relevant for salt water than for fresh water, the notch sharpness must be taken into account (DeFranco et al., 1991). The sharpness or radius of the notch tip is important to reduce scatter during the test and should ideally be close to zero, therefore, the notch tip must be sharpened after cutting the notch. Methods used in the literature to reshape the notch tip are mostly razor blades (Urabe et al., 1980) or surgeon scalpels (Timco & Frederking, 1983). A problem in literature is that the mechanism of reshaping the notch is not described in detail and therefore is hard to replicate. The minor influence of the notch sharpness on sea water ice might be explained by an analogy to concrete, where the formation of micro cracks (i.e. brine or air pores) prevents the formation of a plastic zone (Tuhkuri, 1988). The mode I fracture toughness is also affected by the loading respectively strain rate of the test. It increases with decreasing strain rate (Damsgaard et al., 2021; Tuhkuri, 1988; Urabe & Yoshitake, 1981a, 1981b; Urabe et al., 1980). At low loading rates, the creep behavior in sea ice is accompanied by crack tip blunting which affects the fracture toughness, leading to lower values for the

fracture toughness (Tuhkuri, 1988). On the other hand, if the strain rate is too fast, dynamic effects may modify the results (Lu et al., 2015). It is also noteworthy that larger samples require faster loading rates, so that secondary creep does not increase the apparent fracture toughness (Mulmule & Dempsey, 2000). A best fit strain rate from the mentioned test should be larger than  $\dot{K} > 10 \text{ kPa} \sqrt{\text{m}}/\text{s}$ , sea ice research suggests on a large scale a value dependent on the ice temperature  $-0.5^\circ\text{C}$   $\dot{K} > 20 \text{ kPa} \sqrt{\text{m}}/\text{s}$  (Lu et al., 2015).

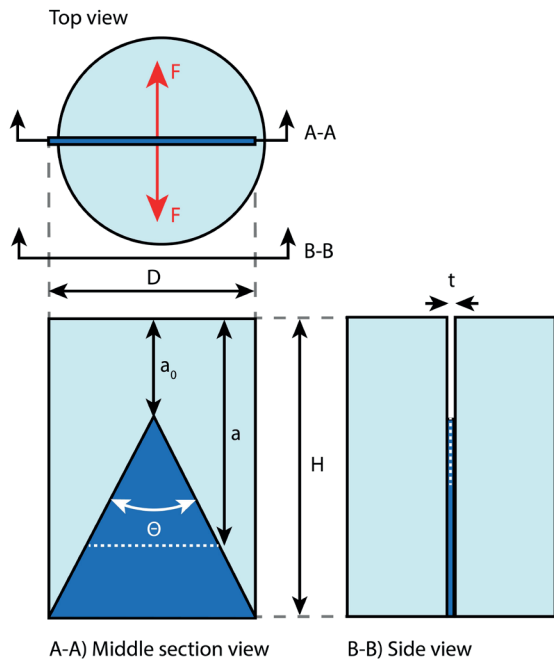


**Fig. 15.** Specimen for the short rod chevron notched test:  $H$  – height;  $D$  – diameter;  $a_0$  – distance from loaded end to chevron tip;  $a$  – crack length,  $\Theta$  – chevron angle;  $F$  – force (drawing after Ouchterlony, 1988)

The second most used test is the short rod chevron-notch (SRCN) test (Rist et al., 1999; Sammonds et al., 1998; Stehn, 1991, 1994). The testing geometry is displayed in Figure 15. Its large benefit is the test geometry which is received by coring in the field, it is proven to give quasistatic crack growth in brittle materials and a high stress concentration at the tip. Even though the short rod chevron notched method has some benefits, its biggest disadvantage is its poor comparability (e.g. impact of porosity on the fracture toughness) to other testing methods (Moslet, 2007; Stehn, 1991, 1994).

Other factors influencing the  $K_{IC}$  fracture toughness of ice are loading history, grain size, heat treatment, surrounding medium (water, air), loading direction, porosity, salinity, thickness and density. Some of these aspects have already been investigated on sea ice, whereas other effects are known from different materials.

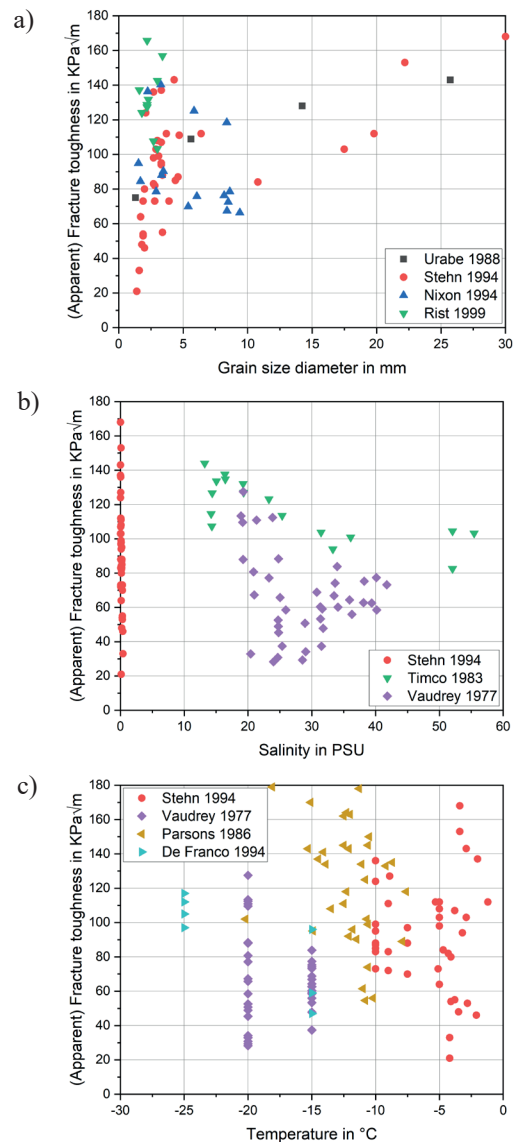


**Fig. 16.** The influence of grains size (a), salinity (b) and temperature (c) on the fracture toughness of sea ice

The grain size effect in salt water has been investigated by some researchers (Nixon & Schulson, 1988; Parsons et al., 1986; Rist et al., 1999; Stehn, 1994; Urabe & Inoue, 1988). Urabe, Stehn and Parsons came to the conclusion that an increasing grain size leads to an increasing fracture toughness. This trend was captured by measurements with a bending test and measurements with the SRCN method. Other authors like Timco & Frederking (1983) and Parsons et al. (1986) obtained an increase in fracture toughness and grain size over the depth, therefore the same conclusion can be drawn from their experiments. Only Nixon & Schulson (1988) concluded a decreasing toughness for increasing grain size. The loading direction has an impact on the fracture toughness. If loaded from the top in a three-point bending test, the fracture toughness is

greater than if the sample gets loaded from the bottom side. The fracture toughness is therefore higher at the bottom where larger grain sizes are present, than at the top where the average grain size is smaller (Ura-be et al., 1980). Stronger ice at the bottom side of ice floes was also observed by Timco & Frederking (1983), while the fracture toughness was constant in the granular region. It is not clear, if the loading direction affects the fracture toughness by itself or through the different grain sizes at the bottom and top. The apparent fracture toughness decreases with increasing brine volume respectively a higher salinity (Fig. 16). A higher brine volume leads to a solid matrix with more brine pockets. Brine pockets and a network of brine channels can lead to stress concentration and the origination of micro cracks (Mulmule & Dempsey, 2000). The influence of the salinity on the fracture toughness was higher for SRCN specimens than for the other testing methods (Stehn, 1994). The impact of temperature on fracture toughness has not yet been quantified. On the one hand, the data in Figure 16 display a slight increase for decreasing temperatures (DeFranco & Dempsey, 1994; Parsons et al., 1986; Stehn, 1994; Vaudrey, 1977), on the other hand, literature suggests that temperature has a minor effect (Rist et al., 1999). Nevertheless, a study showed that ice tested *in-situ* has a strength which is only 30% of ice which is tested in a cold room (Wei & Dai, 2021). Ice shows brittle behavior during fracture toughness tests when it is colder  $-25^{\circ}\text{C}$  and tends to behave in a ductile fashion when it is warmer  $-15^{\circ}\text{C}$  (DeFranco & Dempsey, 1994).

## 2.6. Sea ice storage

Research on the effect of storage temperature on sea ice samples has been limited and only two studies have addressed and attempted to quantify possible changes within samples (Nakawo, 1983; Schwarz J. et al., 1981).

One of the earliest understandings of how samples change with time was presented by Schwarz J. et al. (1981), whereby they state that 10% of brine is initially lost immediately upon sampling and thereafter brine drainage is considered negligible. This claim is presented briefly and is unsubstantiated by any data, thus making it difficult to be confirmed.

Another early study was conducted by Nakawo (1983), with only two sea ice samples. The samples were tested with respect to the porosity, thus this is an important value for mechanical tests as reported before. One sample was tested in the field, while the other samples were stored for six months at  $-40^{\circ}\text{C}$ . In this study, no change of porosity due to storage was detected.

Cox & Weeks (1986), studied the changes in brine volume, porosity and resulting salinity of sea ice samples after storage at  $-50^{\circ}\text{C}$  and  $-30^{\circ}\text{C}$ . After storage and transport at these temperatures, the samples were brought back to their *in-situ* temperatures and the resulting brine volume, porosity and salinity were measured and compared to their prior states. All samples experienced a degree of change in their brine volume, porosity and salinity, and it was found that the greater the difference between the storage temperature and the *in-situ* temperature, the greater the change became in the properties of the ice. The difference can be up to 15%. However, the authors conclude that sea ice samples of *in-situ* temperature colder than  $-10^{\circ}\text{C}$  can be seen as not being affected by cold-storage temperatures and thus any changes are insignificant (Cox & Weeks, 1986). In spite of this, details of the storage time and experimental procedures for sample analysis were not described and thus the extent of change in these samples may not be described fully.

More recent studies have investigated the changes in microstructure of sea ice samples with the change in ice temperature. Whilst the scope of these studies do not refer to the storage temperatures of sea ice, these changes with different temperatures may be relevant for storage considerations. Light et al. (2003), investigated the changes in brine volume and the shape of brine pockets within sea ice with changes in temperature through imaging thin sections. A reduction in temperature from  $-15^{\circ}\text{C}$  to  $-25^{\circ}\text{C}$  reduced the brine volume by 42% and significantly increased the size of crystals within the sample. They also investigated the changes with warming and concluded that brine volume increased 48% from  $-13^{\circ}\text{C}$  to  $-8^{\circ}\text{C}$ . Whilst warming reduces the size of crystals and increased the brine volume, the observed brine pockets also merged to form larger pockets. These samples were subjected to cooling once again and the resultant number of brine and gas pockets did not revert back to their original number suggesting that changes in ice temperature do affect the structure of the sample (Light et al., 2003). Similarly, studies that use MRI to observe the thermal evolution of the microstructure of sea ice samples has yielded similar results and conclusions (Eicken et al., 2000, 2005). Therefore, future research into potential changes in sea ice properties with storage is justified.

### *Sea ice transport*

The transport of sea ice from collection sites in the Arctic and Antarctic refers to the storage and movement of the samples on-board a research vessel and the transportation of these samples from the ship to the research base where the samples are often stored and analyzed.

Studies surrounding the effects of transportation have yet to be accomplished as many assume little or no changes in sample structure and its properties during the transportation process. It is assumed by Cox & Weeks (1986), that gravity drainage of brine due to transportation is negligible for most sea ice samples at temperatures below  $-23^{\circ}\text{C}$ . Temperatures below this for storage of samples during transportation is common practice and the use of dry-ice guarantees cold temperatures within the range of  $-50^{\circ}\text{C}$  and  $-60^{\circ}\text{C}$  during the transport process (Cox & Weeks, 1986; Wolff et al., 1988). Any changes in physical or structural properties of sea ice owing to the movement of samples has yet to be explored and has been limited to the effect of the changes in storage temperature during the transport process.

Both sea ice storage and transport have been grossly underestimated by previous studies and full realization of the extent of potential changes in sample properties remains to be determined. The lack of literature on this topic calls for a greater scope to include a variety of storage times, storage methods, storage temperatures, transport methods and transport temperatures. A detailed analysis into these variables will yield a better understanding of these procedures and allow for more informed decisions around the storage and transport of sea ice.

### 3. Medium to large scale observation

#### 3.1. Overview

Satellite remote sensing is the most prevalent approach for large-scale monitoring of the polar regions and mapping of sea ice extent, thickness and snow cover in both the Arctic and Antarctic as well as discriminating between seasonal and persistent ice types. Satellite active and passive sensors use bands of the visible, infrared and microwave electromagnetic spectrum to measure parameters such as sea-level height (altimetry), surface temperature, surface roughness (scatterometers), ice movement and fluorescence from chlorophyll. Polar nights and large scale cloud cover limit the effectiveness of visible and infrared sensors in these regions leading to the adoption of SAR and radiometer sensors which can observe the Earth's surface irrespective of cloud cover or lack of visible illumination. However, there are some limitations to satellite remote sensing in polar regions. The orbital inclination of satellites does not allow measurements of latitudes above  $80^{\circ}$ . Additionally, satellite remote sensing measurements require calibration and validation against data models, which tend to under represent climate change in the region,

sensors have limited fine scale spatial resolution over short-time periods making sea ice type characterization difficult as well as being restricted by the time taken between re-sampling a particular region (Alberello et al., 2020; Emery et al., 1997; Turner et al., 2017). Lastly, due to the lack of habitation in the Southern Ocean, commercial interest has historically not been strong enough to fund studies. Hence, the coverage of the Antarctic is much coarser (both in terms of spatial and temporal resolutions). This has been changing of late because of the emerging commitment by international bodies towards climate change monitoring and control. For example, the Polar Operational Environmental Satellites (POES) constellation has been getting more sensors and better coverage. Other noteworthy projects consist of NASA's Icesat-2 and ESA's Cryosat-2 which are especially designed to measure sea ice in the Antarctic.

To complement, calibrate, and validate satellite based techniques, additional airborne, ship based, direct and autonomous sensing observation and sampling approaches have been used. Data collection is heavily constrained by large voyage costs. Limited collection opportunities due to safety concerns in these inhospitable regions physically limit airborne and shipping access to these remote locations during the winter months. The data sets that can be collated from these seasonal collections is sparse, localized, and of low resolution, contributing to poorly resolved understanding of the specific processes underlying sea ice formation and composition during the autumn advance and the properties determining melt during the summer sea ice retreat (Kennicutt II et al., 2014, 2016; Lee et al., 2012, 2017; Maksym et al., 2012).

Key to improving the acquisition of these data is the development of innovative instrumentation (Kennicutt II et al., 2016), designed to operate remotely under extreme conditions. These should be capable of taking concurrent measurements of key atmospheric-ice-ocean variables, through seasonal variations, for longitudinal studies. Advances in autonomous technology have already allowed for increased monitoring and persistent sampling of the polar sea ice regions (Alberello et al., 2020; Doble et al., 2017; Kohout et al., 2015; Lee et al., 2017; Polashenski et al., 2011; Rabault et al., 2020; Vichi et al., 2019).

To improve our knowledge of sea ice properties, there has been a history of coordinated observational experiments in the sea ice regions of both the Arctic and Antarctic to better characterize these physical sea ice processes through single-season single-ship experiments to large scale multinational multi-year experiments.

### 3.2. Sea ice observation

Of the two polar regions, the majority of direct measures of sea ice state and dynamics have been performed in the Arctic due to its proximity to Northern countries and historical exploration as a potential shipping route. However, these two regions have distinct metocean conditions and exhibit significant differences in seasonal sea ice composition, coverage and dynamics.

The first multi-national sea ice observational endeavor was conducted from 1970 to 1976 off the coast of Alaska. The Arctic Ice Dynamics Joint Experiment (AIDJEX) was a joint US/Canadian initiative to improve the understanding and model the mechanisms of sea ice mechanics in relation to external stress fields. Direct measurements of sea ice physical parameters were taken by personnel stationed at ice camps, from instruments on aircraft and helicopters, data buoys as well as from Landsat satellite imagery (Lee et al., 2012; Untersteiner et al., 2007).

The next large scale study of the Arctic MIZ occurred during the multinational Marginal Ice Zone Experiment (MIZEX) (Cavalieri et al., 1983; Group, 1986). The MIZEX was designed to study meso and large scale Arctic MIZ processes in the Bering and Greenland Seas, including wave-ice interaction, ice and ocean dynamics, polar frontal studies, eddies and bands and acoustics through a set of field based programs held over a series of winter and summer seasons from 1983 to 1986. These observations were conducted from a number of research vessels (M/V Polarbjørn, R/V Polarstern, M/S Kvitbjørn, M/V Polar Circle, Polar Queen, Discoverer, Håkon Mosby, Valdivia) and research aircraft (Cavalieri et al., 1983; Group, 1986; Lee et al., 2012).

This was then followed the Co-ordinated Eastern ARctic EXperiment (1988-1989), which had a series of MIZ experimental components. This included ice drift measurements from the Norwegian vessel the M/V Polarbjørn, which was purposefully frozen in the ice, a sea ice edge experiment used as validation for the design of the ESA ERS-1 satellite as well as oceanographic and acoustic measurements taken from two ice camps (1989) (Lee et al., 2012).

The Labrador Ice Margin EXperiment (LIMEX) was conducted in 1987 to 1989 as a calibration and validation experiment for SAR observation of the MIZ. Aircraft were fitted with SAR and flown over the MIZ in the Labrador Sea with a number of ships also deployed in the region to obtain ground truth data to validate the SAR measurements. These experiments were also used as part of the validation process for the new SAR satellites (RADARSAT and ESA ERS-1) (Lee et al., 2012; McNutt et al., 1988).

Driven by the need to better understand the decline in Arctic sea ice coverage and its extent, the US Navy recently funded two large scale sea ice observational experiments, the Marginal Ice Zone experiment (Lee et al., 2012) and the Sea State and Boundary Layer Physics of the Emerging Arctic Ocean experiment Thomson J. & Persson (2021) in the Beaufort Sea. These experiments utilized a host of modern observational platforms to measure a range of atmospheric, ocean and ice variables. In particular they used a wide variety of autonomous instruments, which had two way telemetry allowing for easy data transfer.

These observational platforms included:

- ice-based instruments, which were deployed directly on sea ice to measure ice drift, wave parameters, air temperature, wind velocity, humidity, pressure, solar radiation, snow and ice thickness, thermal structure of ice (Ice Mass Balance Buoys – Jackson et al., 2013; Wave Buoys – Doble et al., 2017; Ice-Tethered Profilers – Krishfield et al., 2008; Autonomous Ocean Flux Buoys; Automated Weather Stations; Acoustic Navigation Beacons);
- ocean-based drifting platforms measuring wave parameters, winds, currents and temperature (Surface Wave Instrument Float with Tracking Drifters – Thomson J., 2012);
- mobile autonomous platforms (sea gliders – Eriksen et al., 2001; Jaguar Autonomous Underwater Vehicle, Wave Gliders – Manley & Willcox, 2010; unmanned aerial vehicles – DJI Phantom 3);
- moorings to record a time-series of surface wave parameters;
- shipboard sensors on R/V Sikuliaq used to measure air-ice-ocean parameters (towed CTD, meteorological flux package and a Sea Ice Measurement System);
- remote sensing including SAR and sea ice imagery (Satellite SAR, shipborne radar, video and LIDAR).

These experiments illustrated that, although ships and aircraft are still needed as part of the experimental operation, extensive sampling and measurement can be conducted by less costly distributed networks of autonomous instruments deployed over larger spatial areas. For a detailed overview of these studies see (Lee et al., 2017).

Doble et al. (2017) alluded to a series of environmental considerations when designing the Wave Buoy systems, which were used extensively in the Marginal Ice Zone experiment (MIZ, 2014) (Lee et al., 2012). One such consideration is the frosting over/rimming of the device due to freezing ocean spray. Additionally long periods of heavy cloud cover and no sunlight can

affect the performance of the solar powered battery systems (Doble et al., 2017). Twenty buoys were deployed in the Arctic Marginal Ice Zone with each device anchored by drilling a hole in the ice and placing the keel inside. Nineteen buoys survived the deployment, with one system failing to boot. The buoys survived for extremely long periods with twelve systems surviving for 200 days off a single alkaline battery pack (Doble et al., 2017). Seven systems ran for 70 days on alkaline batteries before switching over to the solar powered lead-acid batteries. During this period, the devices transmitted continuously over the Iridium network and were able to interpolate sea ice phases from the tilt of the buoy (Doble et al., 2017). Eventually, the systems by Doble et al. (2017) lost transmission 300 days after their deployment. Individual device failure was primarily attributed to depletion of the alkaline battery packs, but also due to ice mechanics which resulted in some buoys being crushed by the floes due to rafting, evidence of which was captured by webcams on the buoy shortly before transmission ended. Devices also experienced freeze-over or were buried under snow which resulted in the devices going offline for temporary periods (Doble et al., 2017). Buoys that survived the spring melt refroze during the gradual refreezing of the ice. During the second cycle, none of the buoys rebooted when the ice melted in the spring (Doble et al., 2017).

Kohout et al. (2015) deployed five Wave in Ice Observational Systems (WIIOS) in the East Antarctic Marginal Ice Zone during the Sea Ice Physics and Ecosystem Experiment (SIPEX) mission with the goal of capturing wave-in-ice events (Kohout et al., 2015). Three devices were deployed using helicopters on ice floes while two devices were deployed from the R/V *Aurora Australis*'s 7 ton crane. Kohout et al. (2015) notes that deployment via crane was successful in spite of 7 m swell and 25 m/s winds. The device was fitted inside a Pelican case with a sealed membrane surrounded by a tire for protection and flotation in case of ice melting, see (Kohout et al., 2015). Consequently, this places the buoy directly on the surface of the floe, rendering it susceptible to snow build up and flooding. After deployment, the crew received 600 samples of data over 39 days in total. However, the first device failed 20 hours after deployment coinciding with the first large wave event captured the buoys (Kohout et al., 2015). The second large wave event resulted in the failure of two more systems just 9 days after deployment (Kohout et al., 2015). The fourth buoy lasted for 17.5 days, with the final buoy surviving a total of 39 days. As a result, only one device lasted for the expected time with the majority of data captured during calm events.

Two WIIOS buoys were deployed during the winter of 2017 similar to the ones by Kohout et al. (2015) (Alberello et al., 2020; Vichi et al., 2019). Two devices were deployed on two separate ice floes 3 m in diameter and 100 km from the ice edge. One system survived for 8 days and 18 hours while sampling every 15 minutes before transmission ended. The second buoy, however, survived for 6 days, sampling every 15 minutes until it switched to power saving mode and surviving for a total time frame of 3 weeks (Alberello et al., 2020; Vichi et al., 2019). Alberello et al. (2020) and Vichi et al. (2019) deployed a second pair of WIIOS buoys. However, the first buoy stopped responding after three days, while the second buoy survived for 16 days (Vichi et al., 2019). While the buoys' survival is largely attributed to power optimization, the lifespan could be influenced by the selection of the ice floe. Ice floe size and proximity to the ice edge affect the exposure of the floe to open-ocean processes and storms (Vichi et al., 2019). This could result in failure due to ice mechanics.

Rabault et al. (2020) deployed a Waves In Ice Buoy (WIIB) on landfast ice in the Ross Sea to test the device's performance in the Southern Ocean. This buoy was largely designed using off-the-shelf low cost sensing and processing technology. In a similar fashion to the WIIOS buoy, the device was placed in a Pelican case and attached to a flotation device. However, expected survival time for this device was significantly lower compared to the WIIOS devices: a maximum of 8 days of continuous operation (Rabault et al., 2020). The buoys by Kohout et al. (2015) were designed to be expendable whereas the buoys by Rabault et al. (2020) were designed to be retrievable. Additionally, the WIIB devices were deployed in the summer. Two devices were deployed in close proximity to each other. However an ice break event resulted in the separation of the devices. The devices survived for 2.5 weeks, with device failure attributed by Rabault et al. (2020) to the buoys having been crushed by ice and wave activity in the region. Despite this, the devices were able to record significant wave events and maintain a fully charged battery throughout the deployment which Rabault et al. (2020) attributes to the solar panel.

Finally, the ice-tethered buoys developed by Kohout et al. (2015) and Rabault et al. (2020) sit close to the surface of the ice floes. As discussed previously, during the winter cycles, snow accumulates on the surface and can reach up to 1 m in height. This snow formation can result in flooding where the floe becomes submerged. Prolonged burying under snow may have resulted in the device freezing over thereby losing contact while prolonged contact with the seawater may

have resulted in the buoys failing on several occasions (Alberello et al., 2020; Kohout et al., 2015; Rabault et al., 2020; Vichi et al., 2019). Finally, Vichi et al. (2019) discusses the findings surrounding the failure of the first WIOS system. Vichi et al. (2019) observed a major cyclonic event. The cyclone formed on 2 July 2017 and achieved lysis on 5 July 2017 which coincided with the buoy deployment. Following the event, four more cyclonic events were recorded with three explosive cyclones characterizing a change of pressure over 24 hours (Vichi et al., 2019). During this time, Vichi et al. (2019) observed winds speeds of up to 33 m/s while noting that the air temperatures had increased to values “close to melting”. Additional observations found an increase in significant wave height in the activ-

ity. These conditions indicate deformation Vichi et al. (2019) which may have subjected the buoys to forces experienced by Doble et al. (2017) during their Arctic deployment which were verified against the temperature and pressure readings of the second WIOS during the cyclonic event. The buoys were deployed close to the ice edge exposed to greater open ocean processes and cyclonic activities than other semi-consolidated and consolidated regions (Vichi et al., 2019). As a result, air advection, storms, and large wave movement delay the consolidation of sea ice considerably (Vichi et al., 2019). Hence, the ice floes were more likely to experience rafting, ridging, extended flooding, and freezing over which may have caused the failures of the WIOS buoys.

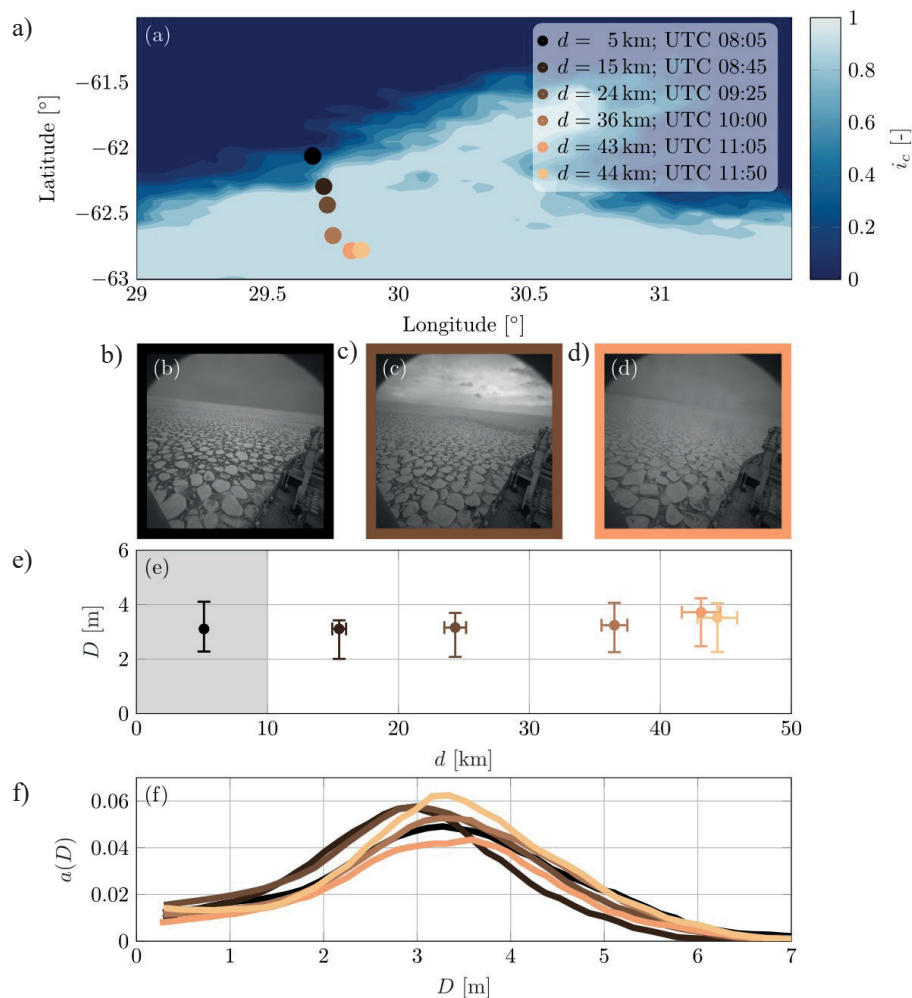


**Fig. 17.** Sea-ice properties on the 4<sup>th</sup> July 2017: a) overview of study area with sea-ice concentration from AMSR2 on the 4<sup>th</sup> July 2017 (longitude and latitude are horizontal and vertical axes, respectively), with bullets indicating six mean measurement locations during 20min acquisitions; b–d) example of image acquisitions (axes in pixels) at  $d = 5$  km, 24 km and 43 km from the ice edge, respectively; e) median pancake floe diameter ( $D$  – vertical axis) versus distance from the edge ( $d$  – horizontal axis) shown as bullets, plus 25<sup>th</sup> and 75<sup>th</sup> diameter percentiles (vertical error bars) and uncertainty in distance from ice edge (horizontal error bars); shaded background denote the measurement location in intermediate ice concentration; f) area weighted floe size distribution ( $a$  – vertical axis) as a function of floe diameter ( $D$  – horizontal axis) at each measurement location; color coding is used in all panels to denote the distance from ice edge (after Alberello et al., 2022)

Deployment of buoys may become a challenge under harsh weather conditions. Circumventing the perilous task of their active installation or the loss of the buoys themselves, stereo-optical techniques from the icebreaker herself have been successfully employed to measure the wave dynamics in the MIZ in the same cyclonic event in 2017 (Alberello et al., 2022). The fundamental question to be answered is the interrelation between ice floe coverage of the ocean surface, the respective sizes and relative thicknesses of the floes and the attenuation of waves from the open ocean edge of the MIZ into the denser and finally consolidated ice cover. These dynamics determine the overall growth rate of the ice shield and its final possible extension at the end of winter. Alberello et al. (2022) showed that the local winds generate the largest contribution (70%) to the wave height at the edge of the MIZ. Irrespective of the wave height, the attenuation of single mode waves is similar to the benchmark value reported earlier (Kohout et al., 2020). Attenuation thus appears to be independent of wave height. Only the complex dynamics in the center of the cyclone exhibited dynamics that could not be described at the present stage of understanding. The extension of wave dynamics into the fully covered ice field was much further than typically assumed. In particular, the fully covered sections that contain a large frazil ice fraction were shown to be subject to the influence of the wind conditions above, much more so than previously assumed.

It is thus of fundamental importance to further understand the role of frazil ice in the dynamics of ice cover formation. In the first 50 km inwards, floe sizes differed much less than expected (see Fig. 17f) reflecting the long extent of similar floe dynamics into the fully covered ice field. As can be seen from the series of experiments conducted over the period 1970 to 2020 an improved design of and access to autonomous instruments capable of persistent, accurate in situ sampling at finer spatial resolutions and over the autumn/winter seasons in the MIZ of both the Arctic and Antarctic would permit to refine dynamic models for these regions. Hence, designing and delivering robust in situ sensing instruments capable of long-term functionality in these regions is a high priority for polar science (Kennicutt II et al., 2016). A successful device should (1) support autonomous or sustained deployment; (2) have adequate sensing capabilities for the variables of interest, (3) be capable of real-time data collection, transfer and analysis, (3) be supported by improved, robust power supplies, and finally but critically (5) survive for extended durations under extreme weather conditions.

## 4. Computational mechanics

Sea ice dynamics, its formation, growth, melting, cracking and evolution covers a wide range of scales in space and time. Modelling such a complex system offers many challenges to computational mechanics and applied mathematics. The computational mechanical treatment of sea ice is reviewed in this section. We cover the modeling of sea ice and all related effects from large to small scale.

### 4.1. Large-scale sea ice dynamics modeling

The components and interacting forces determining the sea ice dynamics are presented in Figure 18. The first global climate models can be traced back to Budyko (1969) and Sellers (1969). They developed energy balance models that accounted for ice-albedo effects by parameterizing sea surface albedo as a function of sea surface temperature. In contrast, the model described by Untersteiner (1961) and Maykut & Untersteiner (1971) takes into account the thermal inertia of brine pockets. However, an extension of the underlying models at that time was limited by available computer capacity, and numerical simulation was too computationally intensive. Thus, the models often remained simplified and considered only basic extensions. A real breakthrough occurred in 1979, when Hibler developed a basin-scale model that treats sea ice as a viscous-plastic (VP) material, and another model that explicitly models the ice thickness distribution, see Hibler III (1979). Following Hibler III (1979), sea ice motion on the large scale can be described by:

$$\rho_{ice} H_{ice} \left( \frac{dV}{dt} + f_c e_r \times v \right) - \sigma - \tau_{ocean} - \tau_{air} + \rho_{ice} H_{ice} g \nabla H_d = 0 \quad (9)$$

with the material time derivative  $D(\cdot)/D(t) = \partial(\cdot)/\partial(t) + \nabla(\cdot)v$ , which includes an advective fluid flow.  $\nabla$  denotes the gradient operator with  $\nabla := (\partial_x, \partial_y)^T$  in the two-dimensional case. The constitutive relation of visco-plasticity, proposed by Hibler III (1979) gives a definition of the sea ice Cauchy stress tensor  $\sigma = \sigma(\dot{\epsilon}, P)$  in terms of  $\dot{\epsilon}$  and the so-called ice strength factor  $P$ :

$$\sigma = 2\eta\dot{\epsilon} + (\xi - \eta)tr\dot{\epsilon}I - \frac{P}{2}I \quad \text{with } \eta, \xi \geq 1 \quad (10)$$

$$\text{and } P = H_{ice} P^* \exp(-C(1 - A_{ice})) \quad (11)$$

$P^*$  and  $C$  denote fixed empirical constants,  $A_{ice}$  and  $H_{ice}$  denote the ice concentration and mean ice layer thickness, respectively.



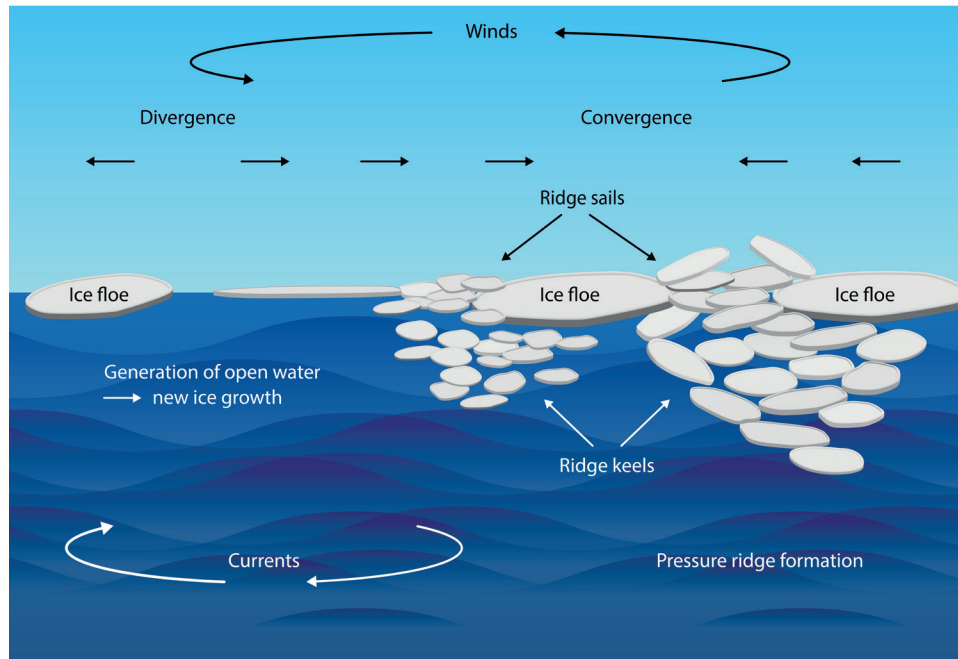


Fig. 18. Sea ice dynamics components and forces (after Thomas, 2017)

The work of Hunke & Dukowicz (1997) succeeded in providing a fundamental extension of the VP model to an elastic-viscous-plastic (EVP) material behavior. This extension in detail is a numerical approximation of the VP model, which is numerically more efficient and robust. Nowadays, both the VP and EVP models are widely used in sea ice modeling. Current sea ice models can be classified into the Los Alamos Sea ice Model CICE (see, e.g. Hunke, 2001; Hunke & Dukowicz, 1997, 2002; Hunke & Lipscomb, 2010); The Model of the University of Victoria (see, e.g. Bitz et al., 2001; Weaver et al., 2001); the Thickness and Enthalpy Distribution (TED) ice model (e.g. Zhang & Rothrock, 2001); the Louvain-la-Neuve ice model (e.g. Vancoppenolle et al., 2009a, 2009b); the Max-Planck-Institute global ocean/sea ice model given in, (e.g. Marsland et al., 2003; Uotila et al., 2012); the ICON Earth System Model (see Jungclaus et al., 2022); and the Finite-Element/volume Sea ice-Ocean Model (FESOM) by the AWI (see, e.g. Danilov et al., 2004, 2015; Timmermann et al., 2009; Wang Q. et al., 2014). A recent overview of sea ice models in climate studies is provided by e.g. Hunke et al. (2010), Notz (2012), and Fox-Kemper et al. (2019). Comparative work on the numerical simulations and the underlying physical observations can be found in Lindsay et al. (2003).

Already in the Arctic Ice Dynamics Joint Experiment (AIDJEX) project of 1973, the Finite Element Method (FEM) was used to simulate crack propagation in sea ice, see e.g. Mukherji (1973). The great utility of

an unstructured grid, such as can be easily used in FEM, was also recognized early, by Becker (1976). In 1980, Sodhi & Hibler III (1980) presented a FEM implementation of ice drift in the complex region of the Strait of Belle Isle in eastern Canada that separates the Labrador Peninsula from the island of Newfoundland. Thomson N.R. et al. (1988) investigate various constitutive laws for Eulerian and Lagrangian descriptions of short-term ice motion in the Beaufort Sea in the Arctic Ocean.

In addition to the aforementioned simulation approaches based on the FEM, a fundamental approach is the application of the Finite Difference Method (FDM). In many cases, the methods and approaches developed here have become established in the vocabulary of the discipline. The Finite Volume Method (FVM) is also an established approach to the solution of the sea ice dynamics equations (cf. Danilov et al., 2017; Gao et al., 2011).

### Solver types

In recent years, tremendous efforts have been made by various groups on the Finite Element Method (FEM) in sea ice modeling. The University of Louvain group has made significant contributions to both sea ice and ocean modeling (see e.g. Lietaer, 2011; Lietaer et al., 2008), mainly related to the Arctic. Timmermann et al. (2009) show a simulation of a global configuration with a coupled ice-ocean model, which was the first result of the finite element sea ice model developed at the Alfred Wegener Institute already in 2003 as part of the finite element sea ice-ocean circulation model. In 2014, the AWI group published the second

version of FESIM (see Wang Q. et al., 2014 and Danilov et al., 2015, as well as Losch & Danilov, 2012, and Losch et al., 2014). Mehlmann & Richter (2017a, 2017b) made proposals for a finite element implementation to efficiently and robustly solve the sea ice dynamics problem using a modified Newton solver. This approach can be seen as an improvement of the existing EVP solver and a Picard solver developed by Zhang & Hibler III (1997). The solution to the sea ice viscosity in this approach is shown in Figure 19.

Lemieux & Tremblay (2009) and Lemieux et al. (2014, 2010), invented an improvement of this rather slow solution method; they introduced a Jacobi-free Newton–Krylov solver. Mehlmann & Korn (2021) present a discretization of sea ice dynamics on triangular grids that can be coupled straightforwardly to an ocean model on a triangular grid with Arakawa C-type staggering. Their approach is based on non-standard FE interpolation, namely the Crouzeix–Raviart finite element and shows promising results. Another type of non-standard FE methods can be seen in the Least-Squares Finite Element Method (LSFEM). The LSFEM is based on formulating a minimization problem in terms of partial differential equations.

It is shown in Mehlmann et al. (2021), that at high spatial grid resolution, often with a grid spacing of less than 5 km, viscous-plastic sea ice models begin to produce linear kinematic features. The quantity and definition of simulated LKFs may be influenced by factors other than grid spacing, like discretization specifics. The results of sea ice models with various grid spacings, mesh types, and numerical discretization approaches are contrasted in an idealized setting to examine these effects, see Figure 20. Similar numbers of LKFs are produced by the A-grid approximation on triangular meshes and the A, B, and C-grid discretizations of sea ice dynamics on quadrilateral meshes (with the same number of vertices). In comparison to traditional Arakawa A-grid, B-grid, and C-grid techniques, the discretization on an Arakawa CD-grid on structured quadrilateral and triangular meshes resolves the same amount of LKFs. This is because the CD-grid technique discretizes the velocity field with a greater number of degrees of freedom. The CD-grid discretization is a desirable substitute for traditional discretizations because of its improved resolving capabilities. As an example, Figure 21 shows the solution of the sea ice concentration for the FESOM and the Gascoigne model on triangular and quadrilateral meshes.

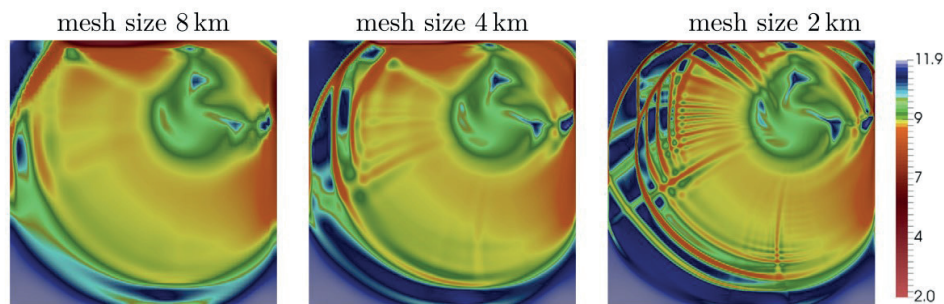


Fig. 19. Plot of the sea ice viscosity in a logarithmic scale (after Mehlmann & Richter, 2017b – reproduced with permission from Elsevier)

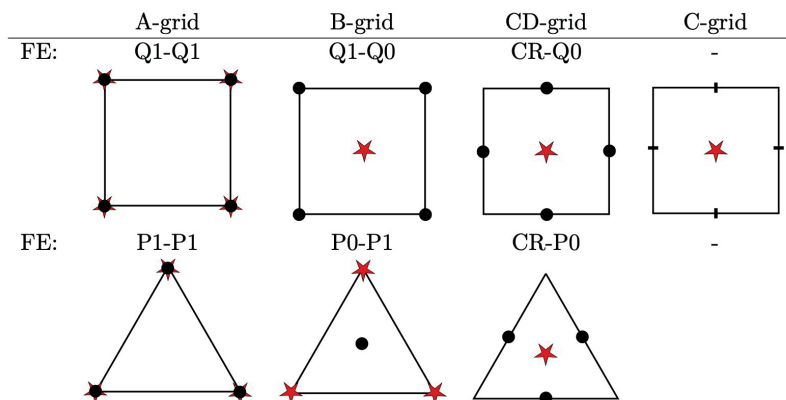
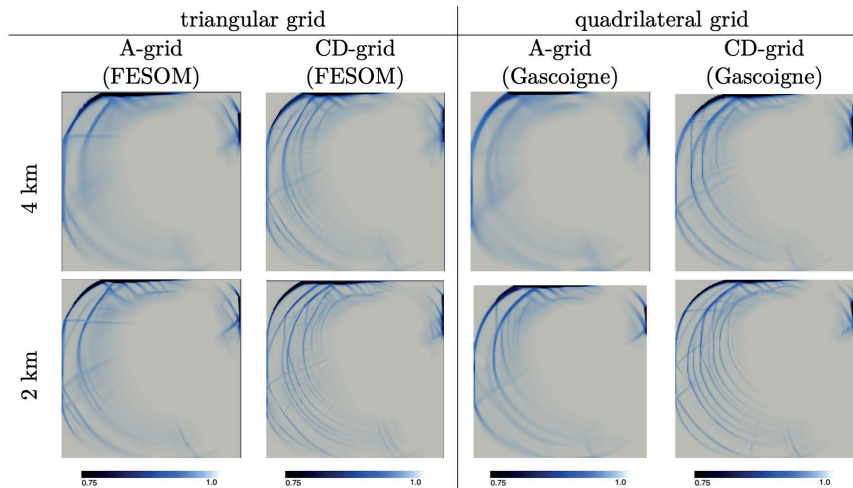


Fig. 20. Different staggering and their finite element (FE) equivalents, with indications the placement of the horizontal velocity  $v = (v_1, v_2)$ , the normal component of the velocity and the staggering of the tracers by  $\bullet$ ,  $-$ , and  $\star$ , respectively (after Mehlmann et al., 2021)



**Fig. 21.** Sea ice concentration on triangular and quadrilateral meshes for selected sea ice models (after Mehlmann et al., 2021)

Despite recent developments, the vast majority of sea ice models are based on viscous-plastic rheology by Hibler III (1979). One of the most efficient methods to obtain accurate solutions for the highly nonlinear VP model is an implicit Jacobian-free Newton–Krylov solver (Lemieux et al., 2010, 2012; Losch et al., 2014), but such solvers are still very computationally expensive. More recent developments have been the modified Newton solver proposed in Mehlmann & Richter (2017a), the so-called operator-related damped Jacobi method, with a globalization of the line search method. They show an implicit scheme with improved convergence properties by combining an inaccurate Newton method with a Picard solver.

Alternatives include explicit Elastic-Viscous-Plastic (EVP) schemes, where an elasticity term is added to the stress equation to loosen the restrictive time-step limitation of VP models, see Hunke & Dukowicz (1997) and Hunke (2001). This idea is widely used in numerical sea ice modeling. Numerous other works show stabilizations and extensions of the EVP model to achieve adequate solutions. Kimmritz et al. (2015) and subsequent further publications that full convergence of the extended EVP model is too expensive for all practical purposes. The problems identified in the investigations show a strong mesh dependence. Although the quality of the solutions for the simulations with a coarse resolution is not affected, the stability problems may become more critical for simulations with finer grids. It is expected that on finer grids, more dynamic properties of the ice are solved with larger gradients in the solutions. This places high demands on the convergence of the solvers. Stability Investigations on the stability of the VP material model were already carried out in the 1990s. For example, Gray & Killworth (1995) investigated the Hibler VP model under uniaxial deformations using linear perturbation analysis and found it unstable when opened. The central ideas are whether

the constitutive law dissipates energy and whether the VP model has solutions sensitive to small changes in the initial conditions. The solutions are not limited, if the constitutive law generates energy. Small perturbations of the initial conditions (or of the solution at any point in time) grow causing initially nearby solutions to be different when the solutions are sensitive to the initial conditions. Schulkes (1996), Dukowicz (1997) and Gray & Killworth (1997) showed that the uniaxial model is globally stable because the constitutive law always dissipates energy during uniaxial opening or closing. Finally, Gray (1999) showed that the model is hyperbolic during uniaxial closing but loses the hyperbolic structure during the uniaxial opening, and numerically showed improper behavior. In all these investigations, the original VP law Hibler III (1979) was used, while Pritchard (2005) discusses the stability of the isotropic visco-plastic sea ice model with replacement closure (see Ip et al., 1991).

## 4.2. Small-scale sea ice modeling

### 4.2.1. Small-scale dynamics modeling

A typical feature of the Antarctic MIZ, particularly during the winter expansion (Alberello et al., 2019b), is the presence of highly mobile round pancake ice floes with interstitial grease ice and areas of open water (Kohout et al., 2014) that form in wavy conditions (Shen H.H. et al., 1987). Pancake ice floes exhibit characteristic diameters of 1 m to 10 m which are much smaller than ocean wavelengths (Alberello et al., 2019a). This is in contrast to ice floes found when consolidated ice breaks up during spring (Squire et al., 1995) and forming floes of a size comparable to the wavelengths typical for the Southern Ocean, ranging from 100 m to 200 m (Bennetts et al., 2017; Dolatshah et al., 2018).

## FESOM2 - Icepack Parameterizations

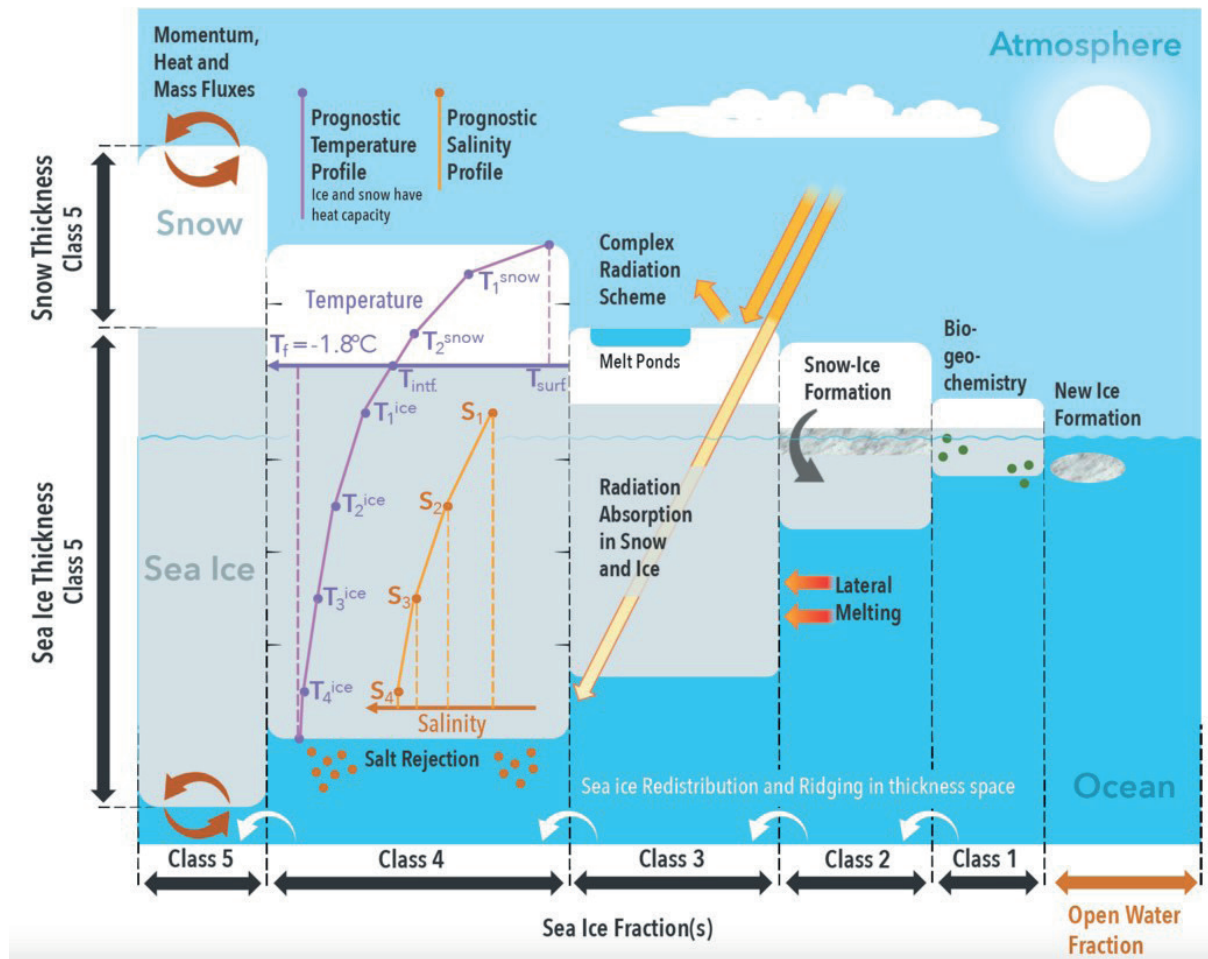


Fig. 22. Small-scale components of sea ice modeling (after <https://fesom.de>)

The latest models incorporate small-scale effects, e.g. floe-wave-interaction and others, into the modeling of large scale dynamics. As an example, Zampieri et al. (2021) implemented an advanced set of sea ice parameterizations derived from the single-column sea-ice model Icepack into FESOM2, see Figure 22. Further small-scale and multi-phase modeling approaches of sea ice formation are discussed in the following section.

### 4.2.2. Small-scale, multi-phase modeling of sea ice formation

Pancake sea ice morphology and dynamics are characterized by relatively free-floating floes of approximately 1–10 m in diameter, which is significantly smaller than the length of ocean waves (Alberello et al., 2019a). Due to the small ratio of pancake floe diameter to wavelength ratio, wave attenuation is dominated by dissipation (Bennetts & Squire, 2012; Squire, 2018). Only for the high wave energy regime at the ice edge, dissipation is attributed to turbulence generation, vortex shedding,

wave breaking, overtopping, overwashing of floes, floe fracture, and floe ridging (Squire, 2020). Due to the small freeboard of pancake floes, overwash is likely to occur as long as the incident ocean waves have not yet significantly attenuated (Nelli et al., 2020; Skene et al., 2015; Toffoli et al., 2015). Further inwards with the energetic high-frequency wave eliminated, dissipative effects are predominantly linked to friction, cohesion, and ridging in the floe-floe interaction (Lu et al., 2008; Rabatel et al., 2015; Shen H.H. & Squire, 1998; Sutherland et al., 2019; Yiew et al., 2017). Damping mechanisms due to the viscous interstitial grease ice as well as the turbulent boundary layer underneath the ice floe are characterized by eddy viscosity (Herman et al., 2019; Sutherland et al., 2019; Weber, 1987; Zhao & Shen, 2018). This behavior is short-range and governed locally, which is in contrast to consolidated ice (Weiss & Dansereau, 2017). When the consolidated ice breaks up in spring (Squire et al., 1995), the ice floes form with sizes comparable to the 100–200 m wavelengths typical

of the Southern Ocean (see Bennetts et al., 2017; Dolatshah et al., 2018). Floe size distributions have only recently been introduced in numerical large-scale models (Bennetts et al., 2017; Roach et al., 2018) showing that the simulated concentration of sea ice (covered area) can be significantly affected by the floe size.

### Reduction

Even with very detailed in situ sea ice and wave dynamics measurements, it remains difficult to link wave attenuation to specific dissipation mechanisms, if the spatial distribution of ice characteristics such as thickness, floe size, the area fraction of grease ice, and rheological properties, is unknown. Consequently, the fitting of elastic and viscous parameters of well-established phenomenological models results in a large spread of estimated values (Shen H.H., 2019). In particular, there is uncertainty regarding wave dissipation due to the choice of the post-collision restitution coefficient (Sutherland et al., 2019). The interpretation of the observed attenuation rates is extremely difficult, as it would require the simultaneous measurement of several wave and ice characteristics over large distances. For example, although synthetic aperture radar data provide information on the variability in wave height and direction over large spatial domains, the lack of accompanying spatial distribution of ice properties (thickness, floe size, elastic modulus, etc.) makes inferences regarding possible causes of that variability challenging (Herman et al., 2019). Furthermore, SAR-derived ice motion fields have a rather long interval between two images. Very seldom time difference between two images is less than a day making it impossible to infer any information on collisional rheology at the scale of a few seconds.

Most developed sea ice numerical models are based on a continuum or a discrete particle approach. Large-scale sea ice models are generally continuum models, of which the most well-known climate system model is the viscous-plastic model by Hibler III (1979). Finer-scale models mainly use the discrete element method on a floe-level (Leppäranta, 2011), in which the sea ice layer is modeled as a collection of interacting particles, i.e. ice floes. The discrete element models are mutually different in terms of the sea ice characteristics, collision mechanics between ice floes and the applied numerical methods (Herman, 2016).

Due to better computing capacities, an increasing interest in high-resolution sea ice predictions is being witnessed. Furthermore, the rapid decrease of sea ice is leading to more economic activity in polar regions. Zhang (2021) studied the sensitivity of sea ice properties for varying high-resolution sea ice models, show-

ing the insensitivity of large-scale sea ice properties, such as sea ice concentration, thickness, velocity, and the orientation of leads, to varying resolution within the multi-floe scale (less than 10 km). According to Zhang (2021) the parameters used in a coarse resolution model can be applied in a high-resolution model without modification of the parameter values. Heorton et al. (2018) and Ringeisen et al. (2019) state that the VP sea ice material law can be used for models with an even higher resolution (less than a km). However, the question remains as to whether the sea ice properties mentioned by Zhang (2021) need to be adjusted for these high resolutions.

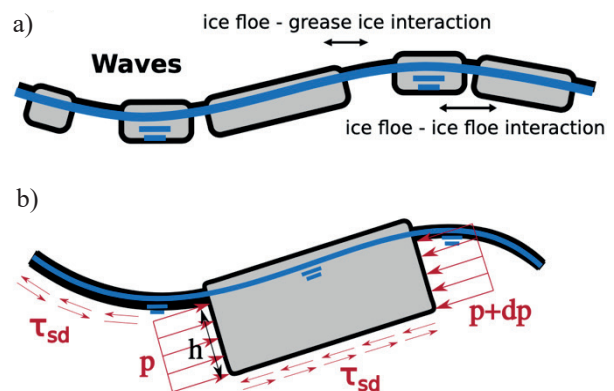


**Fig. 23.** Ice floe-ice floe and ice floe-grease ice interaction (a) and Froude-Krylov force acting at the circumference of ice floes and the skin drag acting at both the bottom of grease ice and ice floes (b) (Marquart et al., 2021)

Marquart et al. (2021) developed a high-resolution small-scale sea ice dynamics model that, unlike most existing fine-scale sea ice models, is described in a continuum form using the Eulerian approach. This model focuses on a region deeper in the marginal ice zone that is completely covered by realistically shaped pancake ice floes, obtained from *in-situ* camera images in the Antarctic MIZ (Alberello et al., 2019b), and interstitial grease ice. A wave load, represented by the sketch in Figure 23 and consisting of Froude-Krylov and skin drag components, are applied as an external force on the sea ice region leading to collisions of ice floes and interaction between ice floes and fat ice. Form drag is implicitly accounted for by the continuum approach due to velocity differences between the two types of ice and acts at the periphery of the ice floe. In addition to describing the coalescence and separation of ice floes, as discussed above, it is equally important to model the porous structure of sea ice and its associated formation processes. The freezing of the ocean surface below the freezing point of seawater heralds sea ice formation with the production of frazil ice crystals, compare to *Section 2.1.1*.

### Ice thickness distribution

A basic goal of physical sea ice models on scales of a millimeter to a meter is to predict the evolution of the ice thickness distribution (ITD) in time and space. The thermodynamic growth and melt rates are calculated by dividing the ice in each grid cell of the global climate model into thickness categories.

The ITD function  $g(x, h, t)dh$  describes the fractional area covered by ice in the thickness range  $(h, h + dh)$  at a given time and location. Its formulation covers the various physical processes with:

$$\frac{\partial g}{\partial t} = -\nabla \cdot (g \cdot v) + \psi - \frac{\partial}{\partial h}(f \cdot g) + \theta^g \quad (12)$$

where  $v$  is the two-dimensional horizontal ice velocity,  $\psi$  the mechanical redistribution function and  $f$  is the vertical growth rate. Vancoppenolle et al. (2013) extend Equation (12) by the additional term  $\theta^g$ , which accounts for one-dimensional bio-geo-chemical (BGC) models in undeformed sea ice. Current models calculate the physical component based on the generic thermodynamic framework by Maykut & Untersteiner (1971) by dividing the sea ice column into  $N$  layers, covered by snow.

Changes in ice thickness are derived by balancing the interfacial heat budgets considering oceanic, inner conductive, and atmospheric fluxes. The model introduced by Bitz & Lipscomb (1999) also considers the dependence of salinity and temperature on the thermal properties and constitutes the reference thermodynamic component of several large-scale sea ice models.

Brine dynamics have to be included as they are an important part of the small-scale sea ice formation and essential to describe nutrient concentration and transport. Recently, the volume averaging mushy layer theory has been applied to model the multiphase, reactive porous nature of sea ice (cf. Vancoppenolle & Tedesco, 2017). The theoretical framework of the mushy layer theory provides conservation equations for a two-phase system of solid and liquid fractions, averaged over a representative volume. Consistent formulations for the conservation of heat, mass, salt, and further concentrations are given in combination with an additional equation to describe the phase equilibrium between salty brine and the surrounding freshwater. The latest studies of Vancoppenolle et al. (2010), Turner et al. (2013), Griewank & Notz (2013), Jeffrey & Hunke (2014) and Rees Jones & Grae Worster (2014) applied the mushy layer theory in the context of 1D sea ice models across the thickness, using differing brine transport formulations.

Vancoppenolle et al. (2010) and Jeffrey et al. (2011) have developed schemes to couple dissolved tracers (nutrients, salt) to brine dynamics, but this approach has not been coupled to the biogeochemical processes.

Wells et al. (2013) investigated the mushy layer convection applied to sea ice. All of these contributions treat the solid ice as undeformable (rigid). A mushy layer model for the turbulent transport of salt and heat between ice and ocean, with a constant friction velocity, is proposed in (McGuinness, 2007). A simplified model for the diffusive controlled growth of mushy layers with modest cooling versus the solutal freezing-point depression is presented in (Wells et al., 2019).

In terms of sea ice growth, different approaches regarding numerical models have been developed. Grae Worster & Rees Jones (2015) have presented three models that take account of brine drainage, the corresponding fluxes as well as dynamic salinity profiles for growing sea ice using the balance of energy. Golden et al. (2020) and Oertling & Watts (2004) expand the set of equations by evaluating conservation of mass, momentum, salt concentration as well as energy. In the work by Golden et al. (2020), the ITD, as given in Equation (12), is stated to be a fundamental of modeling sea ice as it takes mass transport, ridging, and other mechanical processes into consideration. Here, the presented model evaluates ice growth, porosity, salinity, and emerging brine channels. Oertling & Watts (2004) make use of the principles of the mixture theory which leads to a binary model, also computing ice growth, salinity profiles as well as resulting dynamic brine fluxes inside the ice over time. Notz & Worster (2006) set up a 1D enthalpy model, simulating the ice fraction and salinity over time. The model focuses on brine movement where general procedures are given in Notz (2005). To implement enthalpy and salinity changes due to moving brine, a parameter is introduced which represents vertical brine displacements as a mean value for the entire horizontal area.

### TPM in general

Another approach for the multiphase description of sea ice formation is the Theory of Porous Media (TPM), which has the advantage of including a deformable solid. In Schwarz A. et al. (2020) a thermodynamically consistent macroscopic model based on the TPM is presented, which allows for the simulation of the coalescence and separation of ice floes due to frost-thawing cycles in calm sea and different weather conditions. The binary model used consists of the phases ice and liquid (seawater), where both phases are considered as incompressible material, i.e., the real densities of the constituents are constant. The main focus of the investigation lies on the temperature development in space and time as well as on the phase transition between water and ice and vice versa. The phase changes due to freezing, thawing or drying processes (liquid turns into vapor) are first-order phase transitions (see e.g. Elwell & Pointon, 1972). The de-

scription of thermo-mechanical processes in porous media in connection with heat and mass transport is given by Bear & Bachmat (1990) and Bear (2004).

Furthermore, the deformations of the ice phase are also considered. The influence of a gas and pore solution (gel water and non-freezable water, respectively) is not taken into account, i.e., the compensation of the volume expansion of water during freezing by a gas phase, the suction of water assigned to the gel water during thawing (see Setzer, 2001), and capillary effects (compare Helmig, 1997 and Ricken & de Boer, 2003), are not considered. The durability of water-infiltrated solids like concrete or soils under frost-thaw attack is of major significance in engineering (see Domone & Illston, 2010). The behavior of fluid-saturated porous media under cyclic freezing and thawing processes is strongly influenced by the phase transition as well as heat and mass transfer. Coussy (2005) discusses a macroscopic ternary model consisting of liquid, ice, and solid analyzing the effect of cooling rate and pore radius distribution during ice formation of water infiltrated porous materials below the freezing point is discussed. The model is to be understood as an extension of both the standard theory of poroelasticity (Biot, 1941) and the energy approach of poromechanics (see Coussy, 2004). Coussy (2005), Zhou M. & Meschke (2011), Meschke et al. (2011) and Zhou M.-M. (2013) presented a ternary model (solid, liquid and ice) in view of the description of the thermo-hydro-mechanical behavior of fluid saturated porous materials during freezing. Based on the TPM, Bluhm et al. (2009, 2011) and Ricken & Bluhm (2010) discussed an incompressible ternary model for the simulation of liquid saturated porous solids under freezing-thawing load. The influence of energetic effects during the phase transitions was demonstrated in (Bluhm et al., 2014). A history and overview of mathematical models of soil freezing and thawing have been given in (Kurylyk & Watanabe, 2013). Looking into this in more detail, the growth conditions and stages of sea ice determine whether sea ice has a columnar or granular texture. The crystal structure of ice plays an essential role in the formation of the porous structure. The crystal lattice structure is characterized by the rejection of salts from the ice solid matrix (Petrich & Eicken, 2010).

### Ice growth

The research interest in modeling the formation of the porous structure of sea ice dates back more than 100 years, with the first model of ice growth presented by Stefan (1891). This was a one-dimensional mathematical description of ice growth with a sharp moving boundary and negligible heat transport between the ice and the ocean. A variety of mathematical models have been proposed since. In works by Quincke (1905), Tiller et al. (1953), and Chalmers (1964), ice is polluted with salt as a liquid jelly, and the freezing process of salty water is considered as a solidification of binary alloys. A model investigating the brine channel volume, salinity profile or heat expansion without pattern formation is presented by Cox (1983) and Cox & Weeks (1983, 1988). A percolation model by Golden et al. (1998, 2006) is used to describe the role of percolation transitions in brine trapping during the solidification of seawater. In the work by Pringle et al. (2009), the percolation theory is presented to analyze the pore space connectivity using an X-ray computed tomography imaging of sea ice single crystals. The morphology and variability of brine networks in a vertical column of first-year sea ice are described using a percolation model by Lieblappen et al. (2018). A mushy layer model of sea ice is proposed in the paper by Feltham et al. (2006) following the thermodynamic sea ice model presented by Maykut & Untersteiner (1971). However, all these models do not provide a realistic pattern formation of the sea ice structure (Morawetz et al., 2017). The first investigations on a TPM model for the freezing process in sea ice is presented in the work by Schwarz A. et al. (2021), giving the results shown in Figure 24. They showcase a simulation of the freezing processes occurring between two ice floes.

They describe the findings on the development of ice in detail, including the mass exchange between the components and the temperature distribution in calm seas. A thermodynamically consistent approach is proposed for the identification of energy effects pertaining to the characterization and description of the phase transition.

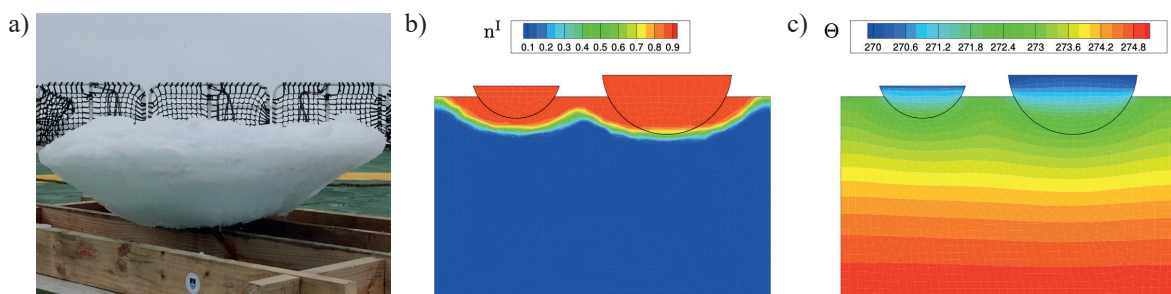


**Fig. 24.** Side view picture of a pancake ice flow (a), volume fraction ice  $n^I$  (b) and temperature  $\theta$  (c) for simplified two pancakes in sea water (after Schwarz A. et al., 2021)

### 4.3. Ocean-sea ice- and wave-sea ice-forcing

In the MIZ, highly dynamic processes take place in which wind, ocean currents, and waves interact with sea ice. In particular, wave-ice interactions play an important role in ice floe formation, retreat, bending, and fragmentation, depending on wave and sea ice properties (Shen H. et al., 2018; Stopa et al., 2018). Propagation of waves from the ice-free ocean into ice-covered waters results in momentum transfer from the ocean to ice floes due to wave dissipation and wave scattering. This effect is taken into account in modeling by means of an additional source term. This was given by Hibler III (1979) with:

$$\tau_{ocean} = C_{ocean} \rho_{ocean} (v - v_{ocean}) |v - v_{ocean}| \quad (13)$$

Here, the ocean water density is given with  $\rho_{ocean}$ ,  $C_{ocean}$  denotes the ocean drag coefficient and the ocean velocity is denoted as  $v_{ocean}$ . However, only the ocean dynamics can be considered on a large scale. In addition, wave sloshing and collisions with ice floes contribute to the loss of wave energy. Therefore, the wave-ice interactions are defined as a two-way street, since the wavefield changes the size distribution of the floes, while the presence of ice floes also changes the wave field. The interactions between waves and ice occur on small to medium scales, but significantly affect the large-scale dynamics and thermodynamics of sea ice. Conversely, ice sheet deformation is determined on a large scale by wind and ocean currents (Williams et al., 2013).

### 4.4. Atmosphere-sea ice-forcing

A major influence on the dynamics and thermodynamics of sea ice is the atmospheric boundary layer (ABL). For most of the year, the atmospheric boundary layer over sea ice has a stable or near-neutral stratification (see e.g. Andreas et al., 2000; Grachev et al., 2005; Persson et al., 2002). However, the sea ice cover is rarely uniform, but typically consists of floes of varying size and thickness and is interrupted by smaller and larger areas of open water, which are cracks, leads, and polynyas compare to (e.g. Andreas et al., 1979; Lüpkes et al., 2008).

Compared to the Arctic, the main differences in the lower boundary conditions for the atmosphere over Antarctic sea ice are as follows: Because the sea ice zone surrounds the Antarctic continent, the sea ice cover is thinner on average, ice concentrations are lower and the sea ice zone is at lower latitudes than in the Arctic. Katabatic winds carry cold continental air masses over the sea ice. These factors likely reduce

thermal stratification in the ABL, but the temporal and spatial distribution of stratification is not well known. Representing the atmosphere over sea ice in numerical models is challenging because of the difficulty in representing clouds, especially mixed-phase clouds, modeling the stable ABL correctly accounting for interactions with the surface and its various forms.

As early as 1979, Hibler III formulated a general form to account for wind forces. This model is still used in today's numerical modeling. Thereby, Hibler III describes the forces resulting from wind with:

$$\tau_{air} = C_{air} \rho_{air} v_{air} |v_{air}| \quad (14)$$

with the wind velocity  $v_{air}$  and  $C_{air}$  denoting the air drag coefficient.

In 1982, Thorndike & Colony (1982) took up the question of the influence of the geostrophic wind on the movement of the sea ice and supplemented existing rules of thumb with a further rough calculation. They found that none of the particularly large-scale ice divergences can be explained by the (geostrophic) wind. However, they limited their modeling to the Arctic, basing their data on the investigations of the AIDJEX expedition.

The work of Martinson & Wamser (1990) is based on the data set from the Winter Weddell Sea Project 1986 for the Antarctic winter, on the one hand, to describe the type of observed sea ice drift and the momentum exchange and on the other hand to determine relevant drag coefficients. "In general, the conditions in Antarctica are different than in the Arctic, and while the basic physics that govern the exchange of momentum are essentially independent of the environmental specifics, the parametric values and modeling approaches are not." (see Martinson & Wamser, 1990). This is what the authors point out, and motivates their delimitation from the previous work by Thorndike & Colony (1982), among others. By evaluating the measurements on pack ice for three different modeling approaches, the authors determine the ranges of values to be assumed for the models. It turns out that all three models are equally suitable.

Holland & Kwok (2012) present a data set of satellite-tracked sea-ice motion over the years 1992 to 2010 that demonstrates significant patterns in Antarctic ice drift that, in the majority of sectors, may be connected to regional winds. These trends are considerable and statistically significant. They measure the interior ice pack's dynamic and thermodynamic processes and demonstrate that, in much of West Antarctica, wind-driven changes in ice advection dominate, while wind-driven thermodynamic changes predominate elsewhere, see Figure 25.



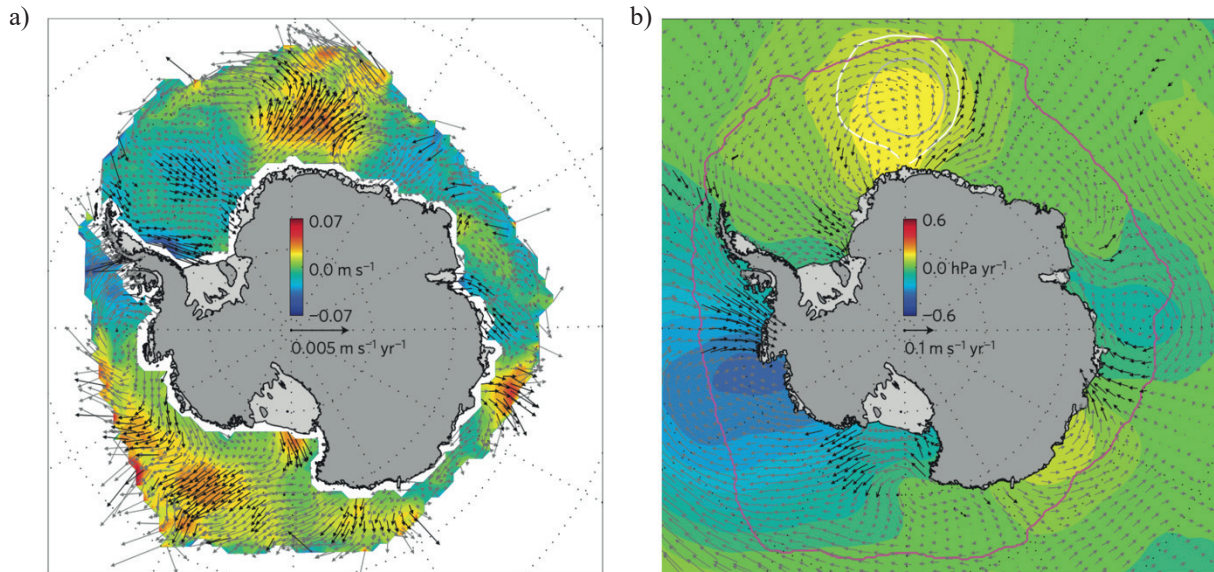


**Fig. 25.** Large and statistically significant changes in ice motion are driven by changes in the winds (taken from Holland & Kwok, 2012): a) ice-motion trend vectors overlaid on 19-year change in meridional ice speed (change is linear trend multiplied by period, positive northwards; black vectors have meridional ice-motion trends significant at >90%); b) ERA-Interim reanalysis 10-m wind trend vectors overlaid on trend in sea-level pressure (white and grey contours show pressure trends significant at 90% and 95%; black vectors have meridional wind trends significant at >90%; magenta contour shows extent of motion trends) (reproduced with permission from Springer Nature)

More recent work is often concerned with the Antarctic continent and shelf ice rather than with the sea ice surrounding the Antarctic. Regional simulations of the atmospheric boundary layer over Antarctic sea ice that have been adequately validated are rare. In Tastula et al. (2012) the Polar Weather Research and Forecasting investigated the mesoscale model to simulate conditions during Ice Station Weddell in the Southern hemisphere autumn and winter of 1992. They thus make an important contribution to understanding existing ABL models.

Atmospheric reanalysis are an important means of determining the relevant forces and offer the possibility of integrating the data sets directly into the modeling of sea ice. The daily cycles of the near-surface meteorological parameters over the Antarctic sea ice in six widely used atmospheric reanalysis (ERA-Interim, ERA-40, JRA-25, NASA-MERRA, NCEP-CFSR, and NCEP-DOE) are based on Tastula et al. (2013) and validated by observations from the Weddell Ice Station. The greatest deviations of the reanalysis from the observations are related to the general overestimation of the snow surface temperature, as well as the near-surface air temperature, the specific humidity, and the wind speed.

In the climate system, sea ice is both an important component and a very sensitive indicator of climate variability and change. The atmospheric boundary layer (ABL) plays an important role as a buffer between sea ice and most of the atmosphere; understanding the physics of the ABL is a prerequisite for reliable modeling

of the current and future climate in both polar regions, see (Thomas, 2017). A realistic description of the ABL is essential for the operational modeling of sea ice conditions, as it influences the wind forcing of the sea ice dynamics as well as the turbulence forcing and radiation.

#### 4.5. Rheological models

In the compressive state, when the stress is increased beyond a certain value, cracks appear, and when the stress is continued beyond this point, the coalescence of these cracks occurs and crushed ice is formed. Thus, from a modeling perspective, in a compression test ice undergoes a transition from a continuum model of the material to a discontinuous model with discrete particles. This requires two constitutive models, one for the solid ice and the other for the crushed ice. In our current discussion, we restrict ourselves to the constitutive model dealing with the solid state of ice.

Modeling sea ice is a challenging task because it exhibits inhomogeneous, anisotropic, and nonlinear viscous-plastic behavior. Important mechanical properties of sea ice such as compressive strength, elastic modulus, and Poisson's ratio depend to varying degrees on grain size and crystallographic orientation, porosity and salinity, strain or stress rate, temperature, confinement, and scale (Sand, 2008). This is discussed in detail in *Section 2*.

First-year ice has columnar crystals that are elongated in the vertical direction and have a substructure of platelets with horizontal  $c$ -axes. In most cases, the  $c$ -axes can be assumed to be randomly oriented in the horizontal plane of the ice sheet. A first-year ice floe is, therefore, anisotropic with different mechanical properties in the directions of the vertical and horizontal planes. When there is no preferred orientation of the  $c$ -axes in the horizontal plane, the ice is said to exhibit transverse isotropy, i.e., the ice floe is isotropic in the plane, but its properties in the vertical direction are different from those in the plane. When the columnar sea ice has a preferential  $c$ -axis orientation, the material is completely anisotropic. Thus, in order to model the constitutive behavior of first-year ice a formulation of a rate-dependent anisotropic, or transverse isotropic, plasticity model is needed.

**Rheological properties on the scale of few interacting ice floes**

The majority of climate models use (elastic-)viscous-plastic or elastic-plastic continuum models to simulate the behavior of sea ice on the large-scale (e.g. Feltham, 2008; Hibler III, 1979; Hunke & Dukowicz, 1997; Thorndike et al., 1975). In these models, sea ice behaves as isotropic plastic material with a hardening or weakening yield surface depending on the sea ice properties. However, continuum formulations do not properly represent sea ice behavior in the marginal ice zone, due to spatial variability in sea ice thickness and concentration resulting in large variations in the mechanical properties (Damsgaard et al., 2018). Feltham (2008) argues that the application of those continuum models implying the statistical average can be taken over a large number of floes are only appropriate, if the mode of failure of a single floe is the same as the failure mode of an agglomeration of floes.

Shen H.H. et al. (1987) described ice floe interactions in an idealized two-dimensional fragmented sea ice field consisting of an assembly of uniform disk shaped ice floes, by means of collisional rheology. Inelastic ice floe collisions cause stress acting in fragmented sea ice. As collisions transfer momentum, internal stress is generated in the deforming ice field. From this, a stress strain rate relationship can be obtained, since collisional energy losses are linked to the deformation energy. Existing collisional rheology models have contributed to the understanding of the sea ice flow in the MIZ, however, the collisional rheology has rarely been used in sea ice modeling, due to the used assumptions and idealized sea ice behavior, resulting in the underestimation of the collisional stress to total stress (Herman, 2016).

Feltham (2005) considered sea ice as a granular material with composite rheology, which describes

the interaction between viscous ice floe collisional and plastic components. This approach is based on previously developed models by Leppäranta & Hibler III (1985) and Shen H.H. et al. (1987). The discriminating feature between both rheological characteristics in the composite rheology is the extent to which random ice floe motions result in floe collisions.

Herman (2016) developed a Discrete-Element bonded-particle sea ice model to study the behavior of ice floes at the floe level. Here, ice floes are represented by disk-shaped floes connected by semi-elastic bonds, subjected to oceanic and atmospheric forcing. The ice floe interaction takes place due to direct contact and/or through bonds. Damsgaard et al. (2018) present a discrete element framework for the approximation of Lagrangian sea ice dynamics, which is also at the floe level. The modeling of fragmented sea ice in the MIZ is improved by using exact solutions for mechanical nonlinearities with arbitrary sea ice concentrations.

**Rheological properties on the scale of ice floe fields**

Considering the sea ice rheology on scales of multiple hundreds of kilometers, the resolution of single ice floes is not target-oriented. The components sea ice, seawater, and frazil ice are described by a single continuum. Here, it was certainly Hibler III (1979) who made a fundamental contribution to the material description of the continuum on this scale. Today, the majority of climate models use (elastic-)viscous-plastic or elastic-plastic continuum models to simulate the behavior of sea ice on the large-scale (e.g. Feltham, 2008; Hibler III, 1979; Hunke & Dukowicz, 1997; Thorndike et al., 1975). In these models, sea ice behaves as an isotropic plastic material, with a hardening or weakening yield surface depending on the sea ice properties, see Figure 26.

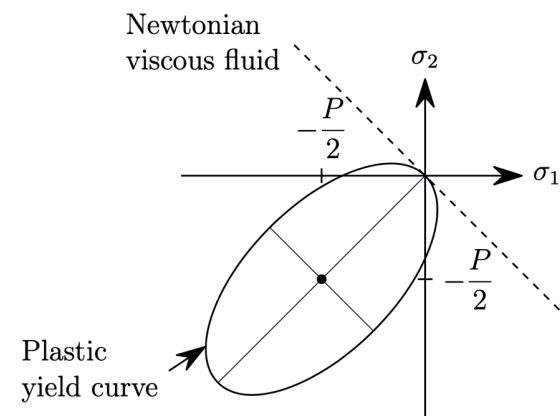


**Fig. 26.** Relationship of the principal components of the stresses ( $\sigma_1$  and  $\sigma_2$ ) for the viscous-plastic material law. The rheology considers an elliptical yield curve with a principal axes ratio of  $e = 2$  (the drawing is based on the illustrations in Hibler III, 1979)

A detailed description of this work and the developments of the rheological model based on it are presented in *Section 4.1*. Alternative rheological descriptions have been proposed recently, (see also Girard et al., 2011; Tsamados et al., 2013; Rampal et al., 2016). The later papers are devoted to the rheological description of sea ice in the Arctic, but nevertheless, provide an important impetus to further improve the rheological description of ice in the Antarctic MIZ as well.

#### 4.6. Fracture mechanics

Fractures within the cover during summer lower the albedo and enable more shortwave absorption by the ocean, which shrinks the cover, reducing its strength and possibly propagating fracturing (Girard et al., 2009; Moritz et al., 2002; Rampal et al., 2009; Zhang et al., 2000). In contrast, fracturing during winter raises the thermodynamically-driven production of new ice and changes the heat and salinity budget in the region (Maykut, 1982). All year round, increased sea ice fracturing and fragmentation promote sea ice drift and export toward lower latitudes (Rampal et al., 2009). These fracture processes are complex and highly nonlinear. They need to be investigated in more detail to understand their role in the climate system, and met-ocean thermodynamics (Rampal et al., 2011). Therefore, modeling the fracturing of Antarctic sea ice reliably is essential to obtain a good representation of the open water fraction, the thickness distribution, and the global sea ice mass balance in climate models (Girard et al., 2009).

Several computational methods have been used to describe the fracture process by predicting the nucleation and propagation of cracks. Some of these methods are finite element methods, which rely on the implementation of sharp crack discontinuities. They are generally implemented using interface element formulations (Camacho & Ortiz, 1996; Gürses & Miehe, 2009; Miehe & Gürses, 2007; Pandolfi & Ortiz, 2002; Xu & Needleman, 1994), nodal enrichment formulations, the so-called extended finite element methods (Belytschko et al., 2003; Fagerström & Larsson, 2006; Song & Belytschko, 2009; Song et al., 2006, 2008) and embedded discontinuities (Armero & Linder, 2009; Linder & Armero, 2009). However, they experience difficulties in handling complex crack branching in three dimensions. Other methods include the discrete element method, which is used to describe the discontinuous distribution characteristics of sea ice (Bateman et al., 2019; Herman et al., 2018; Xu et al., 2012), and the peridynamics method, which is a meshless method

based on the non-local continuous dynamic theory (Liu et al., 2020; Ren et al., 2021; Wang Q. et al., 2018).

In contrast to the above methods, phase-field methods use a diffusive crack approach with a smooth continuum formulation to avoid modeling discontinuities. Since jump discontinuities are not considered, the phase-field method, unlike sharp crack models, can be implemented within a finite element formulation with standard continuous shape functions. Furthermore, no meshing techniques are required to simulate crack growth, since the introduction of the phase-field means that cracks are not represented based on a mesh or geometry. Thus, this method can accurately describe complex topological changes, including multiple branching or the merging of cracks (Miehe et al., 2010). The basic concept of phase-field methods is to add a continuous scalar field, called a phase-field or order parameter, which characterizes the material states. When modeling fractures, this method assigns a value of 0 to the phase-field to denote an undamaged material and a value of 1 for a fractured material. This field bypasses the discontinuous jumps at crack interfaces by interpolating between the phases of the undamaged and fractured material across the diffusion interface. An original length scale parameter is used to determine the width of this crack interface. Thus, the underlying sharp crack recovers when this parameter is infinitesimally small. The evolution of the phase-field is represented by a partial differential equation describing the fracture process. In addition, a degradation function models the change in material stiffness between the undamaged and fractured states by coupling the evolution and elastic field equations (Ambati et al., 2014).

Recently, the phase-field method has gained popularity in modeling the porous structure of sea ice because it allows for the description of a realistic pattern formation (Morawetz et al., 2017). The technique adds the phase-field or order parameter to the other fields, such as temperature and displacement fields. The parameter takes constant values in the bulk of each phase. It continuously interpolates between values in the bulk across a thin boundary layer that describes the interface between the phases. The parameter can be viewed as a tool that characterizes the degree of atomic order or disorder in the phases and allows the interface to be smeared over a diffusion region for numerical convenience. Phase-field models usually use a phenomenological functional of free energy expressed by the phase field and other fields to connect to thermodynamics. Through a dissipative minimization of the free energy, a set of nonlinear differential equations govern the dynamics of order parameters, heat, or mass transport (Provatas & Elder, 2010).

As for phase-field modeling of the structure of sea ice, Kutschan et al. (2010) were the first to present a model for the phenomenological description of the porous structure by including a Ginzburg–Landau equation for the ice–water transition and a reaction–diffusion equation for the salinity parameter. Berti V. et al. (2013) and Grandi (2013) proposed mathematical models that replace the reaction–diffusion equation with a Cahn–Hilliard equation to ensure the concomitant separation between salt and (frozen) water.

Berti V. et al. (2013) proposed a model to describe the porous structure of sea ice, while Grandi (2013) presented a model for the liquid–solid phase transition of saltwater under non-isothermal conditions. These two models consist of three evolution equations: a time-dependent Ginzburg–Landau equation for the liquid–solid phase transition, a diffusion equation of the Cahn–Hilliard type for the salt concentration, and a heat equation for the temperature change. Thoms et al. (2014) and Morawetz et al. (2017) presented a two-dimensional model for sea ice describing the liquid–solid phase transition on short time scales in the absence of spatial temperature gradients in ice or water and used a finite difference scheme to solve the system of equations. Berti A. et al. (2016) proposed a mathematical model for sea ice formation that includes a liquid–solid phase transition and phase separation under non-isothermal conditions, as well as cryoscopic and mechanical effects. Fabrizio et al. (2016) presented a mathematical model for solidification and separation in saline water considering thermal effects.

Current model developments notwithstanding, the understanding of the chemical thermodynamics governing seawater freezing still needs to be improved. In particular, the process leading to the formation of the brine-filled pore and channel structure in sea ice, including the precipitation of salt ions, is poorly understood. Existing mathematical models of sea ice formation that account for the liquid–solid phase transition, ice–salt phase separation, and thermal effects can only be addressed by numerical simulations due to their complexity. Realistic prediction of three-dimensional sea ice growth has not yet been achieved. Precipitation of salt ions also remains unexplored in these models. Therefore, the objective of the present study is to model the formation of sea ice in a realistic three-dimensional domain and to account for the precipitation of salt ions. First, the model will account for the phase transition between liquid and solid, phase separation between ice and salt, cryoscopic and thermal effects, and precipitation of salt ions. Second, the numerical simulations of the model in three dimensions can take into account and allow for quantitative comparisons between exper-

iment and pattern formation prediction (Dong et al., 2017; Middleton et al., 2016; Thoms et al., 2014). Finally, the inclusion of the precipitation of salt ions in the model will help to better understand the influence of salt ions on the freezing kinetics of seawater and thus reliably predict the behavior of sea ice (Petrich & Eicken, 2010).

## 5. Conclusion – recent developments and future directions

To effectively bridge the gap between modeling, observation, and experiment, the following key strategies are proposed:

- Properties such as Young’s modulus, strength, and toughness have mainly been measured in the Arctic region. These values depend on porosity, salinity, and temperature, which are assumed to be different in the Antarctic region than in the Arctic due to variations in environmental conditions. It is currently unknown how reliably data from the Arctic can be applied to Antarctic sea ice. Reliable material properties are essential for numerical calculations that are as realistic as possible. As indicated by the constitutive law, Equation (9), the viscosity and yield strength of sea ice play an important role in the calculation of the constitutive behavior on large scales. Nevertheless, almost no data are available from the MIZ for Antarctic sea ice. Thus, the determination of these data can make an important contribution to improving the numerical modeling of sea ice in the southern hemisphere.
- In addition to the importance of salinity and porosity for deriving mechanical properties, they also provide information on the growth process of sea ice. For the MIZ of Antarctica, only limited data are available in this respect.
- Fracture processes in sea ice are complex and highly nonlinear and need to be studied in more detail to understand their role in the climate system and metocean thermodynamics (Rampal et al., 2011). Thus, reliable modeling of Antarctic sea ice fractures is essential to understand floe coalescence and breakup in order to obtain a good representation of the open water fraction, thickness distribution, and global sea ice mass balance in climate models (Girard et al., 2009).
- It is known that the crystal basal plane growth is the preferred growth direction for ice. It Which angle is the preferred growth direction for sea ice in the transition zone from granular to columnar texture is currently unknown. Is there a threshold

- angle with the highest growth speed, which will succeed in the majority of cases, or is it arbitrary? Does this angle have an influence on the failure plane of sea ice, and if so how does it influence the failure behavior of ice?
- Encapsulated brine pockets are always present in sea ice and are mainly responsible for its special behavior in contrast to fresh-water ice. How do brine pockets change over the freezing and melting period? Do they act as a chemical stress intensity factor for fracture toughness? Do brine pockets show an auto-weakening behavior on sea ice and how does the shape of brine pockets transform over the year?
  - Further research is warranted into investigating and developing precise understandings of the changes of physical and structural properties that samples undergo under differing storage conditions.
  - Filled and unfilled brine pockets have different effects on sea ice strength. Water-filled pores should not influence the compression strength but the shear strength. Further experiments are necessary to determine the difference between open porosity and closed porosity. Brittle fracture statistics (statistical fracture mechanics) will need to be applied.
  - Improvement and further development of the rheological description of sea ice at all scales is an important prerequisite for the reliable modeling of sea ice dynamics and thermodynamics. This needs to be pursued jointly by the scientific branches of experimental investigation, observational strategies, and thermodynamic modeling.
  - It has been noticed that the current literature only deals sporadically with the distinction between First-Year ice and Multi-Year ice. In the Antarctic, however, large parts of the ice are predominantly First-Year ice, while the ice of the Arctic is still in many places Multi-Year ice. The ongoing trend of melting ice in the Arctic also leads to an increased portion of first-year ice. The simulation models must, therefore, be adapted to the changed situation. Deeper knowledge of first-year ice in the Antarctic may contribute to a better understanding of the processes at both poles.
  - Not enough observations have been made to understand the extent to which the lower latitudes, lower sea ice concentrations, and thinner ice in Antarctica affect the structure and processes in the atmospheric boundary layer (ABL), see *Section 4.4*. Due to the lack of accurate observations and the complexity of the highly interactive physical processes associated with mixed-phase clouds, radiative transfer, turbulence, waves, and air-snow-ice coupling, serious challenges remain in modeling the atmosphere over sea ice. Numerical weather prediction models, atmospheric reanalysis, and climate models all have large errors in surface and near surface variables, especially in terms of the currents. More year-round in situ observations from the Arctic and Antarctic sea ice zones are needed to improve this situation, together with closer collaboration between observational and modeling communities, including those involved in remote sensing.

## Acknowledgment

The SCALE cruises are funded by the South African National Research Foundation (NRF) through the South African National Antarctic Programme (SANAP), with contributions from the Department of Science and Innovation and the Department of Environmental Affairs. All authors of this work are deeply grateful to NRF for this continued support. Special thanks to T. Behrendt for their exceptional contribution in designing several figures, enhancing the visual appeal and clarity of our paper's publication.

## Open research

All data used in the creation of this review paper were previously published in different studies. All studies used for this paper are cited and publicly available. Figures are published on Figshare: 10.6084/m9.figshare.22317235.

## References

- Adamson, R.M., Dempsey, J.P., DeFranco, S.J., & Xie, Y. (1995). Largescale in-situ ice fracture experiments: Part I – Experimental aspects. In J.P. Dempsey, Y. Rajapakse (Eds.), *Ice Mechanics, 1995, presented at the 1995 Joint ASME Applied Mechanics and Materials Summer Meeting, Los Angeles, California, June 28–30, 1995* (pp. 107–128). American Society of Mechanical Engineers.
- Alberello, A., Nelli, F., Dolatshah, A., Bennetts, L.G., Onorato, M., & Toffoli, A. (2019a). An experimental model of wave attenuation in pancake ice. In *The 29<sup>th</sup> International Ocean and Polar Engineering Conference*. International Society of Offshore and Polar Engineers.

- Alberello, A., Onorato, M., Bennetts, L., Vichi, M., Eayrs, C., MacHutchon, K., & Toffoli, A. (2019b). Brief communication: Pancake ice floe size distribution during the winter expansion of the antarctic marginal ice zone. *Cryosphere*, *13*(1), 41–48.
- Alberello, A., Bennetts, L., Heil, P., Eayrs, C., Vichi, M., MacHutchon, K., Onorato, M., & Toffoli, A. (2020). Drift of pancake ice floes in the winter Antarctic marginal ice zone during Polar cyclones. *Journal of Geophysical Research: Oceans*, *125*(3), e2019JC015418.
- Alberello, A., Bennetts, L.G., Onorato, M., Vichi, M., MacHutchon, K., Eayrs, C., Ntamba, B.N., Benetazzo, A., Bergamasco, F., Nelli, F., Pattani, R., Clarke, H., Tersigni, I., & Toffoli, A. (2022). Three-dimensional imaging of waves and floes in the marginal ice zone during a cyclone. *Nature Communications*, *13*(1), 4590.
- Aly, M., Taylor, R., Bailey Dudley, E., & Turnbull, I. (2019). Scale effect in ice flexural strength. *Journal of Offshore Mechanics and Arctic Engineering*, *141*(5), 051501.
- Ambati, M., Gerasimov, T., & De Lorenzis, L. (2014). A review on phasefield models of brittle fracture and a new fast hybrid formulation. *Computational Mechanics*, *55*(2), 383–405.
- Andreas, E., Paulson, C., William, R., Lindsay, R., & Businger, J. (1979). The turbulent heat flux from Arctic leads. *Boundary-Layer Meteorology*, *17*(1), 57–91.
- Andreas, E., Claffy, K., & Makshtas, A. (2000). Low-level atmospheric jets and inversions over the western Weddell Sea. *Boundary-Layer Meteorology*, *97*(3), 459–486.
- Arduin, F., Otero, M., Merrifield, S., Grouazel, A., & Terrill, E. (2020). Ice breakup controls dissipation of wind waves across Southern Ocean sea ice. *Geophysical Research Letters*, *47*(13), e2020GL087699.
- Armero, F., & Linder, C. (2009). Numerical simulation of dynamic fracture using finite elements with embedded discontinuities. *International Journal of Fracture*, *160*(2), 119–141.
- Azizi, F. (1989). Primary creep of polycrystalline ice under constant stress. *Cold Regions Science and Technology*, *16*(2), 159–165.
- Bailey, E. (2011). *The Consolidation and Strength of Rafted Sea Ice* [PhD thesis], University College London.
- Bargel, H.-J., Schulze, G. (Hrsg.), Hilbrans, H., Hübner, K.-H., & Krüger, O. (2008). *Werkstoffkunde* (10, bearbeitete Auflage). Springer Berlin.
- Bateman, S.P., Orzech, M.D., & Calantoni, J. (2019). Simulating the mechanics of sea ice using the discrete element method. *Mechanics Research Communications*, *99*, 73–78.
- Bear, J. (2004). Mathematical models of flow and contaminant transport in saturated porous media. In J. Kubik, M. Kaczmarek, & J. Murdoch (Eds.), *Modelling Coupled Phenomena in Saturated Porous Materials. Advanced course, Bydgoszcz, June 2–6, 2003* (pp. 89–178). Centre of Excellence for Advanced Materials and Structures, Institute of Fundamental Technological Research.
- Bear, J., & Bachmat, Y. (1990). *Introduction to Modeling of Transport Phenomena in Porous Media*. Springer Dordrecht.
- Becker, E. (1976). The finite element method in AIDJEX. *AIDJEX Bulletin*, *33*, 144–157.
- Belosi, F., Santachiara, G., & Prodi, F. (2014). Ice-forming nuclei in Antarctica: New and past measurements. *Atmospheric Research*, *145–146*, 105–111.
- Belytschko, T., Chen, H., Xu, J., & Zi, G. (2003). Dynamic crack propagation based on loss of hyperbolicity and a new discontinuous enrichment. *International Journal for Numerical Methods in Engineering*, *58*(12), 1873–1905.
- Bennetts, L.G., & Squire, V.A. (2012). On the calculation of an attenuation coefficient for transects of ice-covered ocean. *Proceedings of the Royal Society A: Mathematical, Physical and Engineering Sciences*, *468*(2137), 136–162.
- Bennetts, L., O’Farrell, S., & Uotila, P. (2017). Brief communication: Impacts of ocean-wave-induced breakup of Antarctic sea ice via thermodynamics in a stand-alone version of the CICE sea-ice model. *The Cryosphere*, *11*(3), 1035–1040.
- Berti, A., Bochicchio, I., & Fabrizio, M. (2016). Transition and separation process in brine channels formation. *Journal of Mathematical Physics*, *57*(2), 023513.
- Berti, V., Fabrizio, M., & Grandi, D. (2013). A phase field model for brine channels in sea ice. *Physica B: Condensed Matter*, *425*, 100–104.
- Biot, M. (1941). General theory of three-dimensional consolidation. *Journal of Applied Physics*, *12*(2), 155–164.
- Bitz, C.M., & Lipscomb, W.H. (1999). An energy-conserving thermodynamic model of sea ice. *Journal of Geophysical Research*, *104*(C7), 15699–15677.
- Bitz, C., Holland, M., Weaver, A., & Eby, M. (2001). Simulating the icethickness distribution in a coupled climate model. *Journal of Geophysical Research: Oceans*, *106*(C2), 2441–2463.
- Blackford, J.R. (2007). Sintering and microstructure of ice: a review. *Journal of Physics D: Applied Physics*, *40*(21), R355–R385.
- Bluhm, J., Ricken, T., & Bloßfeld, M. (2009). *Dynamic Phase Transition Border under Freezing-Thawing Load – A Multiphase Description. Technical Report 47*. J. Schröder (Ed.). Institute of Mechanics, University Duisburg-Essen.
- Bluhm, J., Ricken, T., & Bloßfeld, M. (2011). Ice formation in porous media. In B. Markert (Ed.), *Advances in Extended and Multifield Theories for Continua* (pp. 153–174). Springer Berlin, Heidelberg.
- Bluhm, J., Bloßfeld, W.M., & Ricken, T. (2014). Energetic effects during phase transition under freezing-thawing load in porous media – a continuum multiphase description and FE-simulation. *Journal of Applied Mathematics and Mechanics*, *94*(7–8), 586–608.
- Bonath, V., Edeskär, T., Lintzén, N., Fransson, L., & Cwirzen, A. (2019). Properties of ice from first-year ridges in the Barents Sea and Fram Strait. *Cold Regions Science and Technology*, *168*, 102890.
- Budyko, M. (1969). The effect of solar radiation variations on the climate of the Earth. *Tellus*, *21*(5), 611–619.
- Butkovich, T.R. (1956). *Strength Studies of Sea Ice*. Technical report.

- Butkovich, T.R. (1959). *Some Physical Properties of Ice from the TUTO Tunnel and Ramp, Thule, Greenland*. U.S. Army Snow, Ice, and Permafrost Research Establishment.
- Camacho, G., & Ortiz, M. (1996). Computational modelling of impact damage in brittle materials. *International Journal of Solids and Structures*, 33(20–22), 2899–2938.
- Cavaliere, D., Cowan, A., Gloersen, P., Grenfell, T., Josberger, E., Knight, R., Martin, S., Muench, R., Overland, J., Pease, C., Powell, J., Reynolds, R., Schumacher, J., Squire, V., Wadhams, P., & Wilheit, T. (1983). MIZEX West: Bering Sea marginal ice zone experiment. *Eos, Transactions American Geophysical Union*, 64(40), 578–579.
- Chalmers, B. (1964). *Principles of Solidification*. Wiley.
- Champollion, N., Picard, G., Arnaud, L., Lefebvre, E., & Fily, M. (2013). Hoar crystal development and disappearance at Dome C, Antarctica: observation by near-infrared photography and passive microwave satellite. *The Cryosphere*, 7(4), 1247–1262.
- Chen, X., & Ji, S. (2019). Experimental study on the tensile strength of granular sea ice based on Brazilian tests. In *Proceedings of the 25th International Conference on Port and Ocean Engineering under Arctic Conditions June 9–13, 2019, Delft, The Netherlands*. Port and Ocean Engineering under Arctic Conditions (POAC).
- Colbeck, S.C. (1982). An overview of seasonal snow metamorphism. *Reviews of Geophysics*, 20(1), 45–61.
- Cole, D.M., Gould, L.D., & Burch, W.B. (1985). A system for mounting end caps on ice specimens. *Journal of Glaciology*, 31(109), 362–365.
- Coussy, O. (2004). *Poromechanics*. Wiley.
- Coussy, O. (2005). Poromechanics of freezing materials. *Journal of the Mechanics and Physics of Solids*, 53(8), 1689–1718.
- Cox, G.F.N. (1983). Thermal expansion of saline ice. *Journal of Glaciology*, 29(103), 425–432.
- Cox, G.F.N., & Richter-Menge, J.A. (1984). *Mechanical Properties of Multi-year Sea Ice Triaxial Tests Status Report*. Technical report. U.S. Army Cold Regions Research and Engineering Laboratory, Hanover.
- Cox, G.F.N., & Richter-Menge, J.A. (1985). Tensile strength of multi-year pressure ridge sea ice samples. *Journal of Energy Resources Technology*, 107(3), 375–380.
- Cox, G.F.N., & Weeks, W.F. (1983). Equations for determining the gas and brine volumes in sea ice samples. *Journal of Glaciology*, 29(102), 306–316.
- Cox, G.F.N., & Weeks, W.F. (1986). Changes in the salinity and porosity of sea-ice samples during shipping and storage. *Journal of Glaciology*, 32(112), 371–375.
- Cox, G.F.N., & Weeks, W.F. (1988). Numerical simulations of the profile properties of undeformed first-year sea ice during the growth season. *Journal of Geophysical Research*, 93(C10), 12449–12460.
- Crabeck, O., Galley, R., Delille, B., Else, B., Geilfus, N.X., Lemes, M., Roches, M.D., Francus, P., Tison, J.L., & Rysgaard, S. (2016). Imaging air volume fraction in sea ice using non-destructive X-ray tomography. *The Cryosphere*, 10(3), 1125–1145.
- Cuffey, K.M., & Paterson, W.S.B. (2010). *The Physics of Glaciers* (Fourth ed.). Butterworth-Heinemann/Elsevier.
- Damsgaard, A., Adcroft, A., & Sergienko, O. (2018). Application of discrete element methods to approximate sea ice dynamics. *Journal of Advances in Modeling Earth Systems*, 10(9), 2228–2244.
- Damsgaard, A., Sergienko, O., & Adcroft, A. (2021). The effects of ice floe-floe interactions on pressure ridging in sea ice. *Journal of Advances in Modeling Earth Systems*, 13(7), e2020MS002336.
- Danilov, S., Kivman, G., & Schröter, J. (2004). A finite-element ocean model: principles and evaluation. *Ocean Modelling*, 6(2), 125–150.
- Danilov, S., Wang, Q., Timmermann, R., Iakovlev, M., Sidorenko, D., Kimmritz, M., & Jung, T. (2015). Finite-element sea ice model (FESIM), version 2. *Geoscientific Model Development*, 8(6), 1747–1761.
- Danilov, S., Sidorenko, D., Wang, Q., & Jung, T. (2017). The finite-volume sea ice–ocean model (FESOM2). *Geoscientific Model Development*, 10(2), 765–789.
- DeConto, R.M., & Pollard, D. (2003). Rapid Cenozoic glaciation of Antarctica induced by declining atmospheric CO<sub>2</sub>. *Nature*, 421, 245–249.
- DeFranco, S.J., & Dempsey, J.P. (1994). Crack propagation and fracture resistance in saline ice. *Journal of Glaciology*, 40(136), 451–462.
- DeFranco, S.J., Wei, Y., & Dempsey, J.P.D. (1991). Notch-acuity effects on the fracture toughness of saline ice. *Annals of Glaciology*, 15, 230–235.
- Dempsey, J.P. (1991). The fracture toughness of ice. In S. Jones, J. Tillotson, R.F. McKenna, I.J. Jordaan (Eds.), *Ice-Structure Interaction. IUTAM/LAHR Symposium St. John's, Newfoundland Canada 1989* (pp. 109–145). Springer Berlin, Heidelberg.
- Dempsey, J.P., Bentley, D.L., & Sodhi, D.S. (1986). Fracture toughness of model ice. In *8<sup>th</sup> International Symposium on Ice, Iowa City, August 18–22, 1986* (Vol. 1, pp. 365–376).
- Dempsey, J.P., Adamson, R.M., & Mulmule, S.V. (1999). Scale effects on the *in-situ* tensile strength and fracture of ice. Part II: First-year sea ice at Resolute, N.W.T. *International Journal of Fracture*, 95, 347–366.
- Doble, M.J., Wilkinson, J.P., Valcic, L., Robst, J., Tait, A., Preston, M., Bidlot, J.-R., Hwang, B., Maksym, T., & Wadhams, P. (2017). Robust wavebuoys for the marginal ice zone: Experiences from a large persistent array in the Beaufort sea. *Elementa: Science of the Anthropocene*, 5, 47.
- Dolatshah, A., Nelli, F., Bennetts, L., Alberello, A., Meylan, M., Monty, J., & Toffoli, A. (2018). Letter: Hydroelastic interactions between water waves and floating freshwater ice. *Physics of Fluids*, 30(9), 091702.
- Domone, P., & Illston, J. (Eds.) (2010). *Construction Materials: Their Nature and Behavior*. Spon Press.
- Dong, X.-l., Xing, H., Weng, K.-r., & Zhao, H.-l. (2017). Current development in quantitative phase-field modeling of solidification. *Journal of Iron and Steel Research International*, 24(9), 865–878.

- Dukowicz, J. (1997). Comments on “Stability of the Viscous–Plastic Sea Ice Rheology”. *Journal of Physical Oceanography*, 27(3), 480–481.
- Duval, P., Ashby, M.F., & Anderman, I. (1983). Rate-controlling processes in the creep of polycrystalline ice. *The Journal of Physical Chemistry*, 87(21), 4066–4074.
- Dykens, J. (1967). Tensile properties of sea ice grown in a confined system. In *Physics of Snow and Ice. International Conference on Low Temperature Science. 1. Conference on Physics of Snow and Ice Aug., 14–19, 1966, Sapporo* (pp. 523–537). Institute of Low Temperature Science.
- Dykens, J.E. (1971). *Ice Engineering – Material Properties of Saline Ice for a Limited Range of Conditions*. Technical report. Naval Civil Engineering Lab Port Hueneme Calif.
- Eayrs, C., Holland, D., Francis, D., Wagner, T., Kumar, R., & Li, X. (2019). Understanding the seasonal cycle of Antarctic sea ice extent in the context of longer-term variability. *Reviews of Geophysics*, 57(3), 1037–1064.
- Eicken, H. (1992). Salinity profiles of Antarctic sea ice: Field data and model results. *Journal of Geophysical Research: Ocean*, 97(C10), 15545–15557.
- Eicken, H. (2003). From the microscopic, to the macroscopic, to the regional scale: growth, microstructure and properties of sea ice. In D.N. Thomas, G. Dieckmann (Eds.), *Sea Ice: an Introduction to Its Physics, Chemistry, Biology, and Geology* (pp. 22–81). Blackwell Science.
- Eicken, H., & Lange, M.A. (1989). Development and properties of sea ice in the coastal regime of the southeastern Weddell Sea. *Journal of Geophysical Research*, 94(C6), 8193–8206.
- Eicken, H., Kolatschek, J., Freitag, J., Lindemann, F., Kassens, H., & Dmitrenko, I. (2000). A key source area and constraints on entrainment for basin-scale sediment transport by Arctic sea ice. *Geophysical Research Letters*, 27(13), 1919–1922.
- Eicken, H., Gradinger, R., Gaylord, A., Mahoney, A., Rigor, I., & Melling, H. (2005). Sediment transport by sea ice in the Chukchi and Beaufort Seas: Increasing importance due to changing ice conditions?. *Deep Sea Research Part II: Topical Studies in Oceanography*, 52(24–26), 3281–3302.
- Elwell, L., & Pointon, A.J. (1972). *Classical Thermodynamics*. Penguin.
- Emery, W.J., Fowler, C.W., & Maslanik, J.A. (1997). Satellite-derived maps of Arctic and Antarctic sea ice motion: 1988 to 1994. *Geophysical Research Letters*, 24(8), 897–900.
- Eriksen, C., Osse, T., Light, R., Wen, T., Lehman, T., Sabin, P., Ballard, J., & Chiodi, A. (2001). Seaglider: a long-range autonomous underwater vehicle for oceanographic research. *IEEE Journal of Oceanic Engineering*, 26(4), 424–436.
- Fabrizio, M., Giorgi, C., & Morro, A. (2016). Solidification and separation in saline water. *Discrete & Continuous Dynamical Systems – Series S*, 9(1), 139–155.
- Fagerström, M., & Larsson, R. (2006). Theory and numerics for finite deformation fracture modelling using strong discontinuities. *International Journal for Numerical Methods in Engineering*, 66(6), 911–948.
- Feltham, D.L. (2005). Granular flow in the marginal ice zone. *Philosophical Transactions of the Royal Society A: Mathematical, Physical and Engineering Sciences*, 363(1832), 1677–1700.
- Feltham, D.L. (2008). Sea ice rheology. *Annual Review of Fluid Mechanics*, 40, 91–112.
- Feltham, D.L., Untersteiner, N., Wettlaufer, J.S., & Worster, M.G. (2006). Sea ice is a mushy layer. *Geophysical Research Letters*, 33(14), 1–4.
- Fox-Kemper, B., Adcroft, A., Böning, C., et al. (2019). Challenges and prospects in ocean circulation models. *Frontiers in Marine Science*, 6, 65.
- Frantz, C.M., Light, B., Farley, S.M., Carpenter, S., Lieblappen, R., Courville, Z., Orellana, M.V., & Junge, K. (2019). Physical and optical characteristics of heavily melted “rotten” Arctic sea ice. *The Cryosphere*, 13(3), 775–793.
- Frederking, R., & Sudom, D. (2013). Review of flexural strength of multi-year ice. In *ISOPE-2013 Anchorage conference proceedings. The proceedings of the Twenty-Third (2013) International Offshore and Polar Engineering Conference. Anchorage, Alaska, USA, June 30 – July 5, 2013* (pp. 1087–1093). ISOPE.
- Frederking, R., & Timco, G. (1983). Uniaxial compressive strength and deformation of Beaufort sea ice. In *POAC 83. The seventh international conference on port and ocean engineering under arctic conditions* (Vol. 1: *Sea ice properties and conditions in cold regions*, pp. 89–98). Technical Research Centre of Finland.
- Frederking, R., & Timco, G.W. (1984). Measurement of shear strength of granular/discontinuous-columnar sea ice. *Cold Regions Science and Technology*, 9(3), 215–220.
- Frederking, R., & Timco, G.W. (1986). Field measurements of the shear strength of columnar-grained sea ice. In *Proceedings LAHR Symposium on Ice 1986. Iowa City, August 18–22, 1986* (Vol. 1, pp. 279–292). Inst. of Hydraulic Research.
- Freitag, J., & Eicken, H. (2003). Meltwater circulation and permeability of Arctic summer sea ice derived from hydrological field experiments. *Journal of Glaciology*, 49(166), 349–358.
- Gao, G., Chen, C., Qi, J., & Beardsley, R.C. (2011). An unstructured-grid, finite-volume sea ice model: Development, validation, and application. *Journal of Geophysical Research: Oceans*, 116(C8).
- Girard, L., Weiss, J., Molines, J.M., Barnier, B., & Bouillon, S. (2009). Evaluation of high-resolution sea ice models on the basis of statistical and scaling properties of Arctic sea ice drift and deformation. *Journal of Geophysical Research: Oceans*, 114(C8).
- Girard, L., Bouillon, S., Weiss, J., Amtrano, D., Fichet, T., & Legat, V. (2011). A new modeling framework for sea-ice mechanics based on elasto-brittle rheology. *Annals of Glaciology*, 52(57), 123–132.
- Glen, J.W., & Perutz, M.F. (1954). The growth and deformation of ice crystals. *Journal of Glaciology*, 2(16), 397–403.
- Gold, L.W. (1958). Some observations on the dependence of strain on stress for ice. *Canadian Journal of Physics*, 36(10), 1265–1275.
- Golden, K.M., Ackley, S.F., & Lytle, V.I. (1998). The percolation phase transition in sea ice. *Science*, 282(5397), 2238–2241.



- Golden, K.M., Heaton, A.L., Eicken, H., & Lytle, V.I. (2006). Void bounds for fluid transport in sea ice. *Mechanics of Materials*, 38(8–10), 801–817.
- Golden, K.M., Bennetts, L.G., Cherkaev, E., Eisenman, I., Feltham, D., Horvat, C., Hunke, E., Jones, C., Perovich, D.K., Ponte-Castañeda, P., Strong, C., Sulsky, D., & Wells, A.J. (2020). Modeling sea ice. *Notices of the American Mathematical Society*, 67(10), 1535–1555.
- Goodman, D.J., & Tabor, D. (1978). Fracture toughness of ice: a preliminary account of some new experiments. *Journal of Glaciology*, 21(85), 651–660.
- Grachev, A.A., Fairall, Ch.W., Persson, P.O.G., Andreas, E.L., & Guest, P.S. (2005). Stable boundary-layer scaling regimes: The Sheba data. *Boundary-Layer Meteorology*, 116(2), 201–235.
- Grae Worster, M.G., & Rees Jones, D.W. (2015). Sea-ice thermodynamics and brine drainage. *Philosophical Transactions of the Royal Society A: Mathematical, Physical and Engineering Sciences*, 373(2045), 20140166.
- Grandi, D. (2013). A phase field approach to solidification and solute separation in water solutions. *Zeitschrift für Angewandte Mathematik und Physik*, 64(6), 1611–1624.
- Gray, J. (1999). Loss of hyperbolicity and ill-posedness of the viscous-plastic sea ice rheology in uniaxial divergent flow. *Journal of Physical Oceanography*, 29(11), 2920–2929.
- Gray, J., & Killworth, P. (1995). Stability of the viscous-plastic sea ice rheology. *Journal of Physical Oceanography*, 25(5), 971–978.
- Gray, J., & Killworth, P. (1997). Reply to J. Dukowicz: Comments on stability of the viscous-plastic sea ice rheology. *Journal of Physical Oceanography*, 27(3), 482–483.
- Griewank, P.J., & Notz, D. (2013). Insights into brine dynamics and sea ice desalination from a 1-D model study of gravity drainage. *Journal of Geophysical Research: Oceans*, 118(7), 3370–3386.
- Gross, D., & Seelig, T. (2011). Micromechanics and homogenization. In D. Gross, & T. Seelig (Eds.), *Fracture Mechanics. With an Introduction to Micromechanics* (Second ed., pp. 229–299). Springer Berlin, Heidelberg.
- Group, M. (1986). MIZEX East 83/84: The summer marginal ice zone program in the Fram Strait/Greenland Sea. *Eos, Transactions American Geophysical Union*, 67(23), 513–517.
- Gürses, E., & Miehe, C. (2009). A computational framework of three-dimensional configurational-force-driven brittle crack propagation. *Computer Methods in Applied Mechanics and Engineering*, 198(15–16), 1413–1428.
- Hall, D.K., Chang, A.T.C., & Foster, J.L. (1986). Detection of the depth-hoar layer in the snow-pack of the Arctic coastal plain of Alaska, U.S.A., using satellite data. *Journal of Glaciology*, 32(110), 87–94.
- Han, H., Li, Z., Huang, W., Lu, P., & Lei, R. (2015). The uniaxial compressive strength of the Arctic summer sea ice. *Acta Oceanologica Sinica*, 34(1), 129–136.
- Hawkes, I., & Mellor, M. (1972). Deformation and fracture of ice under uniaxial stress. *Journal of Glaciology*, 11(61), 103–131.
- Helmig, R. (1997). *Multiphase Flow and Transport Processes in the Subsurface. A Contribution to the Modeling of Hydrosystems*. Springer Berlin, Heidelberg.
- Heorton, H., Feltham, D.L., & Tsamados, M. (2018). Stress and deformation characteristics of sea ice in a high-resolution, anisotropic sea ice model. *Philosophical Transactions of the Royal Society A: Mathematical, Physical and Engineering Sciences*, 376(2129), 20170349.
- Herman, A. (2016). Discrete-element bonded-particle sea ice model DESIgn, version 1.3 a – model description and implementation. *Geoscientific Model Development*, 9(3), 1219–1241.
- Herman, A., Evers, K.-U., & Reimer, N. (2018). Floe-size distributions in laboratory ice broken by waves. *The Cryosphere*, 12(2), 685–699.
- Herman, A., Cheng, S., & Shen, H.H. (2019). Wave energy attenuation in fields of colliding ice floes – Part 2: A laboratory case study. *The Cryosphere*, 13(11), 2901–2914.
- Hibler III, W.D. (1979). A dynamic thermodynamic sea ice model. *Journal of Physical Oceanography*, 9(4), 815–846.
- Hicks, F. (2009). An overview of river ice problems: CRIPE07 guest editorial. *Cold Regions Science and Technology*, 55(2), 175–185.
- Holland, P., & Kwok, R. (2012). Wind-driven trends in Antarctic sea-ice drift. *Nature Geoscience*, 5(12), 872–875.
- Hoppmann, M., Richter, M.E., Smith, I.J., Jendersie, S., Langhorne, P.J., Thomas, D.N., & Dieckmann, G.S. (2020). Platelet ice, the Southern Ocean’s hidden ice: A review. *Annals of Glaciology*, 61(83), 341–368.
- Horvat, C.H., & Tziperman, E. (2015). A prognostic model of the sea-ice floe size and thickness distribution. *The Cryosphere*, 9(6), 2119–2134.
- Hosford, W.F. (2006). Sintering. In W.F. Hosford, *Materials Science. An Intermediate Text* (pp. 144–152). Cambridge University Press.
- Hunke, E.C. (2001). Viscous–plastic sea ice dynamics with the EVP model: linearization issues. *Journal of Computational Physics*, 170(1), 18–38.
- Hunke, E.C., & Dukowicz, J.K. (1997). An elastic–viscous–plastic model for sea ice dynamics. *Journal of Physical Oceanography*, 27(9), 1849–1867.
- Hunke, E.C., & Dukowicz, J.K. (2002). The elastic–viscous–plastic sea ice dynamics model in general orthogonal curvilinear coordinates on a sphere–incorporation of metric terms. *Monthly Weather Review*, 130(7), 1848–1865.
- Hunke, E.C., & Lipscomb, W.H. (2010). CICE: the Los Alamos Sea Ice Model, Documentation and Software User’s Manual, Version 4.1.
- Hunke, E.C., Lipscomb, W.H., & Turner, A.K. (2010). Sea-ice models for climate study: retrospective and new directions. *Journal of Glaciology*, 56(200), 1162–1172.
- Hutchings, J.K., Heil, P., Steer, A., & Hibler III, W.D. (2012). Subsynoptic scale spatial variability of sea ice deformation in the western Weddell Sea during early summer. *Journal of Geophysical Research: Oceans*, 117(C1).

- Ip, Ch.F., Hibler III, W.D., & Flato, G.M. (1991). On the effect of rheology on seasonal sea-ice simulations. *Annals of Glaciology*, 15, 17–25.
- Jackson, K., Wilkinson, J., Maksym, T., Meldrum, D., Beckers, J., Haas, C., & Mackenzie, D. (2013). A novel and low-cost sea ice mass balance buoy. *Journal of Atmospheric and Oceanic Technology*, 30(11), 2676–2688.
- Jeffrey, N., & Hunke, E.C. (2014). Modeling the winter-spring transition of first-year ice in the western Weddell Sea. *Journal of Geophysical Research: Oceans*, 119(9), 5891–5920.
- Jeffrey, N., Hunke, E.C., & Elliott, S.M. (2011). Modeling the transport of passive tracers in sea ice. *Journal of Geophysical Research: Oceans*, 116(C7).
- Ji, S.-y., Liu, H.-l., Li, P.-f., & Su, J. (2013). Experimental studies on the Bohai Sea ice shear strength. *Journal of Cold Regions Engineering*, 27(4), 244–254.
- Johnson, S., Khoboko, T., Matlakala, B., Vichi, M., & Rampai, T. (2022). *Crystal size and texture data of sea ice from the Antarctic Marginal Ice Zone collected in Spring 2019*. Zenodo. <https://zenodo.org/records/6966958>.
- Jungclaus, J.H., Lorenz, S.J., Schmidt, H. et al. (2022). The icon earth system model version 1.0. *Journal of Advances in Modeling Earth Systems*, 14(4), e2021MS002813.
- Karulina, M., Marchenko, A., Karulin, E., Sodhi, D., Sakharov, A., & Chistyakov, P. (2019). Full-scale flexural strength of sea ice and freshwater ice in Spitsbergen Fjords and North-West Barents Sea. *Applied Ocean Research*, 90, 101853.
- Kawamura, T., Shirasawa, K., & Kobinata, K. (2001). Physical properties and isotopic characteristics of landfast sea ice around the North Water (NOW) Polynya region. *Atmosphere-Ocean*, 39(3), 173–182.
- Keller, J.B. (1998). Gravity waves on ice-covered water. *Journal of Geophysical Research: Oceans*, 103(C4), 7663–7669.
- Kennedy, J.H., Pettit, E.C., & Di Prinzio, C.L. (2013). The evolution of crystal fabric in ice sheets and its link to climate history. *Journal of Glaciology*, 59(214), 357–373.
- Kennicutt II, M.C., Chown, S.L., Cassano, J.J., Liggett, D., Massom, R., Peck, L.S., Rintoul, S.R., Storey, J.W., Vaughan, D.G., Wilson, T.J., & Sutherland, W.J. (2014). Polar research: Six priorities for Antarctic science. *Nature*, 512(7512), 23–25.
- Kennicutt II, M.C., Kim, Y., Rogan-Finnemore, M. et al. (2016). Delivering 21st century Antarctic and Southern Ocean science. *Antarctic Science*, 28(6), 407–423.
- Kennicutt II, M.C., Bromwich, D., Liggett, D. et al. (2019). Sustained Antarctic research: A 21<sup>st</sup> century imperative. *One Earth*, 1(1), 95–113.
- Kimmitz, M., Danilov, S., & Losch, M. (2015). On the convergence of the modified elastic–viscous–plastic method for solving the sea ice momentum equation. *Journal of Computational Physics*, 296, 90–100.
- Kohout, A.L., Williams, M.J.M., Dean, S.M., & Meylan, M.H. (2014). Storminduced sea-ice breakup and the implications for ice extent. *Nature*, 509(7502), 604–607.
- Kohout, A.L., Penrose, B., Penrose, S., & Williams, M.J.M. (2015). A device for measuring wave-induced motion of ice floes in the Antarctic marginal ice zone. *Annals of Glaciology*, 56(69), 415–424.
- Kohout, A.L., Smith, M., Roach, L.A., Williams, G., Montiel, F., & Williams, M.J.M. (2020). Observations of exponential wave attenuation in Antarctic sea ice during the PIPERS campaign. *Annals of Glaciology*, 61(82), 196–209.
- Krishfield, R., Toole, J., Proshutinsky, A., & Timmermans, M.-L. (2008). Automated ice-tethered profilers for seawater observations under pack ice in all seasons. *Journal of Atmospheric and Oceanic Technology*, 25(11), 2091–2105.
- Kuehn, G.A., Lee, R.W., Nixon, W.A., & Schulson, E.M. (1990). The structure and tensile behavior of first-year sea ice and laboratory grown saline ice. *Journal of Offshore Mechanics and Arctic Engineering*, 112(4), 357–363.
- Kulyakhtin, A., & Tsarau, A. (2014). A time-dependent model of marine icing with application of computational fluid dynamics. *Cold Regions Science and Technology*, 104–105, 33–44.
- Kulyakhtin, A., Kulyakhtin, S., & Løset, S. (2016). The role of the ice heat conduction in the ice growth caused by periodic sea spray. *Cold Regions Science and Technology*, 127, 93–108.
- Kurylyk, B.L., & Watanabe, K. (2013). The mathematical representation of freezing and thawing processes in variably-saturated, non-deformable soils. *Advances in Water Resources*, 60, 160–177.
- Kutschan, B., Morawetz, K., & Gemming, S. (2010). Modeling the morphogenesis of brine channels in sea ice. *Physical Review E: Statistical, Nonlinear, and Soft Matter Physics*, 81(3), 036106.
- Kwok, R. (2018). Arctic sea ice thickness, volume, and multiyear ice coverage: losses and coupled variability (1958–2018). *Environmental Research Letters*, 13(10), 105005.
- Lang, R., Leo, B., & Brown, R. (1984). Observations on the growth process and strength characteristics of surface hoar. In *International snow science workshop (a merging of theory and practice)*. *Proceedings. October 24–27, 1984, Aspen, Colorado USA* (pp. 188–195). ISSW Workshop Committee.
- Lange, M.A., & Eicken, H. (1991). Textural characteristics of sea ice and the major mechanisms of ice growth in the Weddell Sea. *Annals of Glaciology*, 15, 210–215.
- Lange, M.A., Ackley, S., Wadhams, P., Dieckmann, G., & Eicken, H. (1989). Development of sea ice in the Weddell Sea. *Annals of Glaciology*, 12, 92–96.
- Lee, C.M., Cole, S., Doble, M., Freitag, L., Hwang, P., Jayne, S., Jeffries, M., Krishfield, R., Maksym, T., Maslowski, W., Owens, B., Posey, P., Rainville, L., Roberts, A., Shaw, B., Stanton, T., Thomson, J., Timmermans, M.-L., Toole, J., Wadhams, P., Wilkinson, J., & Zhang, Z. (2012). *Marginal Ice Zone (MIZ) Program: Science and Experiment Plan. Technical Report APL-UW 1201*. Applied Physics Laboratory, University of Washington, Seattle.
- Lee, C.M., Thomson, J., The Marginal Ice Zone Team, & The Arctic Sea State Team (2017). An autonomous approach to observing the seasonal ice zone in the Western Arctic. *Oceanography*, 30(2), 56–68.
- Lemieux, J.-F., & Tremblay, B. (2009). Numerical convergence of viscousplastic sea ice models. *Journal of Geophysical Research: Oceans*, 114(C5).

- Lemieux, J.-F., Tremblay, B., Sedláček, J., Tupper, P., Thomas, S., Huard, D., & Auclair, J.-P. (2010). Improving the numerical convergence of viscous-plastic sea ice models with the Jacobian-free Newton–Krylov method. *Journal of Computational Physics*, 229(8), 2840–2852.
- Lemieux, J.-F., Knoll, D.A., Tremblay, B., Holland, D.M., & Losch, M. (2012). A comparison of the Jacobian-free Newton–Krylov method and the EVP model for solving the sea ice momentum equation with a viscous-plastic formulation: a serial algorithm study. *Journal of Computational Physics*, 231(17), 5926–5944.
- Lemieux, J.-F., Knoll, D.A., Losch, M., & Girard, C. (2014). A second-order accurate in time IMPLICIT–EXPLICIT (IMEX) integration scheme for sea ice dynamics. *Journal of Computational Physics*, 263, 375–392.
- Leppäranta, M. (2011). *The drift of sea ice*. Springer Berlin, Heidelberg.
- Leppäranta, M., & Hibler III, W.D. (1985). The role of plastic ice interaction in marginal ice zone dynamics. *Journal of Geophysical Research: Oceans*, 90(C6), 11899–11909.
- Li, Z., Zhang, L., Lu, P., Leppäranta, M., & Li, G. (2011). Experimental study on the effect of porosity on the uniaxial compressive strength of sea ice in Bohai Sea. *Science China Technological Sciences*, 54(9), 2429–2436.
- Lieblappen, R.M., Golden, E.J., & Obbard, R.W. (2017). Metrics for interpreting the microstructure of sea ice using X-ray micro-computed tomography. *Cold Regions Science and Technology*, 138, 24–35.
- Lieblappen, R.M., Kumar, D.D., Pauls, S.D., & Obbard, R.W. (2018). A network model for characterizing brine channels in sea ice. *The Cryosphere*, 12(3), 1013–1026.
- Lietaer, O. (2011). *Finite Element Methods for Sea Ice Modeling* [PhD thesis]. Université Catholique de Louvain.
- Lietaer, O., Fichefet, T., & Legat, V. (2008). The effects of resolving the Canadian arctic archipelago in a finite element sea ice model. *Ocean Modelling*, 24(3–4), 140–152.
- Liferov, P., & Høyland, K.V. (2004). In-situ ice ridge scour tests: experimental set up and basic results. *Cold Regions Science and Technology*, 40(1–2), 97–110.
- Light, B., Maykut, G.A., & Grenfell, T.C. (2003). Effects of temperature on the microstructure of first-year Arctic sea ice. *Journal of Geophysical Research: Oceans*, 108(C2).
- Linder, C., & Armero, F. (2009). Finite elements with embedded branching. *Finite Elements in Analysis and Design*, 45(4), 280–293.
- Lindsay, R., Zhang, J., & Rothrock, D. (2003). Sea-ice deformation rates from satellite measurements and in a model. *Atmosphere-Ocean*, 41(1), 35–47.
- Liu, R., Yan, J., & Li, S. (2020). Modeling and simulation of ice–water interactions by coupling peridynamics with updated Lagrangian particle hydrodynamics. *Computational Particle Mechanics*, 7(2), 241–255.
- Losch, M., & Danilov, S. (2012). On solving the momentum equations of dynamic sea ice models with implicit solvers and the elastic–viscous–plastic technique. *Ocean Modelling*, 41, 42–52.
- Losch, M., Fuchs, A., Lemieux, J.-F., & Vanselow, A. (2014). A parallel Jacobian-free Newton–Krylov solver for a coupled sea ice–ocean model. *Journal of Computational Physics*, 257, 901–911.
- Lu, P., Li, Z.J., Zhang, Z.H., & Dong, X.L. (2008). Aerial observations of floe size distribution in the marginal ice zone of summer Prydz Bay. *Journal of Geophysical Research: Oceans*, 113(C2).
- Lu, W., Løset, S., Shestov, A., & Lubbad, R. (2015). Design of a field test for measuring the fracture toughness of sea ice. In *POAC '15: Proceedings of the 23rd International Conference on Port and Ocean Engineering under Arctic Conditions*. Port and Ocean Engineering under Arctic Conditions (POAC).
- Lüpkes, C., Gryanik, V., Witha, B., Gryscha, M., Raasch, S., & Gollnik, T. (2008). Modeling convection over arctic leads with LES and a non-eddy-resolving microscale model. *Journal of Geophysical Research: Oceans*, 113(C9).
- Lytle, V., & Ackley, S. (2001). Snow-ice growth: a fresh-water flux inhibiting deep convection in the Weddell Sea, Antarctica. *Annals of Glaciology*, 33, 45–50.
- Mackey, T., Wells, J., Jordaan, I., & Derradji-Aouat, A. (2007). Experiments on the fracture of polycrystalline ice. In *POAC '07: Proceedings of the 19th International Conference on Port and Ocean Engineering under Arctic Conditions* (pp. 339–349). Port and Ocean Engineering under Arctic Conditions (POAC).
- Maksym, T., Stammerjohn, S.E., Ackley, S., & Massom, R. (2012). Antarctic sea ice – A polar opposite?. *Oceanography*, 25(3), 140–151.
- Manley, J., & Willcox, S. (2010). The Wave Glider: A persistent platform for ocean science. In *OCEANS'10 IEEE SYDNEY* (pp. 1–5). IEEE.
- Manninen, T., Lahtinen, P., Anttila, K., & Riihelä, A. (2016). Detection of snow surface roughness and hoar at Summit, Greenland, using RADARSAT data. *International Journal of Remote Sensing*, 37(12), 2860–2880.
- Marquart, R., Bogaers, A., Skatulla, S., Alberello, A., Toffoli, A., Schwarz, C., & Vichi, M. (2021). A computational fluid dynamics model for the small-scale dynamics of wave, ice floe and interstitial grease ice interaction. *Fluids*, 6(5), 176.
- Marsland, S., Haak, H., Jungclauss, J., Latif, M., & Röske, F. (2003). The MaxPlanck-Institute global ocean/sea ice model with orthogonal curvilinear coordinates. *Ocean Modelling*, 5(2), 91–127.
- Martinson, D.G., & Wamser, Ch. (1990). Ice drift and momentum exchange in winter Antarctic pack ice. *Journal of Geophysical Research: Oceans*, 95(C2), 1741–1755.
- Massom, R.A., Eicken, H., Hass, C., Jeffries, M.O., Drinkwater, M.R., Sturm, M., Worby, A.P., Wu, X., Lytle, V.I., Ushio, S., Morris, K., Reid, P.A., Warren, S.G., & Allison, I. (2001). Snow on Antarctic sea ice. *Reviews of Geophysics*, 39(3), 413–445.
- Maus, S., Schneebeil, M., & Wiegmann, A. (2021). An X-ray microtomographic study of the pore space, permeability and percolation threshold of young sea ice. *The Cryosphere*, 15(8), 4047–4072.
- Maykut, G.A. (1982). Large-scale heat exchange and ice production in the central Arctic. *Journal of Geophysical Research: Oceans*, 87(C10), 7971–7984.

- Maykut, G.A., & Untersteiner, N. (1971). Some results from a time-dependent thermodynamic model of sea ice. *Journal of Geophysical Research*, 76(6), 1550–1575.
- McGuinness, M.J. (2007). Modelling sea ice growth. *The ANZIAM Journal*, 50(3).
- McNutt, L., Digby, S., Carsey, F., Holt, B., Crawford, J., Tang, C.L., Gray, A.L., & Livingstone, C. (1988). Limex'87: The Labrador ice margin experiment, March 1987 – a pilot experiment in anticipation of RADARSAT and ERS 1 data. *Eos, Transactions American Geophysical Union*, 69(23), 634–643.
- Mehlmann, C., & Korn, P. (2021). Sea-ice dynamics on triangular grids. *Journal of Computational Physics*, 428, 110086.
- Mehlmann, C., & Richter, T. (2017a). A modified global Newton solver for viscous-plastic sea ice models. *Ocean Modelling*, 116, 96–107.
- Mehlmann, C., & Richter, T. (2017b). A finite element multigrid-framework to solve the sea ice momentum equation. *Journal of Computational Physics*, 348, 847–861.
- Mehlmann, C., Danilov, S., Losch, M., Lemieux, J.-F., Hutter, N., Richter, T., Blain, P., Hunke, E., & Korn, P. (2021). Simulating linear kinematic features in viscous-plastic sea ice models on quadrilateral and triangular grids with different variable staggering. *Journal of Advances in Modeling Earth Systems*, 13(11), e2021MS002523.
- Mellor, M., & Hawkes, I. (1971). Measurement of tensile strength by diametral compression of discs and annuli. *Engineering Geology*, 5(3), 173–225.
- Meschke, G., Leonhart, D., Timothy, J.J., & Meng-Meng, Z. (2011). Computational mechanics of multiphase materials – modeling strategies at different scales. *Computer Assisted Methods in Engineering and Science*, 18(1–2), 73–89.
- Middleton, C.A., Thomas, C., de Wit, A., & Tison, J.-L. (2016). Visualizing brine channel development and convective processes during artificial sea-ice growth using Schlieren optical methods. *Journal of Glaciology*, 62(231).
- Miehe, C., & Gürses, E. (2007). A robust algorithm for configurational-force-driven brittle crack propagation with R-adaptive mesh alignment. *International Journal for Numerical Methods in Engineering*, 72(2), 127–155.
- Miehe, C., Welschinger, F., & Hofacker, M. (2010). Thermodynamically consistent phase-field models of fracture: Variational principles and multi-field FE implementations. *International Journal for Numerical Methods in Engineering*, 83(10), 1273–1311.
- Mintu, S., Molyneux, D., & Oldford, D. (2016). A State-of-the-art review of research on ice accretion measurements and modeling. In *Arctic Technology Conference. October 24–26, 2016. St. John's, Newfoundland and Labrador, Canada* (pp. 1–18).
- Morawetz, K., Thoms, S., & Kutschan, B. (2017). Formation of brine channels in sea ice. *The European Physical Journal E*, 40(3), 25.
- Moritz, R.E., Bitz, C.M., & Steig, E.J. (2002). Dynamics of recent climate change in the Arctic. *Science*, 297(5586), 1497–1502.
- Moslet, P.O. (2007). Field testing of uniaxial compression strength of columnar sea ice. *Cold Regions Science and Technology*, 48(1), 1–14.
- Moslet, P.O., Bonnemaire, B., Valkonen, J., Høyland, K.V., Liferov, P., Bjerkås, M., Dybdahl, J., & Løset, S. (2005). Sea ice – vertical pile interaction experiment, Part III: test results 2004. In *POAC '05: Proceedings of the 18th International Conference on Port and Ocean Engineering under Arctic Conditions* (pp. 471–480). Port and Ocean Engineering under Arctic Conditions (POAC).
- Mukherji, B. (1973). Crack propagation in sea ice: a finite element approach. *AIDJEX Bulletin*, 18, 69–75.
- Mulmule, S., & Dempsey, J. (2000). LEFM size requirements for the fracture testing of sea ice. *International Journal of Fracture*, 102, 85–98.
- Munz, D., & Fett, T. (Eds.) (1999). *Ceramics. Mechanical Properties, Failure Behaviour, Materials Selection*. Springer Berlin, Heidelberg.
- Murrell, S.A.F., Sammonds, P.R., & Rist, M.A. (1991). Strength and failure modes of pure ice and multi-year sea ice under triaxial loading. In S. Jones, J. Tillotson, R.F. McKenna, I.J. Jordaan (Eds.), *Ice-Structure Interaction. IUTAM/IAHR Symposium St. John's, Newfoundland Canada 1989* (pp. 339–361). Springer Berlin, Heidelberg.
- Nakawo, M. (1983). Measurements on air porosity of sea ice. *Annals of Glaciology*, 4, 204–208.
- Nelli, F., Bennetts, L.G., Skene, D.M., & Toffoli, A. (2020). Water wave transmission and energy dissipation by a floating plate in the presence of overwash. *Journal of Fluid Mechanics*, 889.
- Newyear, K. (1999). Comparison of laboratory data with a viscous two-layer model of wave propagation in grease ice. *Journal of Geophysical Research: Oceans*, 104(C4), 7837–7840.
- Nicolaus, M., Hoppmann, M., Arndt, S., Hendricks, S., Katlein, C., Nicolaus, A., Rossmann, L., Schiller, M., & Schwegmann, S. (2021). Snow depth and air temperature seasonality on sea ice derived from snow buoy measurements. *Frontiers in Marine Science*, 8.
- Nixon, W.A., & Schulson, E.M. (1988). The fracture toughness of ice over a range of grain sizes. *Journal of Offshore Mechanics and Arctic Engineering*, 110(2), 192–196.
- Notz, D. (2005). *Thermodynamic and Fluid-Dynamical Processes in Sea Ice* [PhD thesis]. University of Cambridge.
- Notz, D. (2012). Challenges in simulating sea ice in Earth System Models. *Wiley Interdisciplinary Reviews: Climate Change*, 3(6), 509–526.
- Notz, D., & Worster, M.G. (2006). A one-dimensional enthalpy model of sea ice. *Annals of Glaciology*, 44, 123–128.
- Oertling, A.B., & Watts, R.G. (2004). Growth of and brine drainage from NaCl-H<sub>2</sub>O freezing: A simulation of young sea ice. *Journal of Geophysical Research: Oceans*, 109(C4).
- Ouchterlony, F. (1988). International Society for Rock Mechanics commission on Testing Methods. *International Journal of Rock Mechanics & Mining Sciences*, 25(2), 71–96.
- Ozeki, T., Tsuda, M., Yashiro, Y., Fujita, K., & Adachi, S. (2020). Development of artificial surface hoar production system using a circuit wind tunnel and formation of various crystal types. *Cold Regions Science and Technology*, 169, 102889.

- Paige, R.A., & Lee, C.W. (1967). Preliminary studies on sea ice in McMurdo Sound, Antarctica, during “Deep Freeze 65”. *Journal of Glaciology*, 6(46), 515–528.
- Pandolfi, A., & Ortiz, M. (2002). An efficient adaptive procedure for three-dimensional fragmentation simulations. *Engineering with Computers*, 18(2), 148–159.
- Parkinson, C.L. (2004). Southern Ocean sea ice and its wider linkages: insights revealed from models and observations. *Antarctic Science*, 16(4), 387–400.
- Parsons, B., Snellen, J., & Hill, B. (1986). Physical modeling and the fracture toughness of sea ice. In *Reliability and Probabilistic Methods, Design and Practical Optimization, Fatigue, Fracture/ Corrosion Control, Stresses, Offshore and Arctic Materials, Structural Mechanics, Ocean Mining, Ocean Energy* (pp. 358–364). The American Soc. of Mechanical Engineers.
- Paul, F., Mielke, T., Schwarz, C., Schröder, J., Rampai, T., Skatulla, S., Audh, R., Hepworth, E., Vichi, M., & Lupascu, D. (2021). Frazil ice in the Antarctic marginal ice zone. *Journal of Marine Science and Engineering*, 9(6), 647.
- Persson, P., Fairall, C., Andreas, E., Guest, P., & Perovich, D. (2002). Measurements near the Atmospheric Surface Flux Group tower at SHEBA: Near-surface conditions and surface energy budget. *Journal of Geophysical Research: Oceans*, 107(C10), SHE 21-1 – SHE 21-35.
- Petrich, C., & Eicken, H. (2010). Growth, structure and properties of sea ice. In D.N. Thomas, G.S. Dieckmann (Eds.), *Sea Ice* (Second ed., pp. 23–77). Blackwell Publishing.
- Petrich, C., & Eicken, H. (2017). Overview of sea ice growth and properties. In D.N. Thomas (Ed.), *Sea Ice* (Third Edition, pp. 1–41). Wiley Blackwell.
- Polashenski, C., Perovich, D., Richter-Menge, J., & Elder, B. (2011). Seasonal ice mass-balance buoys: adapting tools to the changing Arctic. *Annals of Glaciology*, 52(57), 18–26.
- Poplin, J., & Wang, A. (1994). Mechanical properties of rafted annual sea ice. *Cold Regions Science and Technology*, 23(1), 41–67.
- Pringle, D.J., Miner, J.E., Eicken, H., & Golden, K.M. (2009). Pore space percolation in sea ice single crystals. *Journal of Geophysical Research: Oceans*, 114(12).
- Pritchard, R. (2005). Stability of sea ice dynamics models: Viscous-plastic rheology, replacement closure, and tensile cutoff. *Journal of Geophysical Research: Oceans*, 110(C12).
- Provatas, N., & Elder, K. (2010). *Phase-Field Methods in Materials Science and Engineering*. Wiley-VCH.
- Quincke, G.H. (1905). The formation of ice and the grained structure of glaciers. *Proceedings of The Royal Society A: Mathematical, Physical and Engineering Sciences*, 76(512), 431–439.
- Rabatel, M., Labbé, S., & Weiss, J. (2015). Dynamics of an assembly of rigid ice floes. *Journal of Geophysical Research: Oceans*, 120(9), 5887–5909.
- Rabault, J., Sutherland, G., Gundersen, O., Jensen, A., Marchenko, A., & Breivik, O. (2020). An open source, versatile, affordable waves in ice instrument for scientific measurements in the Polar Regions. *Cold Regions Science and Technology*, 170, 102955.
- Rampal, P., Weiss, J., & Marsan, D. (2009). Positive trend in the mean speed and deformation rate of Arctic sea ice, 1979–2007. *Journal of Geophysical Research: Oceans*, 114(C5).
- Rampal, P., Weiss, J., Dubois, C., & Campin, J.M. (2011). IPCC climate models do not capture Arctic sea ice drift acceleration: Consequences in terms of projected sea ice thinning and decline. *Journal of Geophysical Research: Oceans*, 116(C8).
- Rampal, P., Bouillon, S., Ólason, E., & Morlighem, M. (2016). neXtSIM: a new Lagrangian sea ice model. *The Cryosphere*, 10(3), 1055–1073.
- Rayner, N.A., Parker, D.E., Horton, E.B., Folland, C.K., Alexander, L.V., Rowell, D.P., Kent, E.C., & Kaplan, A. (2003). Global analyses of sea surface temperature, sea ice, and night marine air temperature since the late nineteenth century. *Journal of Geophysical Research: Atmospheres*, 108(D14).
- Rees Jones, D.W. & Grae Worster, M. (2014). A physically based parameterization of gravity drainage for sea-ice modeling. *Journal of Geophysical Research: Oceans*, 119(9), 5599–5621.
- Ren, H., Zhang, C., & Zhao, X. (2021). Numerical simulations on the fracture of a sea ice floe induced by waves. *Applied Ocean Research*, 108, 102527.
- Richter-Menge, J.A. (1992). US research in ice mechanics: 1987–1990. *Cold Regions Science and Technology*, 20(3), 231–246.
- Richter-Menge, J.A., Cox, G.F., Perron, N., Durell, G., & Bosworth, H.W. (1986). *Triaxial Testing of First-Year Sea Ice*. CRREL Report 86-16.
- Richter-Menge, J.A., Claffey, K., & Walsh, M.R. (1993). End-capping procedure for cored ice samples used in tension tests. *Journal of Glaciology*, 39(133), 698–700.
- Ricken, T., & Bluhm, J. (2010). Modeling fluid saturated porous media under frost attack. *GAMM-Mitteilungen*, 33(1), 40–56.
- Ricken, T., & de Boer, R. (2003). Multiphase flow in a capillary porous medium. *Computational Materials Science*, 28(3–4), 704–713.
- Ringeisen, D., Losch, M., Tremblay, L.B., & Hutter, N. (2019). Simulating intersection angles between conjugate faults in sea ice with different viscous–plastic rheologies. *The Cryosphere*, 13(4), 1167–1186.
- Rist, M.A., Sammonds, P.R., Murrell, S.A., Meredith, P.G., Doake, C.S., Oerter, H., & Matsuki, K. (1999). Experimental and theoretical fracture mechanics applied to Antarctic ice fracture and surface crevassing. *Journal of Geophysical Research: Solid Earth*, 104(B2), 2973–2987.
- Roach, L.A., Horvat, C., Dean, S.M., & Bitz, C.M. (2018). An emergent sea ice floe size distribution in a global coupled ocean–sea ice model. *Journal of Geophysical Research: Oceans*, 123(6), 4322–4337.
- Rogers, W.E., Thomson, J., Shen, H.H., Doble, M.J., Wadhams, P., & Cheng, S. (2016). Dissipation of wind waves by pancake and frazil ice in the autumn Beaufort Sea. *Journal of Geophysical Research: Oceans*, 121(11), 7991–8007.

- Ryerson, Ch.C. (2013). *Icing Management for Coast Guard Assets*. ERDC/CRREL TR-13-7. Cold Regions Research and Engineering Laboratory.
- Saeki, H., Ono, T., Zong, N.E., & Nakazawa, N. (1985). Experimental study on direct shear strength of sea ice. *Annals of Glaciology*, 6, 218–221.
- Sakharov, A., Karulin, E., Marchenko, A., Karulina, M., & Chistyakov, P. (2019). Mechanism of shear collapse in sea ice. In *Proceedings of the 25<sup>th</sup> International Conference on Port and Ocean Engineering under Arctic Conditions, June 9–13, 2019, Delft, The Netherlands*.
- Sammonds, P.R., Murrell, S.A., & Rist, M.A. (1998). Fracture of multiyear sea ice. *Journal of Geophysical Research: Oceans*, 103(C10), 21795–21815.
- Samuelsen, E.M., Løset, S., & Edvardsen, K. (2015). Marine icing observed on KV Nordkapp during a cold air outbreak with a developing polar low in the Barents sea. In *Proceedings of the 23<sup>rd</sup> International Conference on Port and Ocean Engineering under Arctic Conditions, June 14–18, 2015, Trondheim, Norway*.
- Sand, B. (2008). *Nonlinear Finite Element Simulations of Ice Forces on Offshore Structures* [PhD thesis]. Luleå University of Technology.
- Schneck, C.C., Ghobrial, T.R., & Loewen, M.R. (2019). Laboratory study of the properties of frazil ice particles and flocs in water of different salinities. *The Cryosphere*, 13(10).
- Schulkes, R.M.S.M. (1996). Asymptotic stability of the viscous-plastic sea ice rheology. *Journal of Physical Oceanography*, 26(2), 279–283.
- Schulson, E.M. (1999). The structure and mechanical behavior of ice. *JOM*, 51(2), 21–27.
- Schulson, E.M. (2001). Brittle failure of ice. *Engineering Fracture Mechanics*, 68(17–18), 1839–1887.
- Schulson, E.M., & Duval, P. (2009). *Creep and Fracture of Ice*. Cambridge University Press.
- Schulson, E.M., Fortt, A.L., Iliescu, D., & Renshaw, C.E. (2006). Failure envelope of first-year arctic sea ice: The role of friction in compressive fracture. *Journal of Geophysical Research: Oceans*, 111(C11).
- Schwarz, A., Bluhm, J., & Schröder, J. (2020). Modeling of freezing processes of ice floes within the framework of the TPM. *Acta Mechanica*, 231, 3099–3121.
- Schwarz, A., Bluhm, J., & Schröder, J. (2021). Investigations on modeling of freezing processes within the framework of the theory of porous media. *PAMM*, 20(1), e202000251.
- Schwarz, J., Frederking, R., Gavrillo, V., Petrov, I., Hirayama, K.-I., Mellor, M., Tryde, P., & Vaudrey, K. (1981). Standardized testing methods for measuring mechanical properties of ice. *Cold Regions Science and Technology*, 4(3), 245–253.
- Sellers, W. (1969). A global climatic model based on the energy balance of the Earth-atmosphere system. *Journal of Applied Meteorology and Climatology*, 8(3), 392–400.
- Setzer, M. (2001). Micro-ice-lens formation in porous solid. *Journal of Colloid and interface science*, 243(1), 193–201.
- Shen, H., Perrie, W., Hu, Y., & He, Y. (2018). Remote sensing of waves propagating in the marginal ice zone by SAR. *Journal of Geophysical Research: Oceans*, 123(1), 189–200.
- Shen, H.H. (2019). Modelling ocean waves in ice-covered seas. *Applied Ocean Research*, 83, 30–36.
- Shen, H.H., & Squire, V.A. (1998). Wave damping in compact pancake ice fields due to interactions between pancakes. In M.O. Jeffries (Ed.), *Antarctic Sea Ice: Physical Processes, Interactions and Variability* (pp. 325–341). American Geophysical Union.
- Shen, H.H., Hibler III, W.D., & Leppäranta, M. (1987). The role of floe collisions in sea ice rheology. *Journal of Geophysical Research: Oceans*, 92(C7), 7085–7096.
- Shen, H.H., Ackley, S.F., & Hopkins, M.A. (2001). A conceptual model for pancake-ice formation in a wave field. *Annals of Glaciology*, 33(3), 361–367.
- Shokr, M., & Sinha, N. (2015). *Sea Ice. Physics and Remote Sensing*. John Wiley & Sons.
- Sinha, N.K. (1984). Uniaxial compressive strength of first-year and multiyear sea ice. *Canadian Journal of Civil Engineering*, 11(1), 82–91.
- Sinha, N.K. (1986). Young Arctic frazil sea ice: Field and laboratory strength tests. *Journal of Materials Science*, 21(5), 1533–1546.
- Skene, D., Bennetts, L., Meylan, M., & Toffoli, A. (2015). Modelling water wave overwash of a thin floating plate. *Journal of Fluid Mechanics*, 777.
- Smedsrud, L.H. & Skogseth, R. (2006). Field measurements of Arctic grease ice properties and processes. *Cold Regions Science and Technology*, 44(3), 171–183.
- Snyder, S.A., Schulson, E.M., & Renshaw, C.E. (2015). The role of damage and recrystallization in the elastic properties of columnar ice. *Journal of Glaciology*, 61(227), 461–480.
- Sodhi, D.S., & Hibler III, W.D. (1980). Nonsteady ice drift in the strait of belle isle. In R.S. Pritchard (Eds.), *Sea Ice Processes and Models. Proceedings of the Arctic Ice Dynamics Joint Experiment International Commission of Snow and Ice Symposium* (pp. 177–186). University of Washington Press.
- Song, J.-H., & Belytschko, T. (2009). Cracking node method for dynamic fracture with finite elements. *International Journal for Numerical Methods in Engineering*, 77, 360–385.
- Song, J.-H., Areias, P.M.A., & Belytschko, T. (2006). A method for dynamic crack and shear band propagation with phantom nodes. *International Journal for Numerical Methods in Engineering*, 67(6), 868–893.
- Song, J.-H., Wang, H., & Belytschko, T. (2008). A comparative study on finite element methods for dynamic fracture. *Computational Mechanics*, 42(2), 239–250.
- Squire, V.A. (2018). A fresh look at how ocean waves and sea ice interact. *Philosophical Transactions of the Royal Society A: Mathematical, Physical and Engineering Sciences*, 376(2129), 20170342.
- Squire, V.A. (2020). Ocean wave interactions with sea ice: a reappraisal. *Annual Review of Fluid Mechanics*, 52(1), 37–60.

- Squire, V.A., Dugan, J.P., Wadhams, P., Rottier, P.J., & Liu, A.K. (1995). Of ocean waves and sea ice. *Annual Review of Fluid Mechanics*, 27(1), 115–168.
- Stammerjohn, S., & Maksym, T. (2017). Gaining (and losing) Antarctic sea ice: variability, trends and mechanisms. In D.N. Thomas (Ed.), *Sea Ice* (Third ed., pp. 261–289). Wiley Blackwell.
- Stefan, J. (1891). Ueber die Theorie der Eisbildung, insbesondere über die Eisbildung im Polarmeere. *Annalen der Physik*, 278(2), 269–286.
- Stehn, L. (1991). Fracture toughness of low salinity sea ice using short rod chevron notched specimens. In D.B. Muggeridge, D.B. Colbourne & H.M. Muggeridge (Eds.), *Proceedings – 11<sup>th</sup> International Conference on Port and Ocean Engineering Under Arctic Conditions. St. Jones, Canada* (Vol. 1, pp. 541–555). Ocean Engineering Research Centre.
- Stehn, L. (1994). Fracture toughness and crack growth of brackish ice using chevron-notched specimens. *Journal of Glaciology*, 40(135), 415–426.
- Stopa, J.E., Sutherland, P., & Arduin, F. (2018). Strong and highly variable push of ocean waves on Southern Ocean sea ice. *Proceedings of the National Academy of Sciences*, 115(23), 5861–5865.
- Strong, C., & Rigor, I.G. (2013). Arctic marginal ice zone trending wider in summer and narrower in winter. *Geophysical Research Letters*, 40(18), 4864–4868.
- Style, R.W., & Worster, M.G. (2009). Frost flower formation on sea ice and lake ice. *Geophysical Research Letters*, 36(11), 20–23.
- Sutherland, G., Rabault, J., Christensen, K.H., & Jensen, A. (2019). A two layer model for wave dissipation in sea ice. *Applied Ocean Research*, 88, 111–118.
- Tastula, E.-M., Vihma, T., & Andreas, E.L. (2012). Evaluation of Polar WRF from modeling the atmospheric boundary layer over Antarctic sea ice in autumn and winter. *Monthly Weather Review*, 140(12), 3919–3935.
- Tastula, E.-M., Vihma, T., Andreas, E.L., & Galperin, B. (2013). Validation of the diurnal cycles in atmospheric reanalyses over Antarctic sea ice. *Journal of Geophysical Research: Atmospheres*, 118(10), 4194–4204.
- Thomas, D.N. (2017). *Sea Ice* (Third Edition). Wiley Blackwell.
- Thoms, S., Kutschan, B., & Morawetz, K. (2014). *Phase-Field Theory of Brine Entrapment in Sea Ice: Short-Time Frozen Microstructures*. ArXiv. <https://arxiv.org/abs/1405.0304>.
- Thomson, J. (2012). Wave breaking dissipation observed with “SWIFT” drifters. *Journal of Atmospheric and Oceanic Technology*, 29(12), 1866–1882.
- Thomson, J., & Persson, O. (2021). *Arctic Sea State 2015 Field Campaign, Version 1* [Data Set]. National Snow and Ice Data Center.
- Thomson, J., Squire, V.A., Ackley, S., Rogers, E., Babanin, A., Guest, P., Maksym, T., Wadhams, P., Stammerjohn, S., Fairall, C., Persson, O., Doble, M., Graber, H., Shen, H., Gemmrich, J., Lehner, S., Holt, B., Williams, T., Meylan, M., & Bidlot, J. (2013). *Sea State and Boundary Layer Physics of the Emerging Arctic Ocean*. Technical Report APL-UW TR1306. Applied Physics Laboratory, University of Washington.
- Thomson, N.R., Sykes, J.F., & McKenna, R.F. (1988). Short-term ice motion modeling with application to the Beaufort Sea. *Journal of Geophysical Research: Oceans*, 93(C6), 6819–6836.
- Thorndike, A.S., & Colony, R. (1982). Sea ice motion in response to geostrophic winds. *Journal of Geophysical Research: Oceans*, 87(C8), 5845–5852.
- Thorndike, A.S., Rothrock, D.A., Maykut, G.A., & Colony, R. (1975). The thickness distribution of sea ice. *Journal of Geophysical Research*, 80(33), 4501–4513.
- Tiller, W.A., Jackson, K.A., Rutter, J.W., & Chalmers, B. (1953). The redistribution of solute atoms during the solidification of metals. *Acta Metallurgica*, 1(4), 428–437.
- Timco, G.W., & Frederking, R.M.W. (1983). Flexural strength and fracture toughness of sea ice. *Cold Regions Science and Technology*, 8(1), 35–41.
- Timco, G.W., & Frederking, R.M.W. (1986). Confined compression tests: Outlining the failure envelope of columnar sea ice. *Cold Regions Science and Technology*, 12(1), 13–28.
- Timco, G.W., & Frederking, R.M.W. (1990). Compressive strength of sea ice sheets. *Cold Regions Science and Technology*, 17(3), 227–240.
- Timco, G.W., & O'Brien, S. (1994). Flexural strength equation for sea ice. *Cold Regions Science and Technology*, 22(3), 285–298.
- Timco, G.W., & Weeks, W. (2010). A review of the engineering properties of sea ice. *Cold Regions Science and Technology*, 60(2), 107–129.
- Timmermann, R., Danilov, S., Schröter, J., Böning, C., Sidorenko, D., & Rollenhagen, K. (2009). Ocean circulation and sea ice distribution in a finite element global sea ice–ocean model. *Ocean Modelling*, 27(3–4), 114–129.
- Tison, J.L., Maksym, T., Fraser, A.D., Corkill, M., Kimura, N., Nosaka, Y., Nomura, D., Vancoppenolle, M., Ackley, S., Stammerjohn, S., Wauthy, S., Van der Linden, F., Carnat, G., Sapart, C., de Jong, J., Fripiat, F., & Delille, B. (2020). Physical and biological properties of early winter Antarctic sea ice in the Ross Sea. *Annals of Glaciology*, 61(83), 241–259.
- Toffoli, A., Bennetts, L.G., Meylan, M.H., Cavaliere, C., Alberello, A., Elsnab, J., & Monty, J.P. (2015). Sea ice floes dissipate the energy of steep ocean waves. *Geophysical Research Letters*, 42(20), 8547–8554.
- Totman, A., Uzorka, O.E., Dempsey, J., & Cole, D. (2007). Sub-size fracture testing of FY sea ice. *6<sup>th</sup> International Conference on Fracture Mechanics of Concrete and Concrete Structures*.
- Tsamados, M., Feltham, D.L., & Wilchinsky, A.V. (2013). Impact of a new anisotropic rheology on simulations of arctic sea ice. *Journal of Geophysical Research: Oceans*, 118(1), 91–107.
- Tuhkuri, J. (1988). The applicability of LEFM and the fracture toughness of sea ice. In W.M. Sackinger, & M.O. Jeffries (Eds.), *Port and Ocean Engineering under Arctic Conditions* (Vol. 1, pp. 21–32). Geophysical Institute, University of Alaska.

- Turner, A.K., Hunke, E.C., & Bitz, C.M. (2013). Two modes of sea-ice gravity drainage: A parameterization for large-scale modeling. *Journal of Geophysical Research: Oceans*, 118(5), 2279–2294.
- Turner, J., Phillips, T., Marshall, G.J., Hosking, J.S., Pope, J.O., Bracegirdle, T.J., & Deb, P. (2017). Unprecedented springtime retreat of Antarctic sea ice in 2016. *Geophysical Research Letters*, 44(13), 6868–6875.
- Untersteiner, N. (1961). On the mass and heat budget of Arctic sea ice. *Archiv für Meteorologie, Geophysik und Bioklimatologie, Serie A*, 12(2), 151–182.
- Untersteiner, N., Thorndike, A., Rothrock, D., & Hunkins, K.L. (2007). Aidjex revisited: A look back at the U.S.-Canadian Arctic ice dynamics joint experiment 1970–78. *Arctic*, 60(3), 327–336.
- Uotila, P., O’Farrell, S., Marsland, S., & Bi, D. (2012). A sea-ice sensitivity study with a global ocean-ice model. *Ocean Modelling*, 51, 1–18.
- Urabe, N., & Inoue, M. (1988). Mechanical properties of Antarctic sea ice. *Journal of Offshore Mechanics and Arctic Engineering*, 110(4), 403–408.
- Urabe, N., & Yoshitake, A. (1981a). Fracture toughness of sea ice – in-situ measurement and its application. In *IAHR International Symposium on Ice, Quebec, 1981. Proceedings = Symposium international sur la glace de l’AIRH, Quebec, 1981. Comptes rendus* (pp. 356–365). University Laval.
- Urabe, N., & Yoshitake, A. (1981b). Strain Rate dependent fracture toughness of pure ice and sea ice. In *IAHR International Symposium on Ice, Quebec, 1981. Proceedings = Symposium international sur la glace de l’AIRH, Quebec, 1981. Comptes rendus* (pp. 551–563). University Laval.
- Urabe, N., Iwasaki, T., & Yoshitake, A. (1980). Fracture toughness of sea ice. *Cold Regions Science and Technology*, 3(1), 29–37.
- Vancoppenolle, M., & Tedesco, L. (2017). Numerical models of sea ice biogeochemistry. In D.N. Thomas (Ed.), *Sea Ice* (Third ed., pp. 492–515). Wiley Blackwell.
- Vancoppenolle, M., Fichefet, T., Goosse, H., Bouillon, S., Madec, G., & Maqueda, M. (2009a). Simulating the mass balance and salinity of Arctic and Antarctic sea ice. 1. Model description and validation. *Ocean Modelling*, 27(1–2), 33–53.
- Vancoppenolle, M., Fichefet, T., & Goosse, H. (2009b). Simulating the mass balance and salinity of Arctic and Antarctic sea ice. 2. Importance of sea ice salinity variations. *Ocean Modelling*, 27(1–2), 54–69.
- Vancoppenolle, M., Goosse, H., de Montety, A., Fichefet, T., Tremblay, B., & Tison, J. (2010). Modeling brine and nutrient dynamics in Antarctic sea ice: The case of dissolved silica. *Journal of Geophysical Research*, 115(C2).
- Vancoppenolle, M., Meiners, K.M., & Michel, Ch., Bopp, L., Brabant, L., Carnat, G., Delille, B., Lannuzel, D., Madec, G., Moreau, S., Tison, J.-L., van der Merwe, P. (2013). Role of sea ice in global biogeochemical cycles: emerging views and challenges. *Quaternary Science Reviews*, 79, 207–230.
- Vancoppenolle, M., Madec, G., Thomas, M., & McDougall, T.J. (2018). Thermodynamics of sea ice phase composition revisited. *Journal of Geophysical Research: Oceans*, 124(1), 615–634.
- Vaudrey, K. (1977). *Ice Engineering: Study of Related Properties of Floating Sea-Ice Sheets and Summary of Elastic and Viscoelastic Analyses*. Technical Report R 860. Civil Engineering Laboratory.
- Vichi, M., Eayrs, C., Alberello, A., Bekker, A., Bennetts, L., Holland, D., de Jong, E., Joubert, W., MacHutchon, K., Messori, G., Mojica, J.F., Onorato, M., Saunders, C., Skatulla, S., & Toffoli, A. (2019). Effects of an explosive Polar cyclone crossing the Antarctic marginal ice zone. *Geophysical Research Letters*, 46(11), 5948–5958.
- Voermans, J.J., Rabault, J., Filchuk, K., Ryzhov, I., Heil, P., Marchenko, A., Collins, C.O., Dabboor, M., Sutherland, G., & Babanin, A.V. (2020). Experimental evidence for a universal threshold characterizing wave-induced sea ice break-up. *The Cryosphere*, 14(11), 4265–4278.
- Wadhams, P., Lange, M.A., & Ackley, S.F. (1987). The ice thickness distribution across the Atlantic sector of the Antarctic Ocean in midwinter. *Journal of Geophysical Research: Oceans*, 92(C13), 14535–14552.
- Wadhams, P., Parmiggiani, F., & De Carolis, G. (2006). Wave dispersion by Antarctic pancake ice from SAR images: A method for measuring ICE thickness. *European Space Agency, (Special Publication) ESA SP (613)* (unpublished).
- Wählin, J., Leisinger, S., & Klein-Paste, A. (2014). The effect of sodium chloride solution on the hardness of compacted snow. *Cold Regions Science and Technology*, 102.
- Wang, Q., Danilov, S., Sidorenko, D., Timmermann, R., Wekerle, C., Wang, X., Jung, T., & Schröter, J. (2014). The Finite Element Sea Ice-Ocean Model (FESOM) v.1.4: formulation of an ocean general circulation model. *Geoscientific Model Development*, 7(2), 663–693.
- Wang, Q., Li, Z., Lei, R., Lu, P., & Han, H. (2018). Estimation of the uniaxial compressive strength of Arctic sea ice during melt season. *Cold Regions Science and Technology*, 151, 9–18.
- Wang, R., & Shen, H.H. (2010a). Experimental study on surface wave propagating through a grease-pancake ice mixture. *Cold Regions Science and Technology*, 61(2–3), 90–96.
- Wang, R., & Shen, H.H. (2010b). Gravity waves propagating into an icecovered ocean: A viscoelastic model. *Journal of Geophysical Research: Oceans*, 115(6).
- Wang, Y.S., & Poplin, J.P. (1988). Laboratory compression tests of sea ice at slow strain rates from a field test program. *Journal of Offshore Mechanics and Arctic Engineering*, 110(2), 154–158.
- Weaver, A.J., Eby, M., Wiebe, E.C., Bitz, C.M., Duffy, P.B., Ewen, T.L., Fanning, A.F., Holland, M.M., MacFadyen, A., Matthews, H.D., Meissner, K.J., Saenko, O., Schmittner, A., Wang, H., & Yoshimori, M. (2001). The UVic Earth System Climate Model: Model description, climatology, and applications to past, present and future climates. *Atmosphere-Ocean*, 39(4), 361–428.
- Weber, J.E. (1987). Wave attenuation and wave drift in the marginal ice zone. *Journal of Physical Oceanography*, 17(12), 2351–2361.



- Weeks, W. (1961). *Studies of Salt Ice*. Research Report 80. U.S. Cold Regions Research and Engineering Laboratory.
- Wei, M., & Dai, F. (2021). Laboratory-scale mixed-mode I/II fracture tests on columnar saline ice. *Theoretical and Applied Fracture Mechanics*, *114*, 102982.
- Weiss, J., & Dansereau, V. (2017). Linking scales in sea ice mechanics. *Philosophical Transactions of the Royal Society A: Mathematical, Physical and Engineering Sciences*, *375*(2086), 20150352.
- Weiss, J., Schulson, E.M., & Stern, H.L. (2007). Sea ice rheology from in-situ, satellite and laboratory observations: Fracture and friction. *Earth and Planetary Science Letters*, *255*(1–2), 1–8.
- Wells, A.J., Wettlaufer, J.S., & Orszag, S.A. (2013). Nonlinear mushy-layer convection with chimneys: stability and optimal solute fluxes. *Journal of Fluid Mechanics*, *716*, 203–227.
- Wells, A.J., Hitchen, J.R., & Parkinson, J.R.G. (2019). Mushy-layer growth and convection, with application to sea ice. *Philosophical Transactions of the Royal Society A: Mathematical, Physical and Engineering Sciences*, *377*(2146).
- Williams, F.M., Everard, J., & Butt, S. (1992). *Ice and snow measurements in support of the operational evaluation of the Nathaniel B. Palmer in the Antarctic winter environment*. Test Report TR-1992-14. National Research Council Canada.
- Williams, T.D., Bennetts, L.G., Squire, V.A., Dumont, D., & Bertino, L. (2013). Wave–ice interactions in the marginal ice zone. Part 2: Numerical implementation and sensitivity studies along 1D transects of the ocean surface. *Ocean Modelling*, *71*, 92–101.
- Wolff, E., Mulvaney, R., & Oates, K. (1988). The location of impurities in Antarctic ice. *Annals of Glaciology*, *11*(1), 194–197.
- Xu, X.-P., & Needleman, A. (1994). Numerical simulations of fast crack growth in brittle solids. *Journal of the Mechanics and Physics of Solids*, *42*(9), 1397–1434.
- Xu, Z., Tartakovsky, A.M., & Pan, W. (2012). Discrete-element model for the interaction between ocean waves and sea ice. *Physical Review E*, *85*(1), 16703.
- Yiew, L.J., Bennetts, L.G., Meylan, M.H., Thomas, G.A., & French, B.J. (2017). Wave-induced collisions of thin floating disks. *Physics of Fluids*, *29*(12), 127102.
- Zampieri, L., Kauker, F., Fröhle, J., Sumata, H., Hunke, E.C., & Goessling, H.F. (2021). Impact of sea-ice model complexity on the performance of an unstructured-mesh sea-ice/ocean model under different atmospheric forcings. *Journal of Advances in Modeling Earth Systems*, *13*(5), e2020MS002438.
- Zhang, J. (2021). Sea ice properties in high-resolution sea ice models. *Journal of Geophysical Research: Oceans*, *126*(1), e2020JC016686.
- Zhang, J., & Hibler III, W.D. (1997). On an efficient numerical method for modeling sea ice dynamics. *Journal for Geophysical Research: Oceans*, *102*(C4), 8691–8702.
- Zhang, J., & Rothrock, D. (2001). A thickness and enthalpy distribution sea-ice model. *Journal of Physical Oceanography*, *31*(10), 2986–3001.
- Zhang, J., Rothrock, D., & Steele, M. (2000). Recent changes in Arctic Sea ice: The interplay between ice dynamics and thermodynamics. *Journal of Climate*, *13*(17), 3099–3114.
- Zhao, X., & Shen, H.H. (2015). Wave propagation in frazil/pancake, pancake, and fragmented ice covers. *Cold Regions Science and Technology*, *113*, 71–80.
- Zhao, X., & Shen, H.H. (2018). Three-layer viscoelastic model with eddy viscosity effect for flexural-gravity wave propagation through ice cover. *Ocean Modelling*, *131*, 15–23.
- Zhou, M., & Meschke, G. (2011). Numerical modelling of coupling mechanisms during freezing in porous materials. *Proceedings in Applied Mathematics and Mechanics*, *11*(1), 495–496.
- Zhou, M.-M. (2013). *Computational Simulation of Soil Freezing: Multiphase Modeling and Strength Upscaling* [PhD thesis]. Ruhr University Bochum.
- Zong, Z. (2022). A Random Pore Model of sea ice for predicting its mechanical properties. *Cold Regions Science and Technology*, *195*, 103473.

